# FREQUENCY-LOCKING OF A CW DYE LASER

# TO ATOMIC ABSORPTION LINES BY A FARADAY FILTER

*by*

*Taisuke ENDO*

*December 1978*

*Kyoto University*

*Kyoto, Japan*

# FREQUENCY-LOCKING OF A CW DYE LASER

# TO ATOMIC ABSORPTION LINES BY A FARADAY FILTER

*by*

*Taisuke ENDO*

*December 1978*

*Kyoto University*

*Kyoto, Japan*

ACKNOWLEDGEMENTS

The author would like to express his great appreciation to Professor Toru Ogawa for continuous guidance, valuable discussions and stimulating suggestions, and for careful reading of the manuscript. The author is much indebted to Dr. Tsutomu Yabuzaki for many fruitful and encouraging discussions, and carefull reading of the manuscript.

The author also wish to express his gratitude to Professor Susumu Kato and Professor Iwane Kimura for valuable comments and suggestions.

The author wish to acknowledge the assistance of Mr. Masao Kitano and Mr. Takashi Sato during much of this work, and of Mr. Hiromitsu Asano during the early stages.

Thanks are also due to other staff members of Ionosphere Research Laboratory and Professor Kimura's group.

Numerical calculation in this work were performed at the Data Processing Center of Kyoto University.

ABSTRACT

This thesis deals with a theoretical and experimental study on the frequency-locking of a CW (continuous wave) dye laser to atomic absorption lines by a Faraday filter.

The dye laser offers the essential feature of being tunable throughout the spectral region from the near ultraviolet to near infrared. The dye laser covers the most interesting spectral region for the purposes of atomic spectroscopy, photo-chemistry and isotope separation. Therefore it plays a prominent role in these fields.

In most of applications of dye lasers, we need a laser oscillation at an atomic absorption line with narrow spectral width. In recent years several methods have been developed to this end. Frequency-locking to the center of a Doppler-broadened absorption line can be achieved by saturated absorption or resonance fluorescence of an atomic beam with extremely high stability. However, in this method the laser system becomes relatively complicated, because one has to prepare a single-mode oscillation by means of frequency selective elements such as prisms, deffraction grating and Fabry-Perot etalons, and because one has to adjust these elements by a feedback control for frequency-locking. On the other hand, frequency-locking to atomic absorption lines can also be achieved by simple elements

using anomalous dispersions in the vicinity of absorption lines, such as a discharge tube using the lens effect or a vapor prism. With this method, the oscillation only on the wing of the absorption line has been attained, and nobody has succeeded to get the oscillation just at the line center.

The Faraday filter which has been developed in the present work also belongs to the method using anomalous dispersions in the vicinity of absorption lines. The Faraday filter has important advantages: the frequency narrowing and the locking of a dye laser are simultaneously possible by a Faraday filter without any other frequency selective elements; the frequency locking can be achieved at line center; and the oscillation frequency cannot detune from the absorption line without complicated frequency control system.

We at first theoretically analyze the Faraday filter. We calculate the absorption and rotation for linearly polarized monochromatic plane wave by the Faraday effect. The laser cavity with a Faraday filter is studied and the transmission of the Faraday filter in the cavity is calculated. As a result, we find that the frequency-locking of a CW dye laser to the center of an atomic absorption line is possible by the Faraday filter and that the Faraday filter with partial polarizers is more suitable than that with perfect ones for this purpose. Furthermore, we consider the saturation effect on the Faraday filter by laser light, and show that the laser light has little effect on the rotation angle by the filter, that is, the condition for the frequency-locking can be calculated by linear theory.

Next we apply the Faraday filter to following atoms: sodium, neon and helium. For sodium, single-mode CW oscillations at the center of the D lines have been obtained by inserting a Faraday filter in argon-laser-pumped dye laser cavity. The oscillations at the $D_1$ and $D_2$ lines can be selected by choosing adequate values of sodium temperature and the magnetic field strength of the Faraday filter. Experimentally obtained conditions to get the single mode oscillations at the center of the D lines are compared with theoretically calculated feature of the Faraday filter, and a relatively good agreement has been found. The shifts of the oscillation frequencies due to the magnetic field are explained by the theory including a spatial hole-burning effect in dye.

Single-mode CW oscillation at some absorption lines from the 1s states to the 2p states of neon in a discharge has been obtained by means of a Faraday filter. This shows that the Faraday filter is applicable to absorption lines from the excited states as well as the lines from the ground state. Particular attention is given to the influence of isotopes on the Faraday filter. The condition for the oscillation at absorption lines and the shifts of the oscillation frequency due to the variation of the magnetic field are theoretically and experimentally obtained for various ratio of the mixtures of $Ne^{20}$ and $Ne^{22}$. Comparison between the experimental results and the theoretical ones is given, and a good agreement has been found. Furthermore, we have developed a new technique for fine tuning of a CW dye laser in the vicinity of the absorption line by means of the isotope effect. We have

also obtained the 1s densities in a positive column of a glow discharge in the presence of a magnetic field by fitting the experimental results to the theory.

In the frequency-locking to the absorption line from the $2^3P$ state to the $3^3D$ state of helium, attention is mainly focused on the effect of the fine structures to the Faraday filter. The transmission of the Faraday filter has a complicated feature due to this effect. We have obtained experimentally a narrow spectrum located on blue wing of the line, which is predicted by the theoretical calculation to be the easiest mode to get.

At the end of this thesis, we propose the Faraday filter with inhomogeneous magnetic field. By the Faraday filter with uniform magnetic field, we can achieve the frequency-locking to the center of the absorption line. However, the frequency-locking to the wing of another line sometimes occurs at the same time. On the other hand, by the Faraday filter with inhomogeneous magnetic field, we can avoid the frequency-locking to the wing of line.

CONTENTS

# CHAPTER I

# GENERAL INTRODUCTION

## 1.1 Introduction

In recent years, several tunable lasers such as dye lasers[1)~3)], semiconductor lasers[4),5)], and color center lasers[6),7)] have been developed. This is in a striking contrast to that most other lasers heretofore provide discrete oscillation frequency determined by the characteristics of the laser mediums. Among the various types of tunable lasers, the dye laser plays a prominent role in the fields of spectroscopy, photo-chemistry and isotope separation[8)] because the dye laser is continuously tunable over a wide frequency range[9),10)] from the near ultraviolet to the near infrared. The dye laser output for various dyes are shown in Fig. 1.1[9)].

The dye laser provides wideband radiation at the frequency near the peak of the dye gain curve in the untuned case. In many applications, the frequency-locking to desired atomic absorption lines and the spectral narrowing are most important steps towards the full utilization of the dye laser potential. These requirements can be met by using frequency selective elements.

We firstly give a brief review of the principles of the dye laser operation in order to understand its properties of wavelength

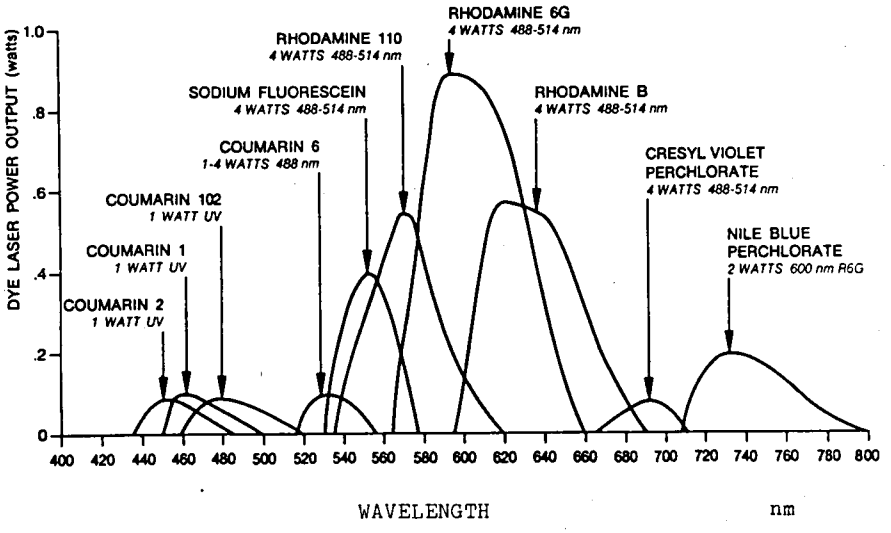


Fig. 1.1 Dye laser output power for various dyes. The position of the output curve with respect to wavelength varies somewhat with the solvent used. The curves in this figure were obtained using ethylene glycol as the solvent.[9)]

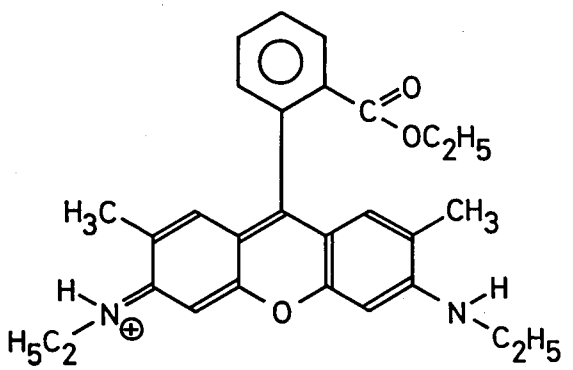


Fig. 1.2 Structure of Rhodamine 6G.

and bandwidth versatility. We also review the methods for frequency selection which have been performed so far, and compare them with the method of Faraday filter which has many advantages as a frequency selective element. Finally, we describe a short review of the present work.

## 1.2 Principles of the Dye Laser

In this section, principles of the dye laser operation are described. The laser dyes are organic compounds containing conjugated double bonds. The constitutional formula of the dye Rhodamine 6G used in the present work is shown in Fig. 1.2 for an example. The dyes are usually get in the state of powder. It is in many cases used in liquid phases solved in organic solvents such as ethyl alcohol[11], ethylene glycol[12], and acetone[11], or solved in water[13]. The dyes can also be used in the solid[14] and vapor phases[15].

The energy level diagram for a dye molecule depends on the dye and the solvent. It can be generally shown[3),16),17)] as Fig. 1.3. The energy levels may be grouped into two series: singlet ($S_0$, $S_1$, $S_2$, ·····) and triplet ($T_1$, $T_2$, $T_3$, ·····) series. The lowest singlet state $S_0$ is the electronic ground state, and the optical transition between singlet and triplet states is forbidden. The rotational and vibrational structure of each electronic state is smeared

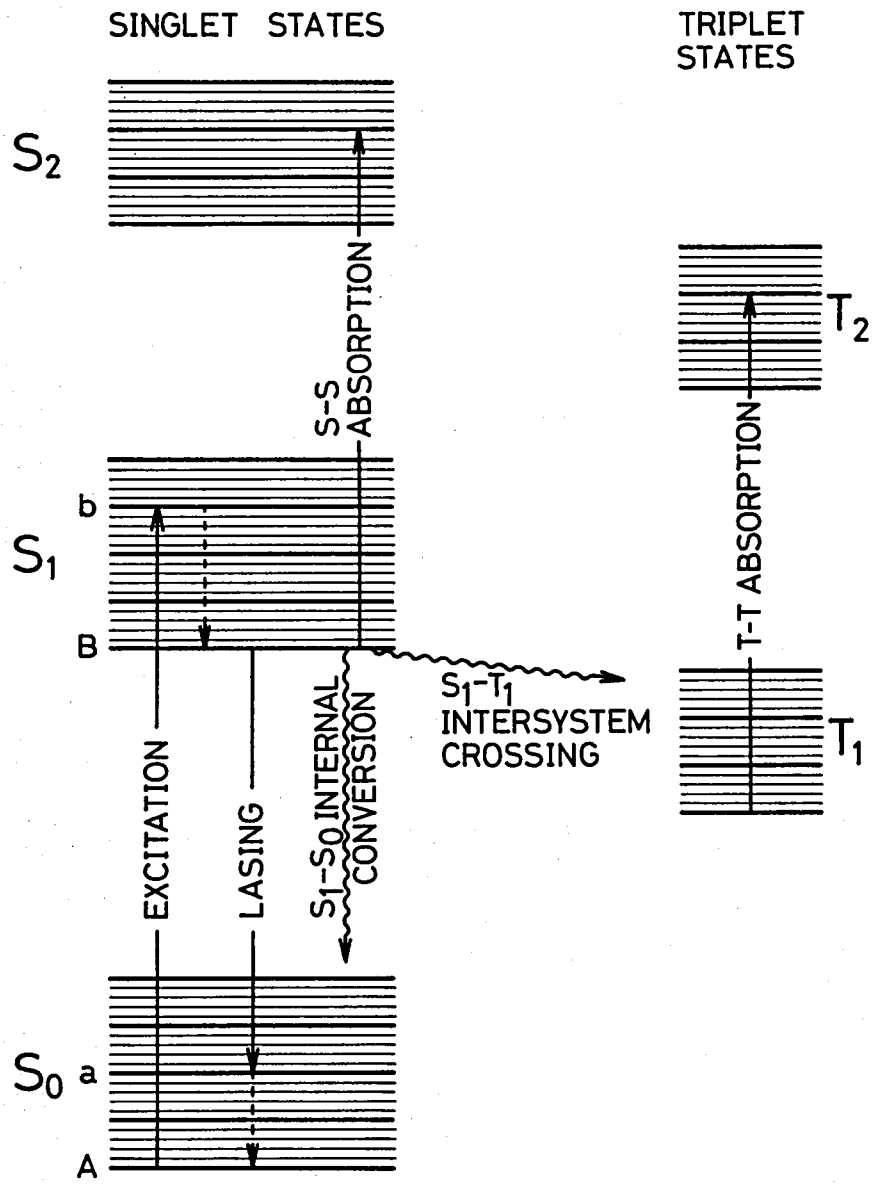


Fig. 1.3 Schematic representation of the energy levels of a dye molecule. The processes of importance in the operation of the CW dye laser are indicated by arrows. The heavy horizontal lines represent vibrational sublevels of the electronic states and the lighter lines represent rotational levels.

out into a broad energy band. The states which contribute to the laser oscillation are $S_0$ and $S_1$. In thermal equilibrium, the dye molecules have energy which is close to the lowest edge of $S_0$. The population of $S_1$ is obtained by optical excitation by a laser[18] or a flashlamp[19] with a wavelength corresponding to the transition from A to b. The molecule excited to b relaxes to B with the rotational and vibrational relaxation time of the order of $10^{-12}$ sec. The broad-band fluorescence spectrum corresponds to the transition from B to a. Since the relaxation time of a is of the order of $10^{-12}$ sec[20] and the lifetime of B is of the order of $10^{-9}$ sec, stimulated emission can occur when the optical excitation is sufficiently strong. Thus, the dye laser operates as a four-level laser. Since the $S_0$ state is widely spread in energy, the laser oscillation can be obtained over the wide wavelength region of the fluorecence band.

A part of molecules which are excited to B does not contribute to laser oscillation. Some of them relax to $S_0$ by the spontaneous emission or the internal conversion without radiation, and the other relax to $T_1$ by the intersystem crossing without radiation. These processes decrease the quantum yield of the laser which is given as

$$\phi = \frac{\sigma_{em}}{\sigma_{em} + \sigma_{sp} + k_{SS} + k_{ST}} \quad , \qquad (1.1)$$

where $\sigma_{em}$ is the stimulated emission cross section, $\sigma_{sp}$ is the spontaneous emission cross section, $k_{SS}$ is the internal

conversion cross section, and $k_{ST}$ is the intersystem conversion cross section.

The molecules in $T_1$ absorb the photon with energy corresponding to the splitting between $T_1$ and $T_2$. Since the absorption spectrum of the triplet state and the fluorescence spectrum of the singlet state overlap partially to each other, the frequency region where the laser oscillation can be obtained is decreased. Therefore, when we consider the laser operation, we must take account of the triplet state as well as the singlet states.

Next, we will consider the wavelength property of the dye laser oscillation. For the calculation of the gain of the dye laser, we need the basic parameters $\sigma_{em}$, $\sigma_s$ and triplet state absorption cross section $\sigma_T$ as functions of a wavelength $\lambda$. The values of these parameters are shown in Fig. 1.4[2),3)] for Rhodamine 6G.

Let us analyze the threshold condition for CW operation.[16)] We define the laser gain as the growth rate of light intensity per unit length given by

$$G(\lambda) = \frac{1}{I}\frac{dI}{dz}, \tag{1.2}$$

where $I$ is the intensity of the laser traveling along the $z$ direction. We may write the rate equation for photon production as

$$\frac{dI}{dz} = I\left(\sigma_{em}N_S - \sigma_s N_0 - \sigma_T N_T - \gamma\right), \tag{1.3}$$

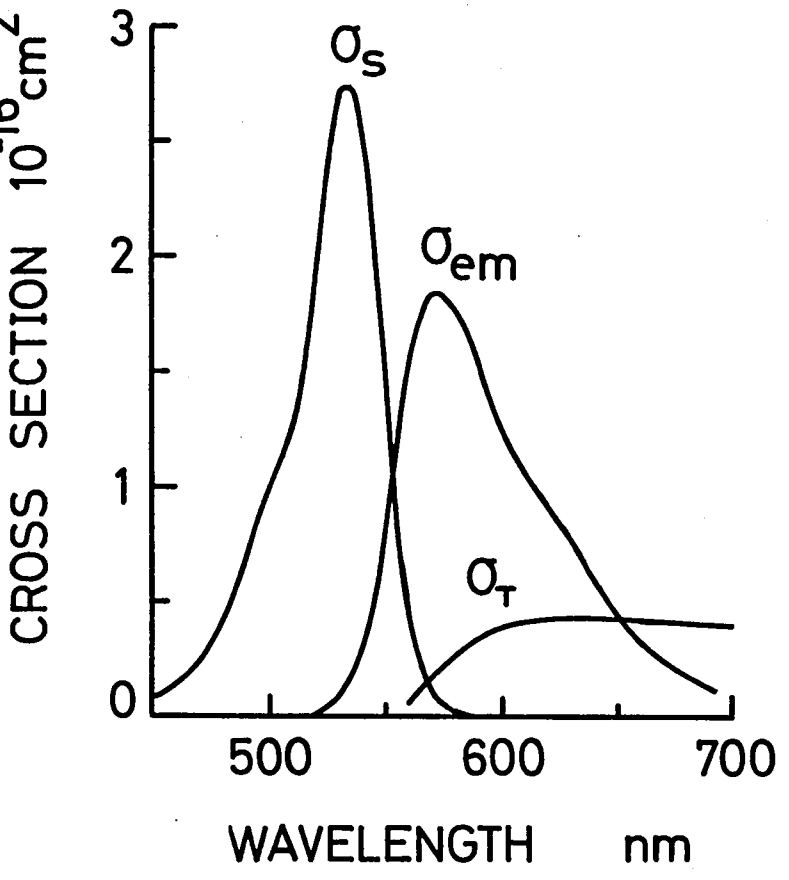


Fig. 1.4 Cross sections for singlet state absorption, $\sigma_S$, singlet state stimulated emission, $\sigma_{em}$, and triplet state absorption, $\sigma_T$ for Rhodamine 6G. [2),3)]

where $N_S$, $N_O$ and $N_T$ are the concentrations of the states $S_1$, $S_O$ and $T_1$, respectively, and $\gamma$ is the rate of the loss of photons per unit active length due to output coupling and other cavity losses. Substituting eq. (1.3) to eq. (1.2), we obtain

$$G(\lambda) = \sigma_{em}N_S - \sigma_S N_O - \sigma_T N_T - \gamma . \tag{1.4}$$

The rate equation for the triplet population may be written as

$$\dot{N}_T = k_{ST}N_S - \frac{N_T}{\tau_T} , \tag{1.5}$$

where $\tau_T$ is the lifetime of the molecule in $T_1$. In the steady state ( $\dot{N}_T = 0$ ), it follows that

$$N_T = \tau_T k_{ST} N_S . \tag{1.6}$$

The total molecular concentration $N$ is given by

$$N = N_O + N_S + N_T . \tag{1.7}$$

Substituting eqs. (1.6) and (1.7) into eq. (1.4), we obtain

$$G(\lambda) = \alpha N_S - \sigma_S N - \gamma , \tag{1.8}$$

where $\alpha$ stands for a growth coefficient given by

$$\alpha = \sigma_{em} + \sigma_S + \sigma_T k_{ST}(\sigma_S - \sigma_T) \quad . \tag{1.9}$$

When the variables $\sigma_{em}$, $\sigma_S$ and $\sigma_T$ are given for a certain dye, the gain $G(\lambda)$ can be regarded as a function of variables: $N_S$, $k_{ST}\tau_T$, $\gamma$ and $\lambda$. It should be noted that $N_S$ and $k_{ST}\tau_T$ depend on the operation condition of the dye laser such as pumping power, solvent and triplet quenching method.

The threshold condition is given by

$$G(\lambda) = 0 \quad . \tag{1.10}$$

Since $k_{ST}\tau_T$ is fixed for a given dye laser system, the threshold condition can be displayed as three-dimensional surface in a coordinate space with axes $N_S/N$, $\gamma/N$ and $\lambda$. The zero-gain surface for Rhodamine 6G is shown in Fig. 1.5,[16] in the case of $k_{ST}\tau_T = 1.0$. This value is close to that found by experiment[21),22)].

We first consider the case of a nondispersive loss, that is $\gamma$ is independent of $\lambda$ and is given by

$$\gamma = \gamma_0 \quad \text{(constant)}. \tag{1.11}$$

As seen in Fig. 1.6(a), when we increase $N_S/N$ by increasing the pumping power, $N_S/N$ attains to the bottom of the valley of the zero-gain surface on a given iso-loss surface $\gamma_0/N$. At the just crossing point, lasing occurs at the wavelength $\lambda_0$. When we vary the loss $\gamma_0$, the crossing point moves along the

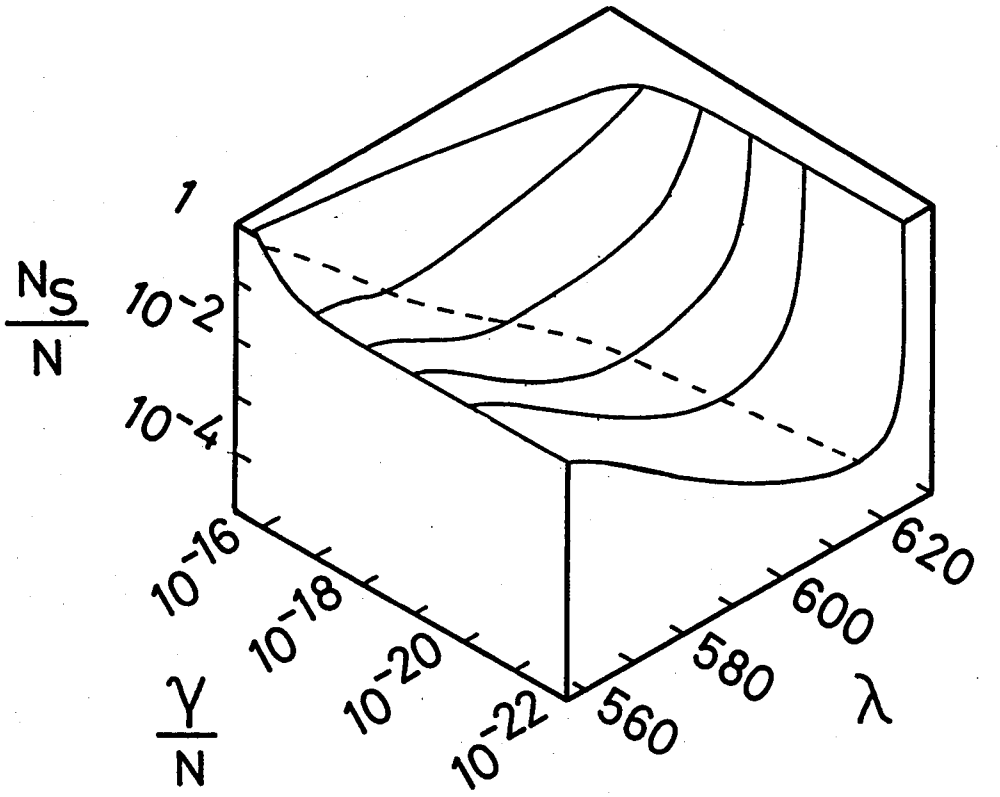


Fig. 1.5 The relative excited state population at threshold, $(N_S/N)_{G=0}$ , in Rhodanine 6G for $k_{ST}\tau_T = 1.0$, as a function of lasing wavelength, $\lambda$ , and normalized extrinsic loss, $\gamma/N$. The iso-loss contours are the intersections of constant-loss planes with the zero-gain surface, and the dotted line represents the locus of minima of these intersections.[16)]

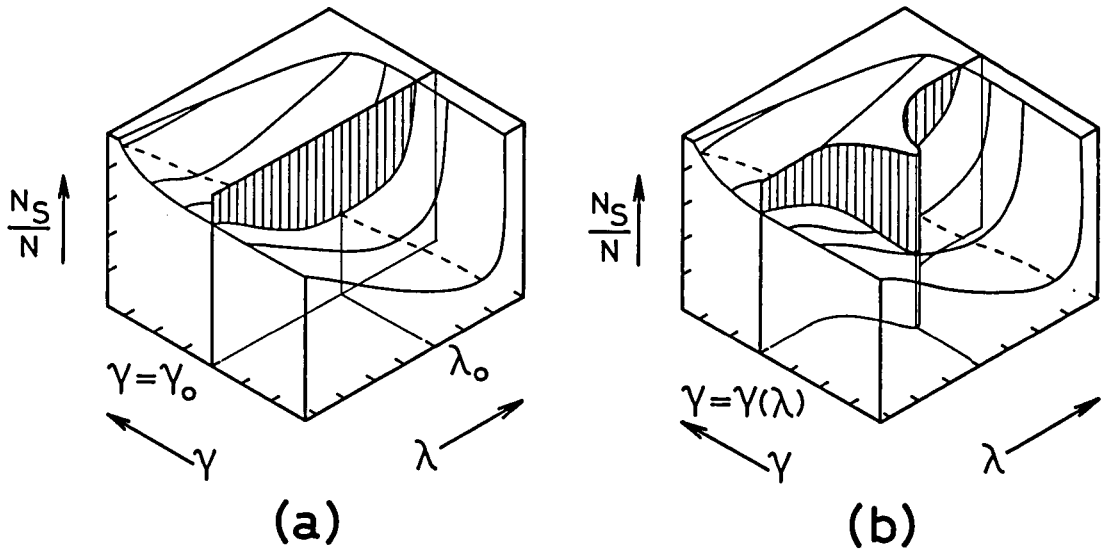


Fig. 1.6 Schematic representation of (a) the self tuning and (b) the external tuning of the dye laser. When the extrinsic loss is nondispersive, it can be represented in (a) by a plane $\gamma = \gamma_0$ which is orthogonal to the $\gamma/N$ axis. The oscillation wavelength $\lambda_0$ is given by the minimum $N_S/N$ point on the intersection of constant loss plane with the zero-gain surface, (the dotted line). When the extrinsic loss is dispersive, it can be represented in (b) by a curved surface $\gamma = \gamma(\lambda)$. The oscillation wavelength agrees with the one giving the minimum loss.

bottom of the valley; i.e. along the dotted line in Fig. 1.6(a). As seen in Fig. 1.6(a), as the loss increases, the oscillation wavelength decreases. Namely we can tune the oscillation wavelength by choosing the loss. This tuning method is referred to as "self-tuning".

Next, we consider the case of a dispersive loss, where $\gamma$ is given by a function of $\lambda$ as

$$\gamma = \gamma(\lambda) . \tag{1.12}$$

The dispersive loss can be achieved by inserting the dispersive elements such as prisms, gratings and so on in the laser cavity. The loss line can be drawn as shown in Fig. 1.6(b). In this case, the lasing occurs at the frequency where the $\gamma$ becomes minimum. It should be noted that in this case the oscillation frequency needs not lie on the bottom of the zero-gain surface. That is, we can tune the oscillation frequency by dispersive elements inserted in the laser cavity. This tuning method is referred to as "external tuning". The oscillation line width depends on the band width of the loss. We can usually obtain the line width narrower than that of the loss due to nonlinear effect of the gain of the dye. This is based on the fact that the homogeneously broadened dye laser medium is extremely sensitive to a frequency dependent cavity Q.

Consequently, we find that the problem of the frequency-locking and spectral narrowing of the dye laser becomes the

problem to realize the dispersive loss having a narrow minimum at desired wavelength. In order to achieve the frequency-locking to an atomic absorption line with high accuracy and stability, we have to prepare the dispersive element having a narrow passband at the line center.

## 1.3 Tuning of the Dye Laser

As described in section 1.1, the dye lasers have the tunability in the wavelength range extended over one hundred nanometers. Without spectral control, the dye laser oscillates at the frequency determined by the self-tuning with a wide spectral width of several tens of nanometers. The frequency selection and spectral narrowing are necessary to make the best use of its tunability. Furthermore, in the most of applications of the dye lasers, the frequency-locking to atomic or molecular absorption lines are essential. In this section, we review the frequency selection methods which have been achieved so far, and compare them with a method using the Faraday filter. Table 1.1 gives a survey of these methods. We give also schematic diagram of these methods in Fig. 1.7.

A is the coarse tuning method utilizing the self-tuning, where we change the oscillation frequency by selection of the dye, the solvent and the concentration of the dye solution. This method is not sufficient when used alone in most of applications of the dye lasers, but should be taken into account before applying

Table 1.1 Tuning methods of dye lasers

| METHOD | | | | FREQUENCY SELECTIVE ELEMENT |
|---|---|---|---|---|
| A | SELF TUNING | | | (DYE, SOLVENT, CONCENTRATION) |
| EXTERNAL TUNING | | B | MECHANICAL TUNING | PRISM, DIFFRACTION GRATING, FABRY-PEROT ETALON, LYOT FILTER, FOX-SMITH TYPE CAVITY |
| EXTERNAL TUNING | | C | SMALL SELECTIVE GAIN | DISCHARGE TUBE |
| EXTERNAL TUNING | | C | ANOMALOUS DISPERSION | DISCHARGE TUBE, VAPOR PRISM, VAPOR MIRROR, FARADAY FILTER |
| D | INJECTION LOCKING | | | (INJECTION OF MONOCHROMATIC RADIATION) |

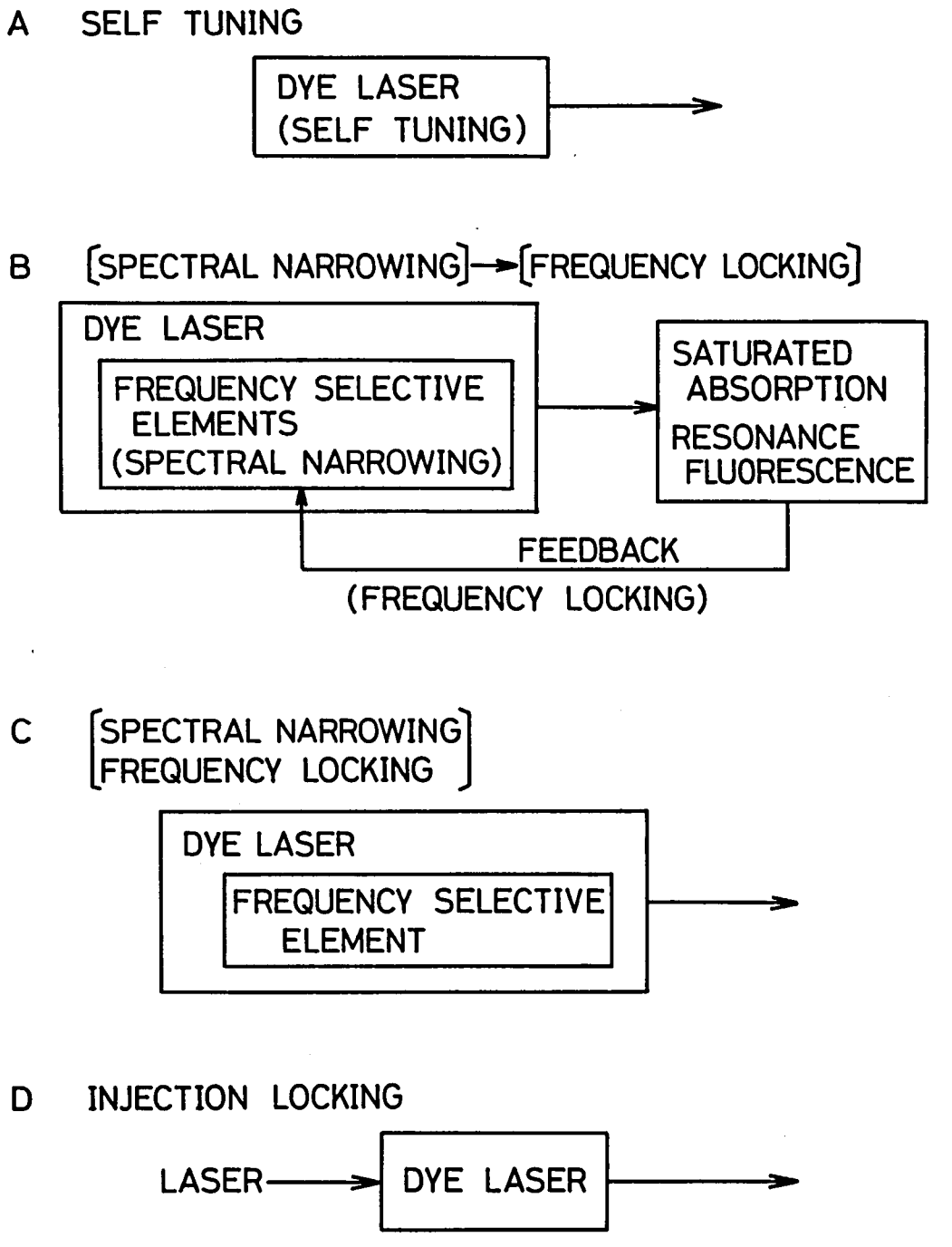


Fig. 1.7 Schematic representation of the frequency tuning or locking methods of dye lasers.

the fine tuning methods described in the following.

The methods of type B is the most orthodox, where we first narrow the spectral width by inserting the dispersive elements, and then lock the frequency by adjusting the positions, angles and tilts of these elements. Prisms[23)~25)], diffraction gratings[26)~28)], Fabry-Perot etalons[29),30)], Lyot filter[31)~34)], and Fox-Smith reflector[35)] have been used as the wavelength selective elements.[36)~43)]

A study of the sodium D lines in saturated absorption[44)~47)] using a repetitively pulsed tunable dye laser was made by Hänsch et al.[44)]. A simplified scheme of the experimental setup is shown in Fig. 1.8. A side-pumped dye cell was placed inside a cavity with a high dispersion grating as a wavelength selective element and reflector. An inverted telescope for collimation and beam expansion was placed inside the cavity. A tilted Fabry-Perot etalon was inserted for line-width reduction. Fine tuning was done by mechanically changing the tilt angle. All parts of the dye laser head were mounted rigidly, with fine adjustments, on a massive metal frame. A piezoelectrically tunable confocal Fabry-Perot interferometer serves as an ultra narrow bandpass filter outside the dye laser cavity. It reduced the line width from 300 to 7 MHz. Two light beams of equal frequency were sent in opposite directions through the resonant atomic vapor, and the changes in absorption for one of the beams (the probe) caused by the other (the bleaching or saturating beam) was recorded. A saturation signal was observed when the laser was tuned close to atomic resonance frequency, so that both light waves interact

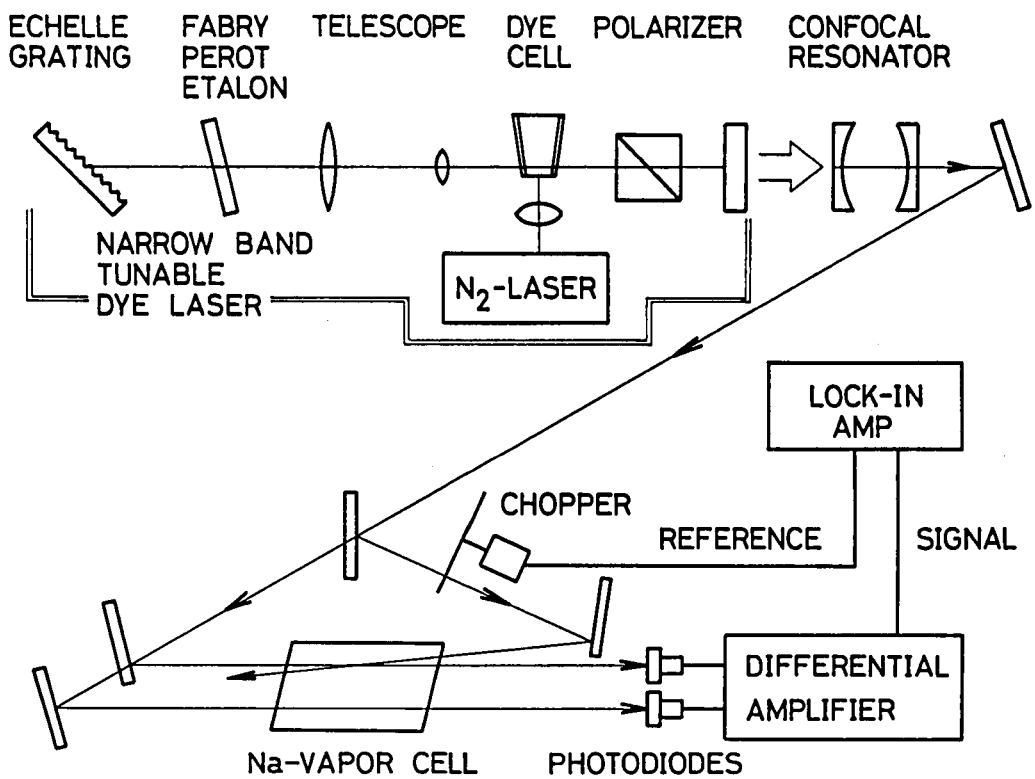


Fig. 1.8 Experimental setup for saturated absorption.[44),48)]

with the same atoms, i.e., those with zero axial velocity.

High resolution spectroscopy of the sodium D lines in atomic beam was carried out by Hartig et al.[49] The experimental setup is shown in Fig. 1.9. The preliminary wavelength selection was performed by a flint glass Brewster angle prism. Single mode operation was obtained by using an uncoated fused quartz intracavity etalon of 5 mm thickness. By varying the length of the laser cavity piezoelectrically, the laser could be tuned continuously over a range of 600 MHz. An atomic beam[40),50)~52)] was used in order to minimize the Doppler width. The sodium atoms were excited by the laser, and the fluorescent light was observed as the laser was tuned across the D lines. The maximum of the signal was observed when the oscillation frequency was just at the absorption lines.

The frequency-locking of a dye laser to atomic absorption lines can be carried out by a feed back control of the frequency-selective elements using the saturated absorption or resonance fluorescence from an atomic beam. In this method, we have to prepare a single-mode or narrow band laser before we apply the frequency-locking methods. Since the oscillation frequency is determined by the positions, angles, and tilts of the tuning elements in this method, we must pay close attention to remove fluctuation of these values. The dye laser is usually mounted on a vibration-isolating table and covered by a box in order to reduce the disturbance which comes from the vibration of the floor and the

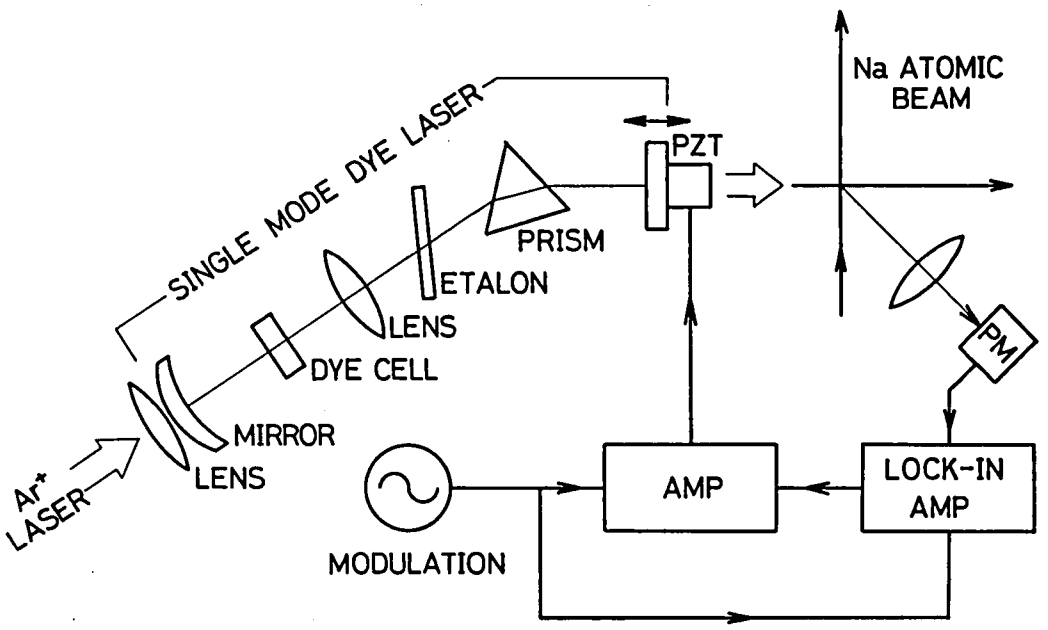


Fig. 1.9 Experimental setup for high resolution spectroscopy by atomic beam.[49)]

thermal effect by air circulation within the laser cavity. When we want to decrease the band width of the laser by narrowing the band width of the tuning elements, we must further decrease the fluctuation of their positions, angles and tilts, and prepare the feedback control system with a electronic circuit and a piezoelectric element with high responce.[53]

With this method, an extremly high frequency-stabilization has now been achieved. For example, the variation of the output frequency of the dye laser was less than $\pm 1.5$ MHz in the experiment by Walther et al.[49] However the stabilizing system generally becomes complicated.

The methods of type C are more conventional, where the spectral narrowing and the locking of a dye laser are simultaneously possible by only one optical element inside the cavity, without any external feedback loop. The Faraday filter in which we are interested in is included in this group. Table 1.2 gives a survey of the methods used so far. The methods can be divided into two groups; one using small selective gain and the other using anomalous dispersion in the vicinity of an absorption or emission line.

It was reported by Klein[54] that a CW dye laser, in which the dye medium was inserted into the pumping argon laser cavity, could be locked to the frequencies of five spontaneous emission transitions in the argon discharge. Although each of the transitions possesses gain, it is too low to bring the system above laser threshold without additional gain from the excited dye. Thus,

Table 1.2 Locking of dye lasers to atomic transitions

| METHOD | ELEMENT | OPERATION | LOCKING TO LINE CENTER | REFERENCE |
|---|---|---|---|---|
| Small selective gain | | | | |
| Ar discharge tube | Ar | CW | o | 54) |
| He-Se discharge tube | Se | CW | o | 55) |
| Anomalous dispersion | | | | |
| Lens effect (gas discharge radial inhomogeneity) | He Na | CW | x | 62) |
| Vapor prism (transvers vapor density gradient) | Na | pulsed | x | 65) 66) |
| Vapor mirror | Na Rb | pulsed | x | 69) |
| Anomalous refractive index in picosecond pulse propagation | Ne | CW (mode locked) | x | 92) 93) |
| Anomalous refractive index of atomic vapor-glass interface | Na | pulsed | x | 70) |
| Anomalous refractive index in flame | Na | pulsed CW | x | 71) |
| Faraday filter | Na | pulsed | x | 78) |
| | Na Ne He | CW | o | This work |

this argon-dye system operating in a narrow line can be called the dye laser locked to a transition in the argon discharge, or the argon laser assisted by the added gain of the excited dye.

Similarly, a CW dye laser which was externally pumped by argon ion laser was locked to inverted transitions in a helium-selenium laser discharge operating within the dye laser cavity by Klein et al.[55]

This method is applicable only to the transition having a gain. In most cases, the transitions which we are interested in for application to photo-chemistry and isotope separation are the absorption lines from the ground state or excited states having long lifetimes, and we cannot apply this method. Instead, we can consider this technique as the opposite effect of the enhancement of absorption, i.e., the existence of quenched regions within a broad oscillation band-width.[56)~61)] The experiment of this type is useful for measuring the existence of small amounts of gain or loss present in the medium within the laser cavity, rather than for the frequency-locking.

Next we will consider the methods using an anomalous dispersion in the vicinity of the line. The frequency-locking of a CW dye laser to atomic absorption lines in a gaseous discharge was carried out by Shank et al.[62], and the mechanism was found to be the lens effect by the nonuniform radial distribution of atoms in the discharge tube. It is well known that strong dispersion can produce a lens in the wings of absorption line under conditions of nonuniform excited state density.[63),64)] The

variation of refractive index at the frequency near line center is shown in Fig. 1.10. It is expected that the excited state density is maximum at the center of the discharge bore, and goes to near zero near the tube wall. The sign of the lens curvature depends on the characteristics of the upper and lower state densities and the relation of the frequency relative to atomic line center. They observed the frequency-locking to the 587.6 nm line ($3^3P$-$3^3D$) of helium and the 589.0 nm line ($3^2S_{3/2}$-$3^2P_{1/2}$) of sodium which was present in the helium discharge tube as an impurity. In the case of helium, both of the upper and lower levels are excited by electron collisions. Since the lower level is more populated than the upper level, the sign of lens at the low frequency side of the line center is positive. The case of sodium, on the other hand, is concerning with a resonance line and, to first order, the ground state density remains uniform across the tube bore, while the excited atoms are nonuniformly distributed. Thus, the sign of lens at frequencies on the low frequency side of the sodium resonance line is negative. In this method, the oscillation frequency depends on the cavity adjustment. It should be noted that the frequency-locking to the line center cannot be achieved because no lens is formed at the line center.

The frequency-locking of a pulsed dye laser was carried out by Yamagishi et al.[65),66)] by a vapor prism placed inside the laser cavity. The vapor prism consists of the heated boat located at the bottom of the cell and water cooled copper pipe placed at the

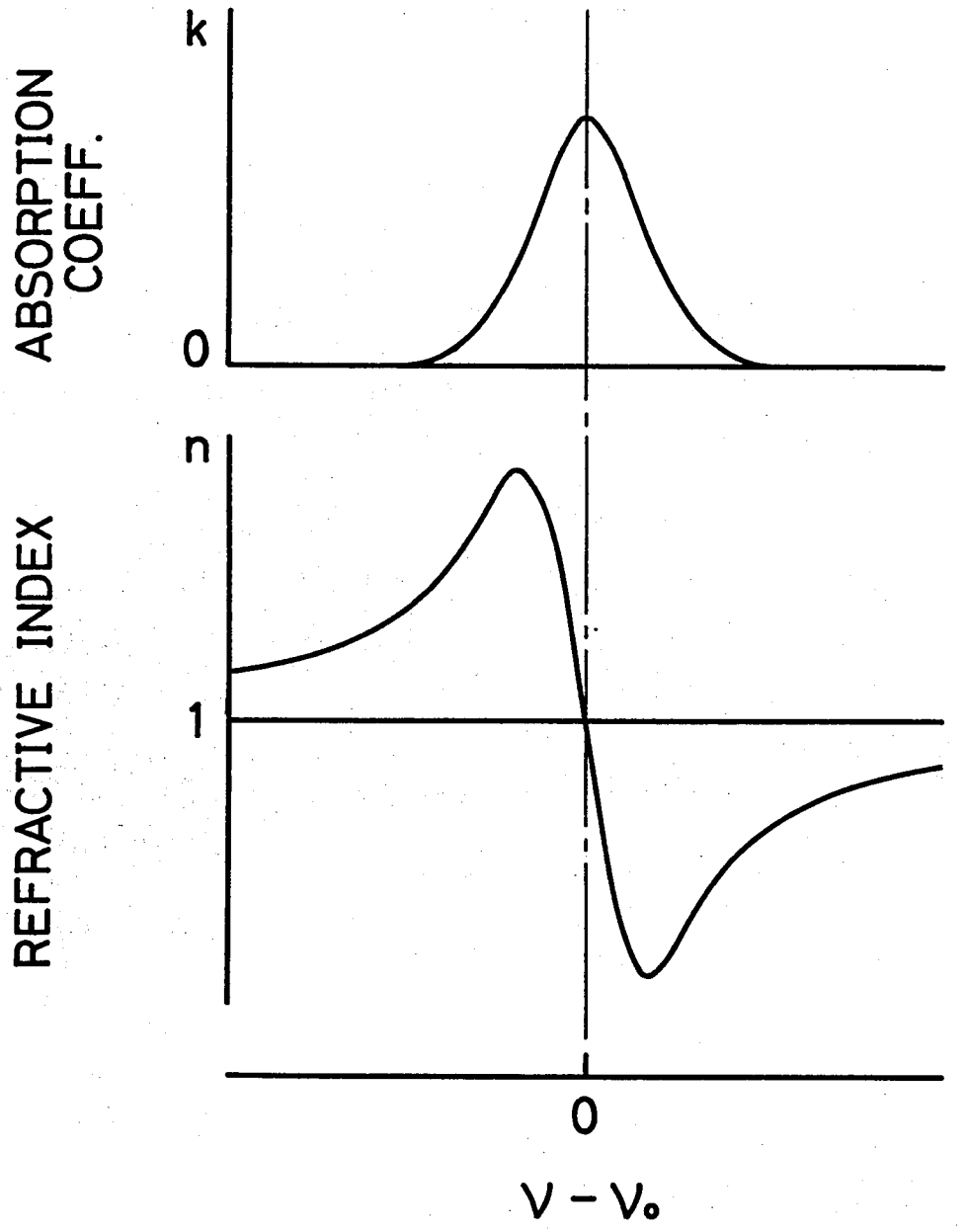


Fig. 1.10 Anomalous dispersion, showing absorption coefficient and refractive index as function of frequency.

top of the cell. The cell is filled with a mixture of sodium vapor evaporated from the boat and of buffer gas. Thus a vapor density gradient is produced in the space between the sodium boat and cooled pipe. This vapor cell behaves as a prism because of the vertical gradient of the refractive index. But the practical use of this vapor prism for frequency-locking at the center of a line has some difficulties by the fact that the anomalous dispersion dominates usually in the wing region of the line.

The frequency-locking to the D lines of the sodium and the 794.8 nm line of the rubidium by means of a vapor mirror[67),68)] was achieved by Bölger et al.[69)] They used a glass cell with a wedged window, containing a small amount of alkali metal, as an external reflector of the optical dye laser resonator. The reflection at the interface between a vapor cell window and the alkali vapor contained is changed by the anomalous dispersion. The reflection coefficient is a function of the frequency. It should be noted that the frequency-locking at both side of the line can be achieved but the frequency-locking at the line center cannot be made since the refraction coefficient becomes zero just at line center.

Some other frequency-locking methods using the anomalous dispersion have been developed: adsorbed atoms on an intracavity glass surface[70)] and atomic vapor produced in a flame inside the cavity[71)]. In these methods, the frequency-locking to the line center is, however, impossible, since the dispersion becomes zero

at line center.

One of the most convenient methods to lock the oscillation frequency of a dye laser to atomic absorption lines is to utilize a Faraday filter, which enables us to achieve the spectral narrowing and the frequency-locking to the line center simultaneously. The Faraday filter[72] consists of cell containing a magnetoactive medium in an axial magnetic field and two polarizers positioned at both ends of the cell, with polarization directions being right angles to each other. When linearly polarized light passes through the cell in the direction parallel to that of the magnetic field, a rotation of the polarization plane occurs, which is known as the Faraday effect[73)~77)]. The Faraday filter has maximum transmission at the rotation angle of $\pi/2$. If the resonant Faraday effect, which rises from anomalous dispersion, is employed, the transmission of the Faraday filter has large frequency-dependence in the vicinity of atomic absorption lines.[72] The frequency giving the maximum transmission is determined by the following parameters: the population density $N$ of the lower level of the associated absorption line, the magnetic field strength $H$, and the length of the cell . The maximum transmission can be obtained at the center of an absorption line by choosing adequate values of these quantities. Inserting the Faraday filter in the dye laser cavity, we can achieve the frequency-locking to the center of the absorption line. The Faraday filter was first proposed by Sorokin et al.[78] and they carried out the locking of the output of a flashlamp-pumped Rhodamine 6G dye laser to the D lines of sodium vapor. However,

they could not get the oscillation at the line center.

In this thesis, we have shown theoretically and experimentally that the frequency-locking at the center of the absorption lines can be achieved by means of the Faraday filter. The reason why the oscillations took place only on the wings of the sodium D lines in the experiment performed by Sorokin et al. is discussed in chapter III.

Finally, we consider the methods of type D.[43),85)] The spectral narrowing of a pulsed dye laser by means of a injection of argon laser was observed by Erickson et al.[79)] Similar results were also obtained when a He-Ne laser[80)], a narrow band flashlamp pumped dye laser[81)] and a CW dye laser was injected.[82)] This method is not essential for the frequency-locking since we must achieve the frequency-locking of the injecting laser before applying this method. However, it is useful to narrow the spectrum of a high power pulsed dye laser, since the narrowing is made by the injection of a very weak monochromatic light without a significant loss of efficiency in the broad-band dye laser.[83),84)]

Consequently, we find that the mechanical tuning and the methods using the anomalous dispersion are important for the frequency-locking of a dye laser to atomic absorption line. By the mechanical tuning, we can get an extremly high frequency stabilization at line center. However, the dye laser system generally becomes complicated. By the methods using anomalous dispersion except for a Faraday filter, we can easily achieve the frequency-locking to the wing of atomic absorption lines, but we

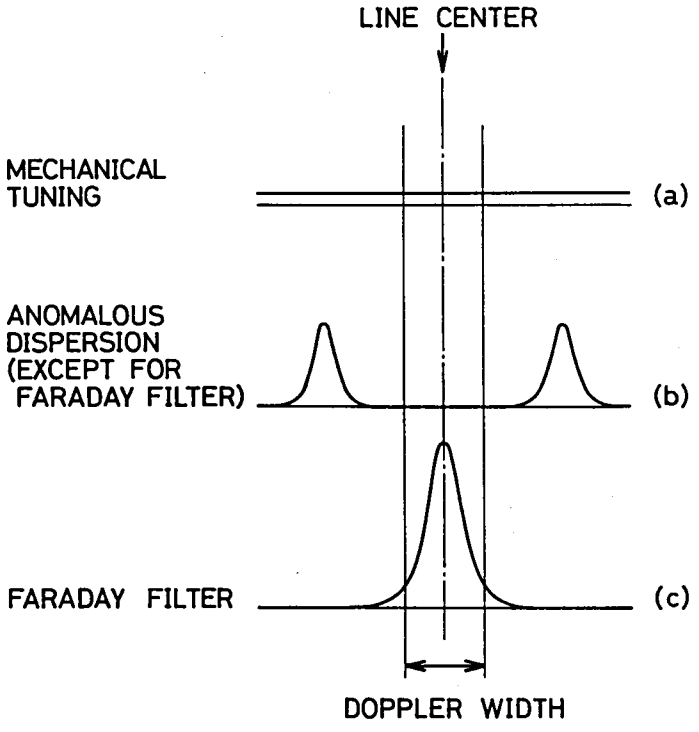


Fig. 1.11 Schmatic representation of the spectral distribution probability (a) by the mechanical tuning, (b) by the anomalous dispersion and (c) by the Faraday filter without fine tuning. By the mechanical tuning (a) we can get an extremly high frequency stabilization with narrow band when the fine tuning by means of the resonance fluoresence or saturated absorption is used. The tuning method using anomalous dispersion (b) leads to locking only on the wings of the line. By the Faraday filter (c), the oscillation frequency cannot be detuned from the absorption line without complicated frequency control system. Furthermore, we can tune the oscillation frequency in the vicinity of the absorption line by choosing adequate values of the parameters of the Faraday filter.

cannot obtain the oscillation at the line center. In contrast with the other methods using anomalous dispersion, the oscillation can easily be locked at the line center by a Faraday filter, and the first experimental success was obtained in our experiment.[86)~88)] The feature of these three tuning methods are schematically shown in Fig. 1.11 as to the spectral destribution probability without fine tuning control. With the mechanical fine tuning control, an extremely narrow-band oscillation can be obtained just at the line center, in both cases of mechanical tuning and Faraday filter.

## 1.4 Outline of the Present Work

Chapter II is devoted to the theoretical analysis of the Faraday filter. At first, we review the anomalous dispersion in the vicinity of atomic absorption lines and the Zeeman effect.[89),90)] We deal with the magneto-optic Faraday effect on the propagation of the monochromatic radiation in the vicinity of an atomic absorption line, propagating along a magnetic field. We analyze the absorption and rotation for a linearly polarized plane wave by the Faraday effect. Next, we study the Faraday filter as a frequency selective element for dye lasers. The laser cavity with a Faraday filter is studied and the transmission of the Faraday filter in a cavity is calculated.[91)] By this calculation, we find that the frequency-locking of a CW dye

laser to the center of an atomic absorption line is possible by inserting a Faraday filter in the laser cavity, and that the Faraday filter with partial polarizers is more siutable than that with perfect ones for this purpose. Furthermore, we consider the saturation effect on the Faraday filter by the lasing, and show that the Faraday filter is of great use as a frequency selective element even in the intense laser light. In other words, we find that the linear approximation is sufficient to give the condition for the frequency-locking by the Faraday filter for a large range of laser intensity.

In chapter III, we study the frequency-locking of a CW dye laser to the sodium D lines by the Faraday filter.[86] We applied the theory described in chapter II to the sodium Faraday filter and discussed about the experiment. Single-mode CW oscillations at the center of the both D lines were obtained. The oscillations at the $D_1$ and $D_2$ lines can be selected by choosing adequate values of the sodium temperature and the magnetic field strength. Experimentally obtained conditions to get the single-mode oscillations at the center of the D lines are compared with the theoretically calculated feature of the Faraday filter, and a good agreement has been found. The shifts of oscillation frequencies due to the magnetic field are also discussed.

In chapter IV, we deal with the frequency-locking to neon absorption lines.[87),88)] Single-mode CW oscillations at absorption lines of neon from the 1s states to the 2p states were

obtained by inserting a Faraday filter in a dye laser cavity. We note that the 1s states are metastable states and quasi-metastable states. Thus the frequency-locking by the Faraday filter may also open a wide range of applications, where the absorption from the excited states is utilized.

Particular attention is given to the influence of isotopes on the Faraday filter. The condition for the oscillation at absorption lines and the shifts of the oscillation frequency due to the variation of the magnetic field strength are theoretically and experimentally obtained for various ratio of the mixtures of $Ne^{20}$ and $Ne^{22}$. Comparison between the experimental results and the theoretical ones is given, and a good agreement has been found. Furthermore, we have developed a new technique for fine tuning of the CW dye laser in the vicinity of the absorption lines by means of the isotope effect.

We also measured the 1s densities in the positive column of the glow discharge in the presence of a magnetic field by fitting the experimental results to the theory.

Chapter V is devoted to the frequency-locking to the 587.6 nm line ($2^3P$-$3^3D$) of helium. We note that the $2^3P$ state is not metastable nor quasi-metastable state, but it has sufficient density for the frequency-locking in the positive column of a glow discharge. One of the different points from the cases of the sodium and neon Faraday filter is that the upper and lower levels of the absorption line have fine structures, and the fine structure coupling cannot be solved in the magnetic field region where the

frequency-locking occurs. Therefore, the transmission of the Faraday filter has complicated magnetic field dependence. We obtained experimentally a narrow spectrum located on the blue wing of the line, which was predicted by the theoretical calculation to be the easiest mode to get.

In chapter Ⅵ, we study the Faraday filter with an inhomogeneous magnetic field. On the point of view of the Faraday filter, the oscillation of the wing is interesting as well as at the line center. However, in many practical applications, the oscillation at the line center must be desired. The oscillations on the wing and at the center compete each other when they exist at the same time. The efficiency of the dye laser locked to the line center is decreased by the oscillation on the wing. We propose the Faraday filter with inhomogeneous magnetic field to avoide the oscillation on the wing. The theoretical calculation shows that this method is usefull for the purpose.

# CHAPTER II

# THEORY OF THE FARADAY FILTER

## 2.1 Introduction

In this chapter, we study on the theory of the Faraday filter.[75),94) 96)] We at first review the classical theory of the dispersion and Zeeman effect[89),97),98)][90]. We investigate the absorption coeffecient and rotation angle for linearly polarized monochromatic plane wave by the resonant Faraday effect[94]. We calculate the transmission of the Faraday filter as a function of the frequency of light for various densities of atoms and magnetic fields of the Faraday filter. We show that maximum transmission can be obtained at the center of an absorption line. Therefore we can achieve the frequency-locking by inserting the Faraday filter in the dye laser cavity.

It should be noted that the transmission of the Faraday filter in the laser cavity differs from that outside the cavity. The reason is that the polarization direction of light must agree itself after a round trip of the cavity. The cavity with a Faraday filter is studied[91] and the effective transmission of the Faraday filter in the laser cavity is calculated to know the features of the Faraday filter as a frequency selective element.

When the Faraday filter is put into a laser cavity, an intense

laser beam irradiates the atoms in the Faraday cell. If the rotation angle for linearly polarized monochromatic plane wave propagating through the Faraday filter is varied due to the saturation effect of the atoms by the laser light, the frequency-locking of the dye laser by the Faraday filter will not be accurate. In order to know this point, we study on the saturation effect on the Faraday filter by laser light, and find that the deviation of the rotation angle from that in the case of a weak light is very small. In other words, the condition for the frequency-locking can be calculated by the linear theory.

## 2.2 Absorption and Dispersion

Atoms are represented by damped harmonic oscillator in the classical theory.[89] Each atom contains charges that can be displaced under the action of an external field, and these charges act as if they were held to positions of equilibium by restoring forces proportional to the displacement. We also introduce a damping force proportional to the velocity. Consider a harmonic oscillator of mass m, charge -e, and resonance frequency $\omega_0$. The equation of motion for the oscillator is then

$$m ( \ddot{x} + \gamma \dot{x} + \omega_0^2 x ) = -eE, \qquad (2.1)$$

where the dots indicate time derivatives and x is the displacement of charge from its equilibrium position. The damping term

$m\gamma\dot{x}$ represents the loss of energy by the oscillating charge owing to emission of electromagnetic radiation. If E varies sinusoidally with time as

$$E = E_0 \exp(-i\omega t), \tag{2.2}$$

we can solve eq. (2.1) by assuming that x varies also as $\exp(-i\omega t)$. We then find the steady state solusion as

$$x = -\frac{e}{m} \frac{E}{\omega_0^2 - \omega^2 + i\omega\gamma} . \tag{2.3}$$

If the density of atoms is $N/cm^3$, the macroscopic electric dipole moment of these atoms is

$$P = -Nex = \frac{e^2}{m} \frac{NE}{\omega_0^2 - \omega^2 + i\omega\gamma} , \tag{2.4}$$

and the dielectric susceptibility $\chi$ is

$$\chi = \frac{P}{\varepsilon_0 E} = \frac{e^2}{\varepsilon_0 m} \frac{N}{\omega_0^2 - \omega^2 + i\omega\gamma} . \tag{2.5}$$

Since there are many absorption lines in atoms, each resonance frequency can no more be associated with a single electron, but in a certain sense, each electron contributes partially to the susceptibility of any resonance frequency. We then find

$$\chi = \sum_i f_i \frac{e^2}{\varepsilon_0 m} \frac{N}{\omega_i^2 - \omega^2 + i\omega\gamma} , \tag{2.6}$$

where, $\omega_i$ is the resonance frequency of the i-th transition, $f_i$ is the oscillator strength which satisfies

$$\Sigma f_i = 1. \tag{2.7}$$

When we consider the susceptibility in the vicinity of the i-th transition, and the contribution of the other transition can be neglected,

$$\chi \simeq f_i \frac{e^2}{\varepsilon_0 m} \frac{N}{\omega_i^2 - \omega^2 + i\omega\gamma}$$

$$\simeq f_i \frac{e^2}{2\varepsilon_0 m \omega_i} \frac{N}{\omega_i - \omega + \frac{i\gamma}{2}} . \tag{2.8}$$

The atoms have Maxwell-Boltzmann velocity distribusion;

$$g(v) = \sqrt{\frac{M}{2\pi k_B T}} \left\{ \exp - \left( \sqrt{\frac{M}{2k_B T}}\, v \right)^2 \right\} , \tag{2.9}$$

where M is the mass of an atom, $k_B$ is the Boltzmann constant and T is the temperature of the gas. An atom which has velocity v along the direction of light propagation has effective resonance frequency $(1 - \frac{v}{c})$ due to the Doppler effect. By replacing $\omega_i$ with $\omega_i(1 - \frac{v}{c})$ in eq. (2.8) and integrating it over the velocity, we obtain the susceptibility of atoms in gas phase,

$$\chi = \frac{f_i N e^2}{2m\omega_i \varepsilon_0} \int_{-\infty}^{\infty} g(v) \frac{1}{\omega_i(1 - \frac{v}{c}) - \omega + \frac{i\gamma}{2}} \, dv. \tag{2.10}$$

This can be written in the form

$$\chi = \frac{k_0 \lambda}{2\pi} i \phi(z), \tag{2.11}$$

where $\phi(z)$ is the complex error function[94),99)] given by

$$\phi(z) = \exp(-z^2) \left\{ 1 - \frac{2i}{\sqrt{\pi}} \int_0^z \exp(y^2)\, dy \right\} \tag{2.12}$$

$$z = (4\pi/\Delta\nu_D) \sqrt{\ln 2}\, (\nu - \nu_0) + ir, \tag{2.13}$$

and $k_0$ is the absorption strength given by

$$k_0 = N f_i e^2 \sqrt{\pi \ln 2} \,/\, m_e \varepsilon_0 c \Delta\nu_D, \tag{2.14}$$

and $\lambda$ is the wavelength of the line. The Voigt parameter of the natural damping ratio r, and the Doppler full-width at half-maximum $\Delta\nu_D$ (FWHM) are given by

$$r = \sqrt{\ln 2}\, \frac{\gamma}{\Delta\nu_D} \tag{2.15}$$

$$\Delta\nu_D = 2 \frac{\nu_0}{c} \sqrt{\ln 2} \sqrt{\frac{2k_B T}{M}}\,. \tag{2.16}$$

Next, we study the propagation of light in dispersive medium. From Maxwell's equations, wave equation for electric field becomes

$$\frac{\partial^2}{\partial z^2} E = \mu_0 \frac{\partial^2}{\partial t^2} (\varepsilon_0 E + P)\,. \tag{2.17}$$

We assume that E varies sinusoidally in both z and t in the form

$$E = E_0 \exp\left\{i(\omega t - Kz)\right\} . \tag{2.18}$$

Substituting eq. (2.18) to eq. (2.17), we get the relation

$$K^2 = \frac{\omega^2}{c^2}(1 + \chi) . \tag{2.19}$$

K is in general complex. It is convenient to introduce an absorption coefficient k and an index of refraction n given by the relation

$$K = \frac{\omega}{c} n - i\frac{k}{2} = \frac{\omega}{c}\left(n - i\frac{ck}{2\omega}\right) \tag{2.20}$$

$$\exp(-iKz) = \exp(-\frac{k}{2}z)\ \exp(-i\frac{\omega}{c}nz) . \tag{2.21}$$

For a gas, the density of atoms is small, so that the second term of eq. (2.19) is small compared with unity. Then we have approximately

$$n - i\frac{c}{\omega}\frac{k}{2} = 1 + \frac{\chi}{2} , \tag{2.22}$$

and if we separate this into real and imaginary parts, we obtain

$$n = 1 + \frac{1}{2}\,\mathrm{Re}\left\{\chi\right\} \tag{2.23}$$

$$k = -\frac{\omega}{c} \mathrm{Im}\{\chi\} = -\frac{2\pi}{\lambda} \mathrm{Im}\{\chi\} \ . \qquad (2.24)$$

Substituting eq. (2.11) into eqs. (2.23) and (2.24), we find

$$n = 1 - \frac{k_0 \lambda}{4\pi} \mathrm{Im}\left\{\phi(z)\right\} \qquad (2.25)$$

$$k = k_0 \, \mathrm{Re}\left\{\phi(z)\right\} \ . \qquad (2.26)$$

## 2.3 Zeeman Effect

In this section, we review the Zeeman effect.[90] We consider an atom which has a quantum number of total angular momentum $\vec{J}$. In a magnetic field, the atom is quantized along the direction of the magnetic field $\vec{H}$ in such a fachion that the projection of the angular momentum $\vec{J}$ on $\vec{H}$ is equal to $M\hbar$, where $M$ takes integral or half of integral values from $M=-J$ to $M=J$. We can write these quantum conditions as

$$\sqrt{J(J+1)} \cos\phi = M, \qquad M = -J, -J+1, \cdots\cdots, J \qquad (2.27)$$

where $\phi$ is the angle formed by two vectors $\vec{J}$ and $\vec{H}$. The vector $\vec{J}$ precesses around $\vec{H}$ with a Larmor angular frequency given by

$$\omega_L = H\, g\, \frac{e}{2mc} , \tag{2.28}$$

where g is the g-factor, c is the velocity of light, and -e is the charge of an electron. Multiplying by the projection of the mechanical angular moment on $\vec{H}$, the energy of this motion becomes

$$W = H\, g\, \frac{e}{2mc} \sqrt{J(J+1)}\, \hbar \cos\phi . \tag{2.29}$$

Substituting eq. (2.27) into eq. (2.29), we find

$$E = M\, g\, H\, \frac{\hbar e}{2mc} . \tag{2.30}$$

Dividing by hc, the energy in wave numbers is given by

$$E(cm^{-1}) = M\, g\, H\, \frac{e}{4\pi mc^2} = M\, g\, L , \tag{2.31}$$

where L is the Lorentz unit given by

$$L = \frac{He}{4\pi mc^2} . \tag{2.32}$$

The selection rules for the transitions between Zeeman substates are given in the following way:

1) When the light propagates perpendicularly to $\vec{H}$,

$M = \pm 1$; linearly polarized perpendicular to $\vec{H}$;

$\sigma_{\pm}$ components

M = 0; linearly polarized parallel to $\vec{H}$;

$\pi$ components,

2) When the light propagates parallel to $\vec{H}$,

$M = \pm 1$; circularly polarized; $\sigma_{\pm}$ components

M = 0; forbidden.

The intensity rules for the Zeeman spectra are given as follows:

1) Transition $J \longrightarrow J$;

$$\begin{aligned} M &\longrightarrow M \pm 1, \quad I = A\,(J \pm M + 1)(J \mp M). \\ M &\longrightarrow M, \quad I = 4\,A\,M^2. \end{aligned} \tag{2.33}$$

2) Transition $J \longrightarrow J+1$;

$$\begin{aligned} M &\longrightarrow M \pm 1, \quad I = B\,(J \pm M + 1)(J \pm M + 2). \\ M &\longrightarrow M, \quad I = 4B\,(J+M+1)(J-M+1). \end{aligned} \tag{2.34}$$

A and B are constants within each Zeeman pattern.

## 2.4 Faraday Rotation and Faraday Filter

We consider, as a simple example, the atoms which have an absorption line from J=0 to J=1. A magnetic field is applied to such atoms, which are filled in a cell as shown in Fig. 2.1(a). The energy levels and spectral strength in the magnetic field are schematically shown in Fig. 2.1(b). When the light passes through the cell along the magnetic field, the absorption coefficients for $\sigma_+$ and $\sigma_-$ lights are given from eq. (2.26) as follows,

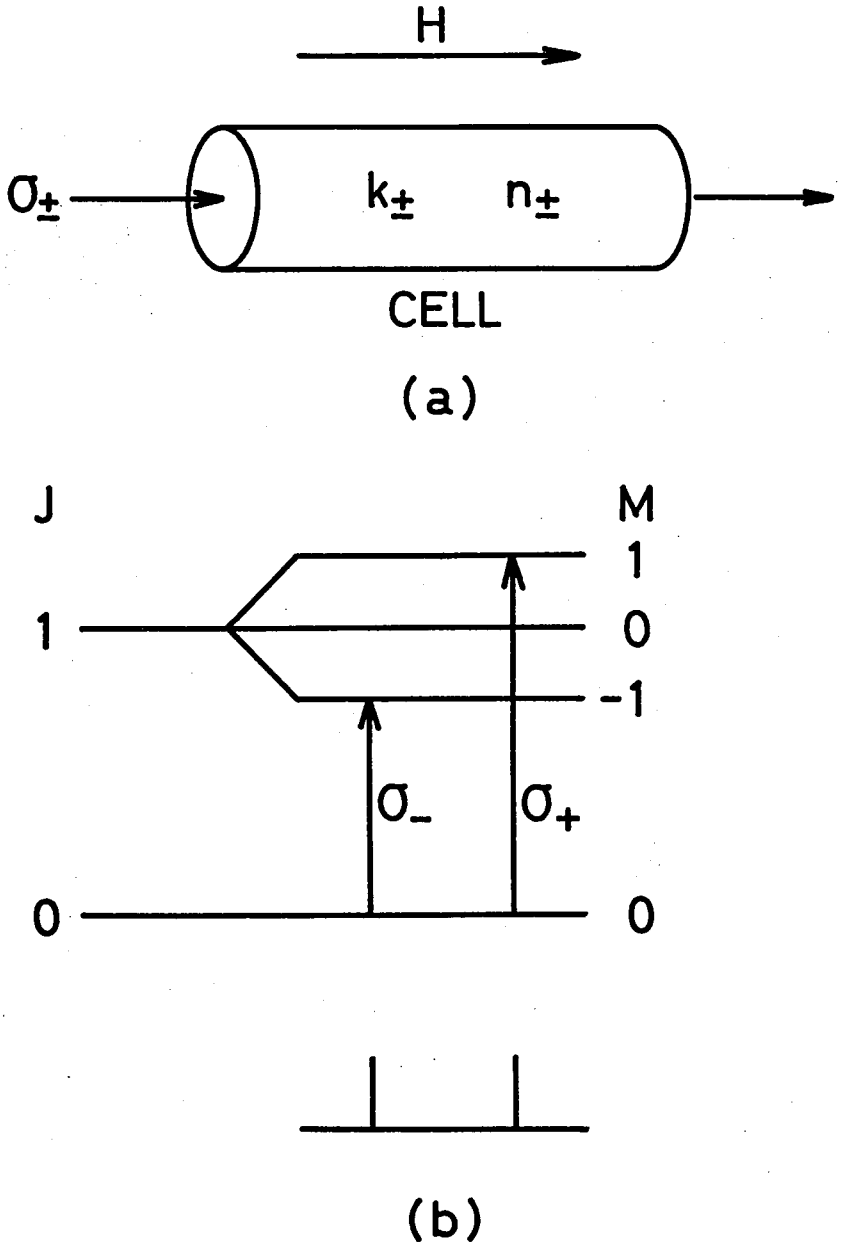


Fig. 2.1 (a) Diagram of apparatus. (b) The resonant two-level system without and with an applied magnetic field H. The corresponding spectra are shown schematically below the level diagram.

$$k_{\pm} = k_0 \, \mathrm{Re}\left\{\phi(z_{\pm})\right\}$$

$$z_{\pm} = (4\pi/\Delta\nu_D)\sqrt{\ln 2}\,(\nu - \nu_0 \mp cL) + ir. \qquad (2.35)$$

The refractive indices are given by

$$n_{\pm} = \left[1 - \frac{k_0\lambda}{4\pi}\,\mathrm{Im}\left\{\phi(z_{\pm})\right\}\right]. \qquad (2.36)$$

The frequency dependence of these quantities in the vicinity of the absorption line is shown in Fig. 2.2(a) and (b).

Now, we consider the case of monochromatic, linearly polarized plane wave. The wave can be divided into two counter rotating waves. These $\sigma_+$ and $\sigma_-$ waves propagate through the cell in the magnetic field with the velocities $c/n_+$ and $c/n_-$, respectively. After passing through the cell of the length $\ell$, the phase difference of two waves is

$$\varphi = \left(\frac{\ell}{c/n_+} - \frac{\ell}{c/n_-}\right)\omega = \frac{2\pi\ell}{\lambda}(n_+ - n_-). \qquad (2.37)$$

The two waves form a linearly polarized wave again at the end of the cell. If we define the rotation angle of the polarization plane as shown in Fig. 2.3, it is given by

$$\theta = \frac{\pi\ell}{\lambda}(n_- - n_+), \qquad (2.38)$$

which is also shown in Fig. 2.2(c). This rotation of the

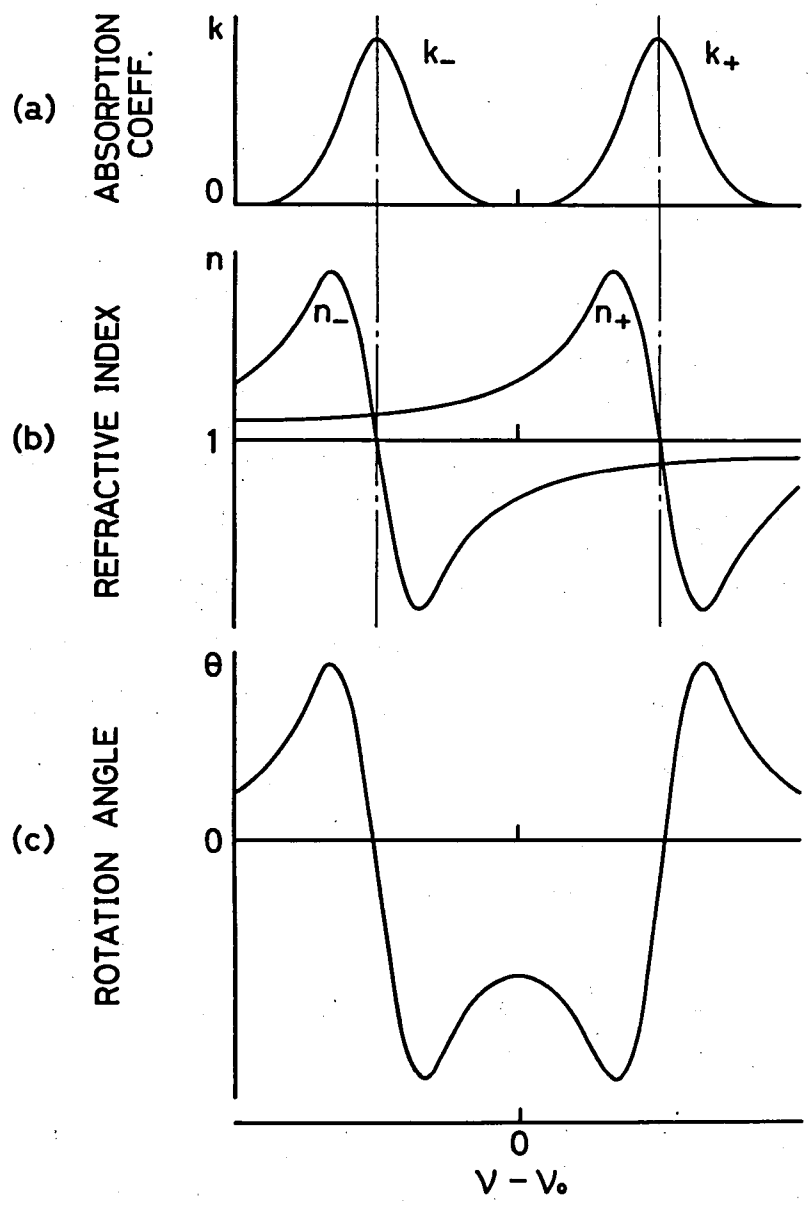


Fig. 2.2 Schematic representation of the resonant Faraday effect. (a) Absorption coefficients $k_{\pm}$ and (b) refractive indices $n_{\pm}$ for $\sigma_{\pm}$ lights. (c) Rotation angle for linearly polarized light.

polarization plane is known as the Faraday effect. On the other hand, the single-pass transmission $\tau_0$ for linearly polarized light is given by

$$\tau_0 = \frac{1}{2}\left\{\exp(-k_+ \ell) + \exp(-k_- \ell)\right\} . \qquad (2.39)$$

It is important that the rotation angle $\theta$ and the transmission $\tau_0$ depend on the frequency $\nu$ of the light in the vicinity of the absorption line and become zero when $\nu$ is far from the line. It should be noted that the rotation angle $\theta$ and the transmission $\tau_0$ are functions of density N and the magnetic field H for a particular medium, because $n_{\pm}$ and $k_{\pm}$ are also the functions of these parameters.

In the next step, we study the Faraday filter. As seen in Fig. 2.3, the Faraday filter consists of the Faraday cell mentioned above and a polarizer positioned at each end of the Faraday cell with the angle of polarization plane $\theta_0$. When monochromatic light enters the Faraday filter from left side, the polarizer on the left side selects one polarization. This linearly polarized light passes through the Faraday cell with the rotation angle of $\theta(\nu)$ due to the Faraday effect. The transmission of the Faraday filter becomes maximum when $\theta(\nu)$ satisfies the relation

$$\theta(\nu) = \theta_0 \qquad (2.40)$$

Therefore, we can select the transmission frequency by two ways.

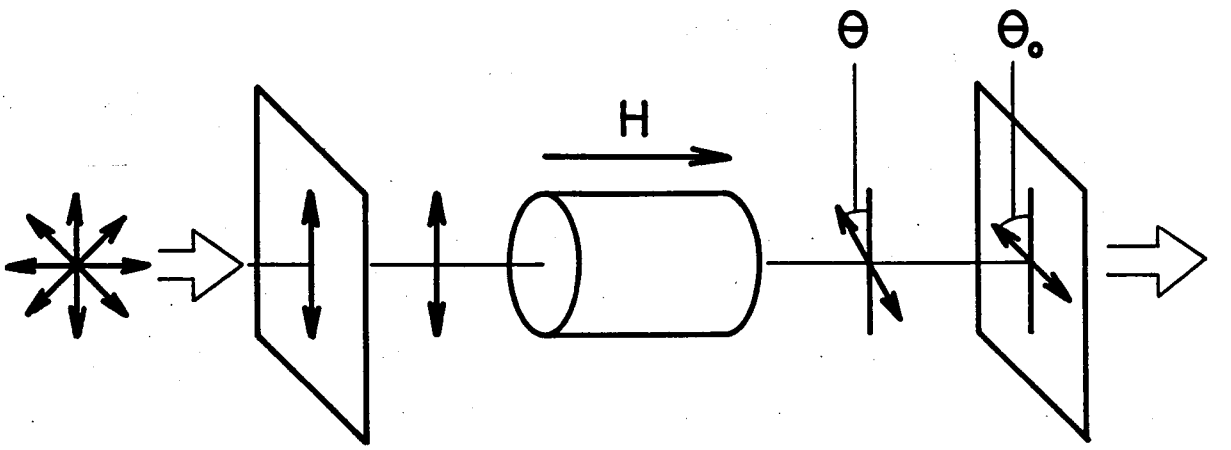


Fig. 2.3 Schematic representation of the Faraday filter.

1) To rotate a polarizer so that $\theta_0$ agrees with $\theta(\nu)$.

2) To select the density N and/or the magnetic field strength so that $\theta(\nu)$ agrees with $\theta_0$.

Now, we apply the Faraday filter as a frequency selective element to a dye laser. As described in 1.3, we can select the oscillation frequency by inserting the Faraday filter in the dye laser cavity as shown in Fig. 2.4. In this case, the polarization direction of the laser light must agrees with itself after a round trip of the cavity. That is,

$$2\theta = n\pi, \qquad n : \text{integer}. \tag{2.41}$$

Therefore, we must take $\theta_0 = \pi/2$. Consequently, when the Faraday filter used as a frequency selective element in a laser cavity, the tuning method 2) should be taken. If we choose the density N and the magnetic field H for a given cell length $\ell$ so that $\theta$ becomes $\pi/2$ and k becomes sufficiently small at the line center, we get the maximum transmission there. By inserting this Faraday filter into the laser cavity, we can achieve the frequency-locking to the line center. In order to know the features of the frequency-locking by the Faraday filter, we must know its transmission as a function of the frequency $\nu$, the density N, and the magnetic field H as

$$\tau = \tau(\nu, N, H). \tag{2.42}$$

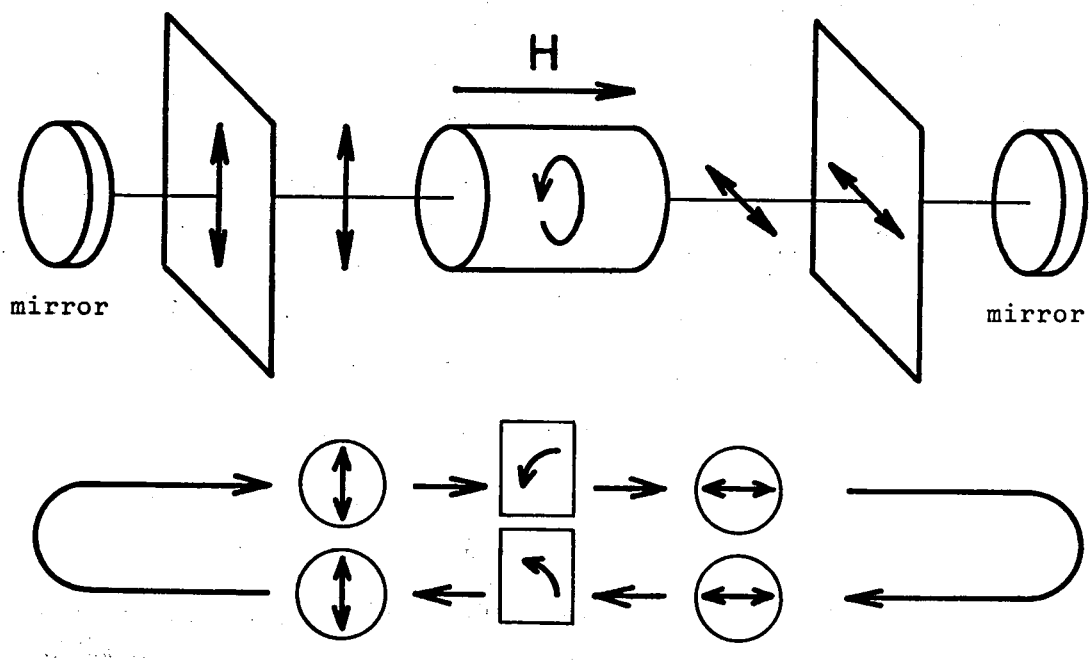


Fig. 2.4 Schematic representation of the laser cavity with the Faraday filter as a frequency selective element.

The transmission $\tau$ is also written as a function of the transmission $\tau_0$ due to light absorption and the rotation angle $\theta$ as

$$\tau(\nu, N, H) = f\left\{\tau_0(\nu, N, H), \theta(\nu, N, H)\right\} . \quad (2.43)$$

In the next section, we will investigate the laser cavity with the Faraday filter to know the function f.

## 2.5 Laser Cavity with a Faraday Filter

In this section, polarization modes and eigenvalues are analyzed for a laser cavity with a Faraday filter. It is shown that a Faraday filter with partial polarizers has higher frequency selectivity than that with perfect ones, when applied to the frequency-locking of a dye laser to atomic absorption lines.

The Faraday filter consists of a cell which includes a magnetoactive medium in an axial magnetic field to get the Faraday rotation, and two polarizers whose polarization directions are set $\pi/2$ apart. By sandwiching the cell between the polarizers, the transmission of the light becomes maximum at the frequency for which the rotation angle is $\pi/2$. From a point of view of the frequency-locking of a dye laser, it is desired that the transmission decreases abruptly as the rotation angle is slightly varied from $\pi/2$. No analysis, however, has yet been given to the laser cavity with a Faraday filter. In this section, we

discuss on the polarization modes and corresponding eigenvalues of this cavity system using a simplified model. As a polarizer, we consider here a perfect polarizer and a partial polarizer such as a Brewster-angle window.

We will consider the optical system shown in Fig. 2.5, where A and B represent the polarizers and $R(\theta)$ represents the optical rotator with no losses. In the following analysis, we assume that the electric fields are in the form of plane waves, and we discuss only on the polarization states of the electric fields ignoring the longitudinal cavity modes. The electric vector can be expressed by two mutually perpendicular components $E_x$ and $E_y$, and it can be represented by a two-component column matrix. In this representation, the actions of the polarizers and the optical rotator can be expressed by two-by-two matrices as

$$A = \begin{pmatrix} 1 & 0 \\ 0 & a \end{pmatrix}, \qquad B = \begin{pmatrix} b & 0 \\ 0 & 1 \end{pmatrix}, \tag{2.44}$$

$$R(\theta) = \begin{pmatrix} \cos\theta & -\sin\theta \\ \sin\theta & \cos\theta \end{pmatrix},$$

where $\theta$ is the single-pass rotation angle, and $a$ and $b$ are are real and positive numbers. In eqs. (2.44), we have assumed that one of the diagonal elements of the matrix A or B is unity,

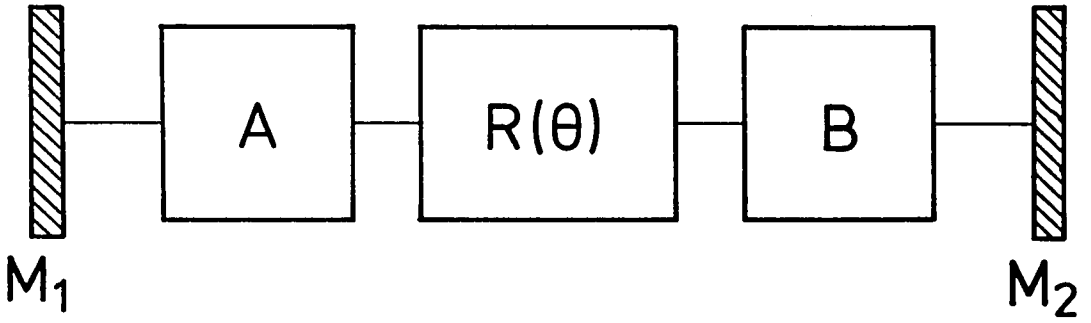


Fig. 2.5 Cavity system to be considered. A and B represent polarizers and R($\theta$) represents an optical rotator. Two mirrors $M_1$ and $M_2$ are assumed to have a perfect reflectance.

but even if it is not so, the results obtained here can be applied as described later.

We are now interested in the modes of polarization of the cavity, i.e. the electric fields having the same polarization after a double-pass through the cavity elements. The modes of polarization and their eigenvalues are determined by solving the following eigenvalue problem,

$$\left\{ B\, R(\theta)\, A\, A\, R(\theta)\, B \right\} E = \Lambda E \,. \tag{2.45}$$

Inserting eqs. (2.44) to eq. (2.45), we have the eigenvalue equation,

$$\Lambda^2 - \frac{1}{2}\left\{ (1+a^2)(1+b^2)\cos 2\theta - (1-a^2)(1-b^2) \right\} \Lambda + a^2 b^2 = 0 \,. \tag{2.46}$$

The quantity $(1- |\Lambda_i|^2)$ represents the cavity loss for the corresponding polarization mode, $\Lambda_i$ being one of the solutions of eq. (2.46). If $\Lambda_i$ is real, the corresponding mode is in the linear polarization state, and if it is complex, the mode is in the elliptical polarization state. In the case that $0<b<a<1$, the moduli of eigenvalues as functions of the rotation angle $\theta$ is shown in Fig. 2.6, together with diagrams illustrating the corresponding polarization states at the mirror $M_2$ in Fig. 2.5. As seen in Fig. 2.6, there exist two linear polarization states in the vicinity of $\theta=0$ or $\pi/2$. For intermediate values of $\theta$, we have two degenerated modes, which are in left-handed and right-handed

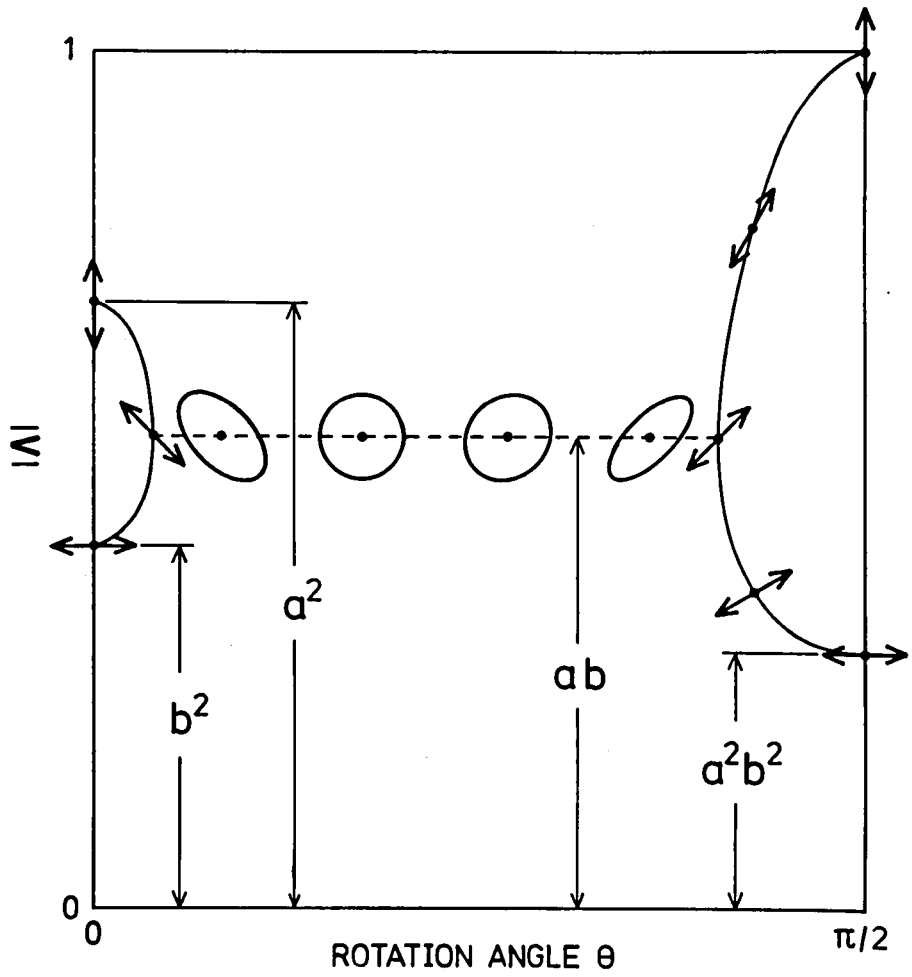


Fig. 2.6 Moduli of eigenvalues as functions of the rotation angle $\theta$ for the case that $0 < b < a < 1$. The solid and dashed lines represent the eigenvalues of linear and elliptical polarization modes respectively. The corresponding polarization states at the mirror $M_2$ are also illustrated.

elliptical polarization states. When the value of a or b decreases, the region of $\theta$ where we have elliptical polarizations becomes small and finally disappears at $a = 0$ or $b = 0$.

As a polarizer in an ordinary optical system, one may use a perfect polarizer or a partial polarizer such as a Brewster-angle window, so that we will consider the following three typical cases:

1) A and B are perfect polarizers; i.e. $a = 0$ and $b = 0$,
2) A is a perfect polarizer and B is a Brewster-angle window; i.e. $a = 0$, $b = 0.84$,
3) A and B are Brewster-angle windows; i.e. $a = 0.84$, $b = 0.84$.

For these three cases, the moduli of eigenvalues as functions of the rotation angle $\theta$ are shown in Fig. 2.7. When $a = 0$ or $b = 0$, one of the eigenvalues is always zero for any values of $\theta$. In the case 2), we see an interesting feature that both of two eigenvalues become zero at a certain value of $\theta$. Among these three cases, the steepest slope of the favored eigenvalue in the vicinity of $\theta = \pi/2$ is obtained in the case 3), so that the frequency selectivity must be largest in this case. Consequently, it can be said that the Faraday filter with partial polarizers is more suitable than that with perfect polarizers for the frequency-locking of a dye laser. It should, however, be noted that the loss of the cavity for the light with a zero rotation angle, i.e. for the light with a frequency far from the absoption line, is not 100 percent in the case of 2) and 3), so that if the gain of the dye laser exceeds this loss, the frequency

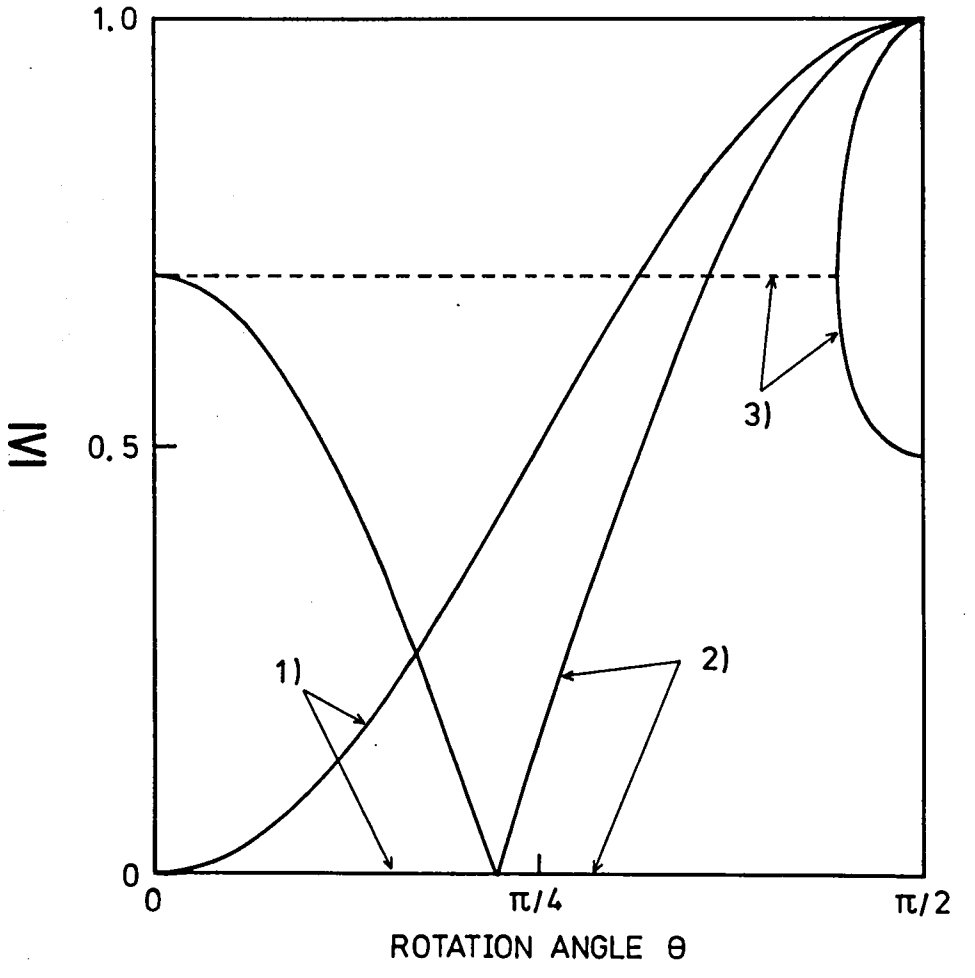


Fig. 2.7 Moduli of eigenvalues as functions of the rotation angle $\theta$ for three cases: 1) A and B are perfect polarizers, 2) A is a perfect polarizer and B is a Brewster-angle window, 3) A and B are Brewster-angle windows.

selectivity may suddenly be destroyed.

In the above analysis, we have treated the simplified cases that the elements $A_{xx}$ and $B_{yy}$ of the matrices A and B are unity and the optical rotator has no losses. For a practical dye laser with a Faraday filter, the cavity system will be more complicated. For example, we have to take account of losses of the polarizers and the anisotropic amplification of the active medium, which depends on the polarization of the pumping light.[100)~102)] In such cases the elements $A_{xx}$ and $B_{yy}$ are not unity, but the results obtained here can be applied only by replacing $\Lambda$ by $\Lambda/A_{xx}^{2}B_{yy}^{2}$, a by $a/A_{xx}$ and b by $b/B_{yy}$. Furthermore the circular dichroism in the Faraday cell must also be important. This effect can easily be introduced by choosing adequate complex numbers as the matrix elements of $R(\theta)$.

In our practical experiment, a Brewster-angle window is employed as a polarizer. As shown in Fig. 3.8, ther are two partial polarizers on the left side of the cell, that is, a cell window and a dye jet stream. Furthermore, polarization dependence of the gain of the dye is determined mainly by the polarization of the argon laser which is in the same direction as the principal axes of above two partial polarizers. Consequently, the polarization selectivity should be very high on the left side of the cell in Fig. 3.8, so we consider a perfect polarizer instead of these partial polarizers. As a result, the cavity system to be considered is the case 2). In this case, the electric field amplitude after one round trip in the cavity is reduced by

a factor of

$$|b^2 \cos^2\theta - \sin^2\theta|. \tag{2.47}$$

Therefore, single-pass transmission due to optical rotation is effectively given by eq. (2.47). The total transmission is given by the product of this and the transmission $\tau_0$ due to light absorption, i.e.,

$$\tau = \tau_0 |b^2 \cos^2\theta - \sin^2\theta| . \tag{2.48}$$

## 2.6 Saturation Effect

So far, we assume that the transmission of the Faraday filter is not varyed by the lasing light. In other words, we assume that the absorption coeffecient and refractive index of the medium are independent of the intensity of the laser light. If this assumption is not proper, the frequency-locking of the dye laser by the Faraday filter becomes very difficult. In order to make this point clear, we investigate the saturation effect on the characteristics of the Faraday filter.

In order to simplify the calculation, we consider the case of a two-level atom which has the upper and lower levels $|a\rangle$ and $|b\rangle$, respectively, as shown in Fig. 2.8. We derive the susceptibility using the density operator.[103] The assumed total

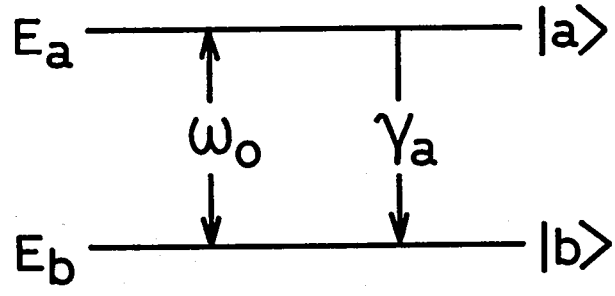


Fig. 2.8 Diagram depicting two energy levels $|a\rangle$ and $|b\rangle$ of the unperturbed Hamiltonian $H_0$. The energies are given by $E_a$ and $E_b$ respectively. The resonance frequency of the transition is $\omega_0$. The decay rates of the population and the coherence are $\gamma_a$ and $\gamma_{ab}$ respectively.

hamiltonian may be written as the sum

$$H = H_0 + V, \tag{2.49}$$

where $H_0$ has following eigenvalues and eigenstates,

$$\begin{aligned} H_0|a\rangle &= E_a\,|a\rangle \\ H_0|b\rangle &= E_b\,|b\rangle\,. \end{aligned} \tag{2.50}$$

The hamiltonian V denotes the interaction between the atom with the electromagnetic field, which is written for electric dipole interaction as

$$V = - \vec{d}\ \vec{E}\ , \tag{2.51}$$

where $\vec{d}$ is the electric dipole operator of an atom, $\vec{E}$ is the electic field vector.

We may next define the density operator as

$$\rho = \rho_{aa} |a\rangle \langle a| + \rho_{ab} |a\rangle \langle b| + \rho_{ba} |b\rangle \langle a| + \rho_{bb} |b\rangle \langle b| \tag{2.52}$$

or in matrix form of

$$\rho = \begin{pmatrix} \rho_{aa} & \rho_{ab} \\ \rho_{ba} & \rho_{bb} \end{pmatrix} \tag{2.53}$$

We may write the equation of motion for $\rho$ as

$$i \hbar \frac{\partial \rho}{\partial t} = \left[ H, \rho \right] + i \hbar \left( \frac{\partial \rho}{\partial t} \right)_{\text{relaxation}} \tag{2.54}$$

In our case the relaxation term is given by

$$\left( \frac{\partial \rho}{\partial t} \right)_{\text{relax.}} = \begin{pmatrix} - \gamma_a \rho_{aa} & - \gamma_{ab} \rho_{ab} \\ - \gamma_{ba} \rho_{ba} & - \gamma_b \rho_{bb} \end{pmatrix}$$

$$= \begin{pmatrix} -\gamma_a \rho_{aa} & -\gamma_{ab} \rho_{ab} \\ -\gamma_{ab} \rho_{ba} & \gamma_a \rho_{bb} \end{pmatrix} , \qquad (2.55)$$

since

$$\gamma_a = -\gamma_b , \qquad \gamma_{ab} = \gamma_{ba} . \qquad (2.56)$$

The rational coefficient $\gamma_a$ represents the relaxation of the atom from the state $|a\rangle$ to the state $|b\rangle$ by the spontaneous emission. The longitudinal relaxation time $T_1$ is given by

$$T_1 = \frac{1}{\gamma_a - \gamma_b} = \frac{1}{2\gamma_a} . \qquad (2.57)$$

The rational coefficient $\gamma_{ab}$ represents the relaxation of the coherence between the states $|a\rangle$ and $|b\rangle$. The transverse relaxation time $T_2$ is given by

$$T_2 = \frac{1}{\gamma_{ab}} . \qquad (2.58)$$

We take circular polarizations to represent the light polarization,

$$\vec{e}_+ = -(1/\sqrt{2})(\vec{e}_1 + i\,\vec{e}_2)$$
$$\qquad (2.59)$$
$$\vec{e}_- = (1/\sqrt{2})(\vec{e}_1 - i\,\vec{e}_2) ,$$

where $\vec{e}_1$ and $\vec{e}_2$ are the mutually perpendicular axes in the plane which is perpendicular to the direction of the propagation of the light. The left circularly polarized light is written as

$$\vec{E} = E_0 \left\{ \vec{e}_- \exp(i\omega t) + \text{c.c.} \right\} . \tag{2.60}$$

The electric dipole moment $\vec{d}$ can be written for the case of $m_a = m_b + 1$ as

$$\vec{d} = \begin{pmatrix} 0 & \vec{e}_- d \\ -\vec{e}_+ d & 0 \end{pmatrix} . \tag{2.61}$$

Therefore, we get as the interaction hamiltonian

$$V = - \vec{d}\,\vec{E} = \begin{pmatrix} 0 & -dE_0 \exp(-i\omega t) \\ -dE_0 \exp(i\omega t) & 0 \end{pmatrix} . \tag{2.62}$$

By substituting eqs. (2.49), (2.50), and (2.62) to eq. (2.54),

$$\dot{\rho}_{aa} = - \gamma_a \rho_{aa} - i\mathcal{E}( \rho_{ab} e^{i\omega t} - \text{c.c.}) \tag{2.63}$$

$$\dot{\rho}_{bb} = \gamma_a \rho_{aa} + i\mathcal{E}( \rho_{ab} e^{i\omega t} - \text{c.c.}) \tag{2.64}$$

$$\dot{\rho}_{ab} = -(i\omega_0 + \gamma_{ab})\rho_{ab} - i\varepsilon e^{-i\omega t}(\rho_{aa} - \rho_{bb}) , \tag{2.65}$$

where

$$\omega_0 = \frac{E_a - E_b}{\hbar} , \qquad \varepsilon = \frac{d E_0}{\hbar} . \tag{2.66}$$

Here, we assume in eq. (2.65)

$$\rho_{ab} = \tilde{\rho}_{ab} e^{-i\omega t} , \tag{2.67}$$

and

$$\dot{\tilde{\rho}}_{ab} = 0 . \tag{2.68}$$

Then we get

$$\tilde{\rho}_{ab} = -i\varepsilon \frac{1}{i\delta + \gamma_{ab}} (\rho_{aa} - \rho_{bb}) , \tag{2.69}$$

where

$$\delta = \omega_0 - \omega . \tag{2.70}$$

By substituting eq. (2.69) to eqs. (2.63) and (2.64),

$$\dot{\rho}_{aa} = -\gamma_a \rho_{aa} - \varepsilon^2 \frac{2\gamma_{ab}}{\gamma_{ab}^2 + \delta^2} (\rho_{aa} - \rho_{bb})$$

$$\dot{\rho}_{bb} = \gamma_a \rho_{aa} + \varepsilon^2 \frac{2\gamma_{ab}}{\gamma_{ab}^2 + \delta^2} (\rho_{aa} - \rho_{bb}) . \tag{2.71}$$

The steady state population inversion becomes

$$\rho_{aa} - \rho_{bb} = -\frac{1}{1 + I\Gamma} , \tag{2.72}$$

where

$$\Gamma = \frac{\gamma_{ab}^2}{\gamma_{ab}^2 + \delta^2} \tag{2.73}$$

and

$$I = \frac{(2\varepsilon)^2}{\gamma_a \gamma_{ab}} \tag{2.74}$$

which is referred to as the saturation parameter.

By substituting eq. (2.72) to eq. (2.69),

$$\tilde{\rho}_{ab} = i\varepsilon \frac{1}{i\delta + \gamma_{ab}} \frac{1}{1 + I\Gamma} . \tag{2.75}$$

The electric dipole moment is given by

$$\langle \vec{d} \rangle = \mathrm{Tr}(\rho \vec{d}) = d(\vec{e}_- \rho_{ba} + \mathrm{c.c.}) . \tag{2.76}$$

Therefore, we find the susceptibility

$$\chi(\omega) = \frac{d}{E_0} \tilde{\rho}_{ba} \quad . \tag{2.77}$$

By substituting eq. (2.75) to eq. (2.77) and use the relation

$$\chi(\omega) = \chi' + i\,\chi'', \tag{2.78}$$

we get

$$\chi' = \frac{d^2}{\hbar} \frac{\omega_0 - \omega}{(\omega - \omega_0)^2 + (I+1)\gamma_{ab}^2} \tag{2.79}$$

$$\chi'' = -\frac{d^2}{\hbar} \frac{1}{\sqrt{I+1}} \frac{\sqrt{I+1}\ \gamma_{ab}}{(\omega - \omega_0)^2 + (I+1)\gamma_{ab}^2} \quad . \tag{2.80}$$

As seen in eqs. (2.79) and (2.80), the line is broadened by the factor of $\sqrt{I+1}$ due to saturation effect. It should be noted that $\chi''$ at $\omega = \omega_0$ is decreased by the ratio of $1/\sqrt{I+1}$ but $\chi'$ is not decreased.

Taking velocity average of eqs. (2.79) and (2.80), and using eqs. (2.25) and (2.26), we obtain

$$n = 1 - \frac{k_0 \lambda}{4\pi} \mathrm{Im}\left\{\phi(z)\right\} \tag{2.81}$$

$$k = \frac{1}{\sqrt{I+1}}\ k_0\ \mathrm{Re}\left\{\phi(z)\right\} \tag{2.82}$$

$$z = ( 4\pi/\Delta\nu_D) \sqrt{\ln 2} \ ( \nu - \nu_0) + i \sqrt{I+1} \ r , \qquad (2.83)$$

where

$$r = \sqrt{\ln 2} \ \frac{2 \gamma_{ab}}{\Delta\nu_D} \qquad (2.84)$$

When the homogeneous line width is much narrower than the Doppler line width, that is $\sqrt{I+1}\ r \ll 1$, the refractive index $n$ is the same as the one for unsaturated case. On the other hand the absorption coefficient $k$ is decreased by the factor of $1/\sqrt{I+1}$. Therefore, the rotation angle for the linearly polarized light is not affected largely by the saturation effect. Consequently, it becomes evident that the feature of the Faraday filter as the frequency selective element in the laser cavity can be calculated by the linear theory.

## 2.7 Conclusions

In this chapter, we have studied on the theory of the Faraday filter. We have reviewed the classical theory of the susceptibility and the Zeeman effect, and obtained the absorption coeffecient and rotation angle for linearly polarized monochromatic plane wave by the resonant Faraday effect.

The laser cavity with a Faraday filter has been studied in

order to obtain the effective transmission of the Faraday filter in the laser cavity. We have found that the Faraday filter with partial polarizers is more suitable than that with perfect polarizers for frequency-locking of a dye laser.

Furthermore, we have studied on the saturation effect on the resonant Faraday effect by the laser light. We have shown that the absorption coefficient is decreased by the factor of $\sqrt{I+1}$, but the deviation of the rotation angle from that in the case of a weak light is very small. That is, we have found that the condition for the frequency-locking can be calculated by the linear theory.

# CHAPTER III

# FREQUENCY-LOCKING TO THE SODIUM D LINES

## 3.1 Introduction

In this chapter, we study on the frequency-locking of a CW dye laser of Rhodamine 6G pumped by an argon ion laser to the center of the sodium D lines by the Faraday filter.[86] Particular attention is given to the condition to get the single-mode oscillations at the center of D lines and the shifts of the oscillation frequency due to variation of the magnetic field strength. Comparison between the experimental results and the theoretical ones is given, and a relatively good agreement has been found.

## 3.2 Transmission of the Faraday Filter

The Faraday filter consists of a sodium cell in an axial magnetic field and two polarizers positioned at both ends of the cell with polarization directions that form right angles to each other. When linearly polarized light passes through the cell in the direction parallel to that of the magnetic field, a rotation

of the polarization plane occurs, which is known as the Faraday effect. The Faraday filter has maximum transmission at the rotation angle $\pi/2$. The transmission of the Faraday filter has large frequency-dependence in the vicinity of the absorption lines of sodium. The frequency with the maximum transmission is given by a sodium vapor density N, a magnetic field strength H, and a length of the cell $\ell$. As shown later, the maximum transmission can be obtained at the center of the D lines by choosing adequate values of these quantities.

Here we will calculate the transmission of the Faraday filter with sodium vapor in the vicinity of the $D_1$ and $D_2$ lines. According to the theoretical analysis in chapter II, the single pass transmission $\tau_0$ and the rotation angle $\theta$ for linearly polarized light are given by

$$\tau_0 = \frac{1}{2}\left\{\exp(-k_+ \ell) + \exp(-k_- \ell)\right\} \tag{3.1}$$

$$\theta = \frac{2\pi\ell}{\lambda}(n_- - n_+), \tag{3.2}$$

with

$$k_\pm = \Sigma \beta_j k_0 \, \mathrm{Re}\left\{\phi(Z_{j\pm})\right\} \tag{3.3}$$

$$n_\pm = \Sigma \beta_j \left[1 - \frac{k_0 \lambda}{4\pi} \, \mathrm{Im}\left\{\phi(Z_{j\pm})\right\}\right] \tag{3.4}$$

$$Z_{j\pm} = \frac{4\pi}{\Delta\nu_D}\sqrt{\ln 2}\left\{\nu - \nu_0 \pm (m_2 g_2 - m_1 g_1)_j cL\right\} + ir, \tag{3.5}$$

where $\beta_j$ is the relative transition strength of the j-th Zeeman component which is normalized so that $\Sigma\beta_j=1$. It should be noted that $\tau_0$ and $\theta$ are functions of the temperature T and the magnetic field strength H, because, for sodium, the density N is a function of the temperature and is given by the relation[104]

$$\log_{10} N = 23.715 - 5257.7/T \ . \qquad (3.6)$$

Next, we will calculate the spectra in the magnetic field in order to get the transmission of the Faraday filter. Since sodium has a nuclear spin of 3/2, we must take account of hyperfine structure to calculate the spectra. The total mechanical moment $\vec{J}$ is coupled with the quantum vector $\vec{I}$, representing the total mechanical moment of the nucleus $\vec{I}\hbar$ to form a resultant $\vec{F}$, where $|\vec{J}|=\sqrt{J(J+1)}$, $|\vec{I}|=\sqrt{I(I+1)}$ and $|\vec{F}|=\sqrt{F(F+1)}$. The model is shown in Fig. 3.1. The resultant $\vec{F}$ is the total mechanical moment of the atom. F takes values differing from each other by unity from the value I-J to I+J when $I \geqq J$, and from J-I to J+I when $J \geqq I$. The interaction energy between the nuclear moment $\vec{I}$ and electron moment $\vec{J}$ is given by

$$\varepsilon_F = A\,\vec{I}\,\vec{J}\cos(\vec{I}\,\vec{J}), \qquad (3.6)$$

where A is a measure of the strength of coupling. The cosine term is evaluated by use of Fig. 3.1. Then we find

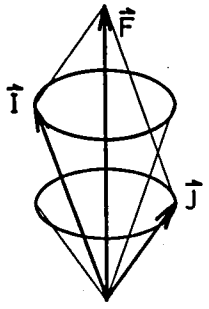


Fig. 3.1 Vector model illustrating the coupling of a nuclear moment $\vec{I}$ with an electron moment $\vec{J}$ to form a resultant $\vec{F}$.

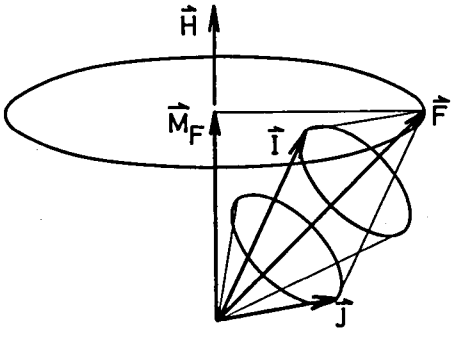


Fig. 3.2 Vector model of an atom with a nuclear spin in a very weak magnetic field.

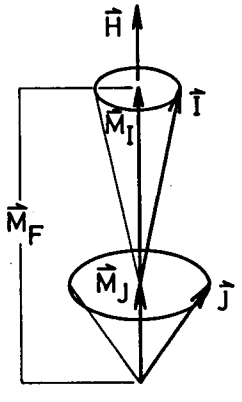


Fig. 3.3 Vector model of an atom with a nuclear spin in a strong magnetic field.

$$\varepsilon_F = \frac{1}{2} A \left( |\vec{F}|^2 - |\vec{I}|^2 - |\vec{J}|^2 \right). \qquad (3.7)$$

In a very weak magnetic field the atom precesses around the field direction $\vec{H}$ subject to the quantum conditions that the projection of the mechanical resultant $\vec{F}\hbar$ on $\vec{H}$ is equal to $M_F\hbar$. The magnetic quantum number $M_F$ takes values differing from each other by unity from $-F$ to $F$. A classical vector model for very weak field is shown in Fig. 3.2. The energies of this precession in wave numbers can be calculated in the similar way to the precession of $\vec{J}$ around $\vec{H}$. We find

$$-E_F = g_F M_F L \ , \qquad (3.8)$$

where a constant $g_F$ is given by

$$g_F = g_J \frac{|\vec{F}|^2 + |\vec{J}|^2 - |\vec{I}|^2}{2|\vec{F}|^2} \ , \qquad g_J = 1 + \frac{|\vec{J}|^2 + |\vec{S}|^2 - |\vec{L}|^2}{2|\vec{J}|^2} . \qquad (3.9)$$

In a strong magnetic field, the coupling between the nuclear moment $\vec{I}$ and the electron resultant $\vec{J}$ is broken down, and each precesses independently around $\vec{H}$. $\vec{I}$ and $\vec{J}$ are quantized separately with the field direction. A classical vector model for strong field is shown in Fig. 3.3. The energy due to the interaction between $\vec{I}$ and $\vec{H}$, and $\vec{J}$ and $\vec{H}$ are given, respectively

$$-E_I = -g_I M_I L \ , \qquad -E_J = g_J M_J L \ . \qquad (3.10)$$

The energy due to the interaction between $\tilde{I}$ and $\tilde{J}$ is

$$\mathcal{E} = A\,\tilde{I}\,\tilde{J}\,\cos(\tilde{I}\,\tilde{J}) \ . \tag{3.11}$$

Referring to Fig. 3.3, the averaged cosine is given by

$$\overline{\cos(\tilde{I}\,\tilde{J})} = \cos(\tilde{I}\,\tilde{H})\cos(\tilde{J}\,\tilde{H}) = M_I M_J \ . \tag{3.12}$$

Substituting this to eq. (3.11),

$$\mathcal{E} = A\,M_I M_J \ . \tag{3.13}$$

Finally, we get the total energy

$$E = -g_I M_I L + g_J M_J L + A\,M_I M_J \ . \tag{3.14}$$

We can neglect the first term since $g_I$ is so small compared with $g_J$. Then we get

$$E = g_J M_J L + A\,M_I M_J \ . \tag{3.15}$$

Let us now apply eqs. (3.8) and (3.15) to the D lines of sodium. The wavelength of the $D_1$ line ($^2S_{1/2}$-$^2P_{1/2}$) and $D_2$ line ($^2S_{1/2}$-$^2P_{3/2}$) are 589.6 nm and 589.0 nm, respectively. The energies in a very weak or strong magnetic field can be calculated by tabulating the factors mentioned above as seen in

Tables 3.1 and 3.2. The resultant energy levels are schematically shown in Fig. 3.4.

As shown later, the magnetic field for the frequency-locking by the Faraday filter is strong enough to break down the coupling[105] between $\vec{I}$ and $\vec{J}$. Selection rules for hyperfine transitions are

$$\Delta M_I = 0 ,$$

$$\Delta M_J = \begin{cases} 0 & \text{for } \pi \text{ component} \\ \pm 1 & \text{for } \sigma \text{ component.} \end{cases}$$

The spectral strengths are similar to eqs. (2.33) and (2.34). Allowed transitions and their relative transition strength are schematically shown in Fig. 3.5. The frequency separation between the hyperfine components calculated from the one without field[39] using Tables 3.1 and 3.2 are also shown in Fig. 3.5.

In order to calculate the absorption and rotation angle profiles of the Faraday cell, we must sum over all hyperfine components as well as Zeeman components performed in eqs. (3.3) and (3.4). Fig. 3.6(a) and (b) show the calculated coefficient $k$ and the rotation angle $\theta$ for the $D_1$ line in the case that the cell temperature $T$ is 441 K and the magnetic field strength $H$ is 2.7 kG. As described in 2.5, the total transmission is given by the product of the transmission due to optical rotation and the transmission $\tau_0$ due to light absorption, i.e.,

Table 3.1 Magnetic-Energy Factors for the Terms $^2S_{1/2}$ and $^2P_{1/2}$

| NO FIELD | | VERY WEAK FIELD (hfs ZEEMAN EFFECT) | | | STRONG FIELD (BACK-GOUDSMIT EFFECT) | | | | | |
|---|---|---|---|---|---|---|---|---|---|---|
| TERM | $\varepsilon_F$ | $M_F$ | $g_F$ | $g_F M_F$ | $M_I$ | $M_J$ | $g_J$ | $g_J M_J$ | $AM_I M_J$ | $M_F$ |
| $^2_2P_{1/2}$ | 3/4A | 2 | 1/12 | 1/6 | 3/2 | 1/2 | 2/3 | 1/3 | 3/4A | 2 |
| | | 1 | | 1/12 | 3/2 | -1/2 | | -1/3 | -3/4A | 1 |
| | | 0 | | 0 | 1/2 | 1/2 | | 1/3 | 1/4A | 1 |
| | | -1 | | -1/12 | 1/2 | -1/2 | | -1/3 | -1/4A | 0 |
| | | -2 | | 1/6 | -1/2 | 1/2 | | 1/3 | -1/4A | 0 |
| $^2_1P_{1/2}$ | -5/4A | 1 | -1/6 | -1/6 | -1/2 | -1/2 | | -1/3 | 1/4A | -1 |
| | | 0 | | 0 | -3/2 | 1/2 | | 1/3 | -3/4A | -1 |
| | | -1 | | 1/6 | -3/2 | -1/2 | | -1/3 | 3/4A | -2 |
| $^2_2S_{1/2}$ | 3/4A | 2 | 1/4 | 1/2 | 3/2 | 1/2 | 2 | 1 | 3/4A | 2 |
| | | 1 | | 1/4 | 3/2 | -1/2 | | -1 | -3/4A | 1 |
| | | 0 | | 0 | 1/2 | 1/2 | | 1 | 1/4A | 1 |
| | | -1 | | -1/4 | 1/2 | -1/2 | | -1 | -1/4A | 0 |
| | | -2 | | -1/2 | -1/2 | 1/2 | | 1 | -1/4A | 0 |
| $^2_1S_{1/2}$ | -5/4A | 1 | -1/2 | -1/2 | -1/2 | -1/2 | | -1 | 1/4A | -1 |
| | | 0 | | 0 | -3/2 | 1/2 | | 1 | -3/4A | -1 |
| | | -1 | | 1/2 | -3/2 | -1/2 | | -1 | 3/4A | -2 |

Table 3.2 Magnetic-Energy Factors for the Term $^2P_{3/2}$

| NO FIELD | | VERY WEAK FIELD (hfs ZEEMAN EFFECT) | | | STRONG FIELD (BACK-GOUDSMIT EFFECT) | | | | | |
|---|---|---|---|---|---|---|---|---|---|---|
| TERM | $\varepsilon_F$ | $M_F$ | $g_F$ | $g_F M_F$ | $M_I$ | $M_J$ | $g_J$ | $g_J M_J$ | $AM_I M_J$ | $M_F$ |
| $^2_3P_{3/2}$ | 9/4A | 3 | 2/3 | 6/3 | 3/2 | 3/2 | 4/3 | 6/3 | 9/4A | 3 |
| | | 2 | | 4/3 | 1/2 | 3/2 | | 6/3 | 3/4A | 2 |
| | | 1 | | 2/3 | -1/2 | 3/2 | | 6/3 | -3/4A | 1 |
| | | 0 | | 0 | -3/2 | 3/2 | | 6/3 | -9/4A | 0 |
| | | -1 | | -2/3 | 3/2 | 1/2 | | 2/3 | 3/4A | 2 |
| | | -2 | | -4/3 | 1/2 | 1/2 | | 2/3 | 1/4A | 1 |
| | | -3 | | -6/3 | -1/2 | 1/2 | | 2/3 | -1/4A | 0 |
| $^2_2P_{3/2}$ | -3/4A | 2 | 2/3 | 4/3 | -2/3 | 1/2 | | 2/3 | -3/4A | -1 |
| | | 1 | | 2/3 | 3/2 | -1/2 | | -2/3 | -3/4A | 1 |
| | | 0 | | 0 | 1/2 | -1/2 | | -2/3 | -1/4A | 0 |
| | | -1 | | -2/3 | -1/2 | -1/2 | | -2/3 | 1/4A | -1 |
| | | -2 | | -4/3 | -3/2 | -1/2 | | -2/3 | 3/4A | -2 |
| $^2_1P_{3/2}$ | -11/4A | 1 | 2/3 | 2/3 | 3/2 | -3/2 | | -6/3 | -9/4A | 0 |
| | | 0 | | 0 | 1/2 | -3/2 | | -6/3 | -3/4A | -1 |
| | | -1 | | -2/3 | -1/2 | -3/2 | | -6/3 | 3/4A | -2 |
| $^2_0P_{3/2}$ | -15/4A | 0 | 0 | 0 | -3/2 | -3/2 | | -6/3 | 9/4A | -3 |

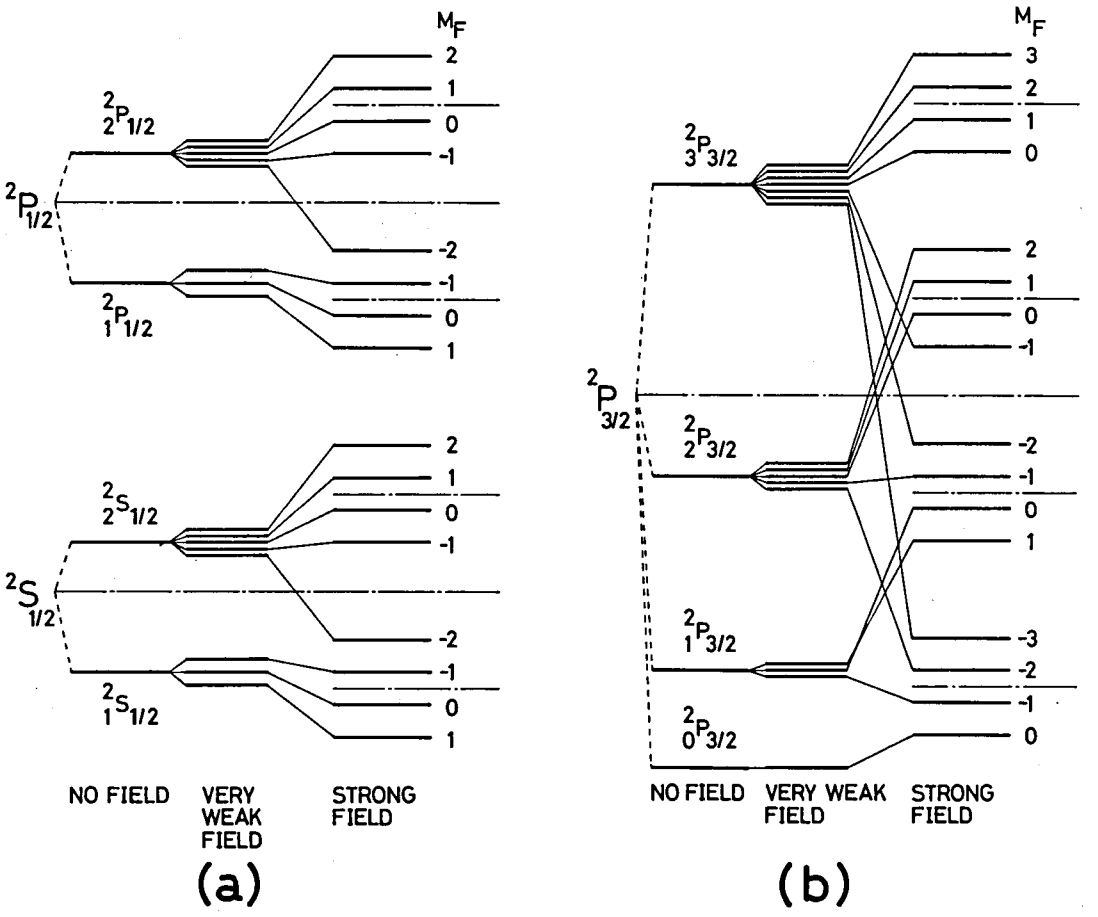


Fig. 3.4 Energy level diagrams in a very weak and strong magnetic field, (a) for the $^2S_{1/2}$ and $^2P_{1/2}$ states and (b) for the $^2P_{3/2}$ states.

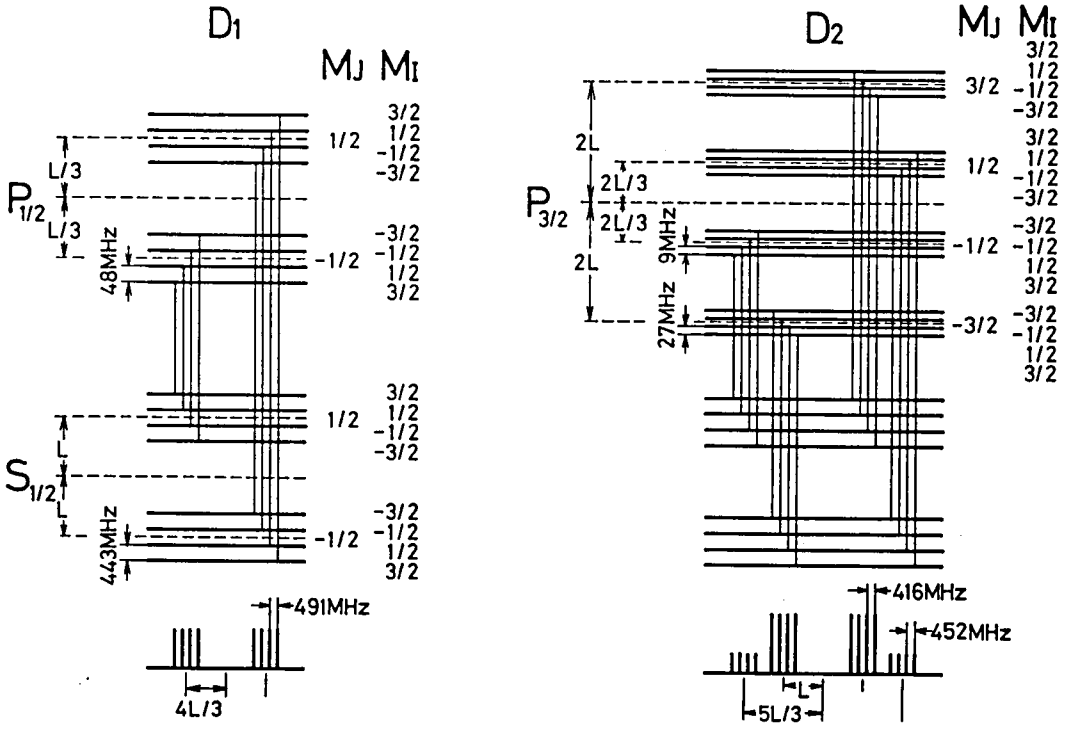


Fig. 3.5 Energy level diagrams for the sodium $D_1$ and $D_2$ lines in a strong magnetic field and allowed $\sigma_+$ and $\sigma_-$ transition components. The corresponding spectra and their relative intensities are also shown in the bottom, where L represents the Lorentz unit.

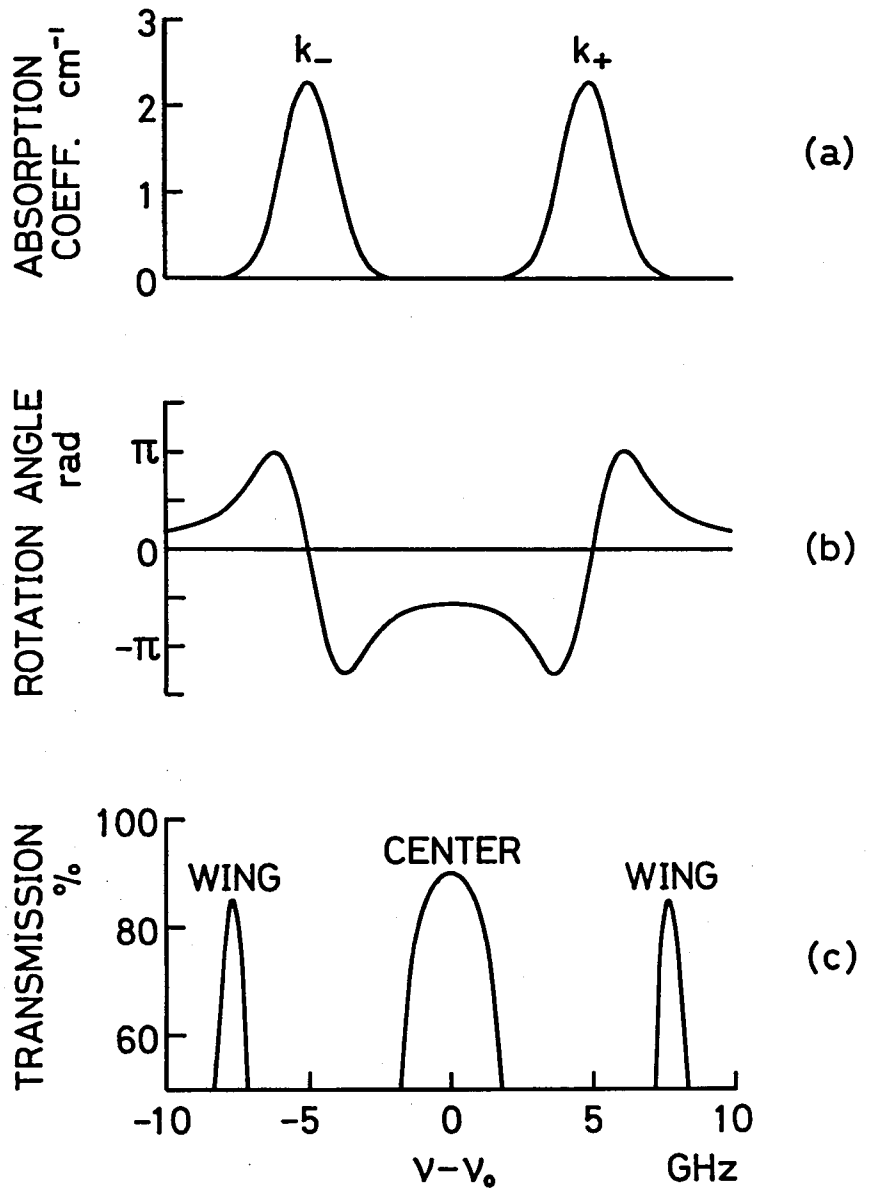


Fig. 3.6 (a) Absorption coefficients of the Faraday filter for $\sigma_+$ and $\sigma_-$ light in the case of the temperature T=441 K and the magnetic field strength H=2.7 kG. (b) Single-pass rotation angle for linearly polarized light. (c) Transmission of the Faraday filter inserted in the laser cavity.

$$\tau = \tau_0 \left| b^2 \cos^2\theta - \sin^2\theta \right| , \qquad (3.16)$$

where b is the transmission of the Brewster-angle window for the electric field perpendicular to the principal axis. In our case b=0.84. The values of $\tau$ for the $D_1$ line in the same case as in Fig. 3.6(a) and (b) are shown in Fig. 3.6(c). As shown in Fig. 3.6(c), the transmission curve generally has three peaks; one is in the center region, and the others are positioned on the wings symmetrically. It should be noted that the "line center" used in this chapter means the geometrical center of $\sigma_+$ and $\sigma_-$ absorption lines. When the Faraday filter is inserted in the dye laser cavity, the oscillation takes place in the frequency region where the single-pass gain of the dye exceeds the cavity loss given by $1-\tau$. The transmission $\tau$ varies with the sodium temperature and the magnetic field strength, as seen in the above argument. The condition of the cell temperature and the magnetic field strength for which the transmission $\tau$ is larger than 0.9 is calculated by using all of the above equations, and the results are shown in Fig. 3.7.

As seen in a later section, the transmission has a single peak in the center region in a weak magnetic field. When increasing the magnetic field strength H, the peak value grows, and at a certain value of H, the single peak splits into two peaks (see Fig.3.12). The separation of two peaks increases monotonically with the increase of H. The single-mode and the two-mode oscillation may take place when the transmission curve

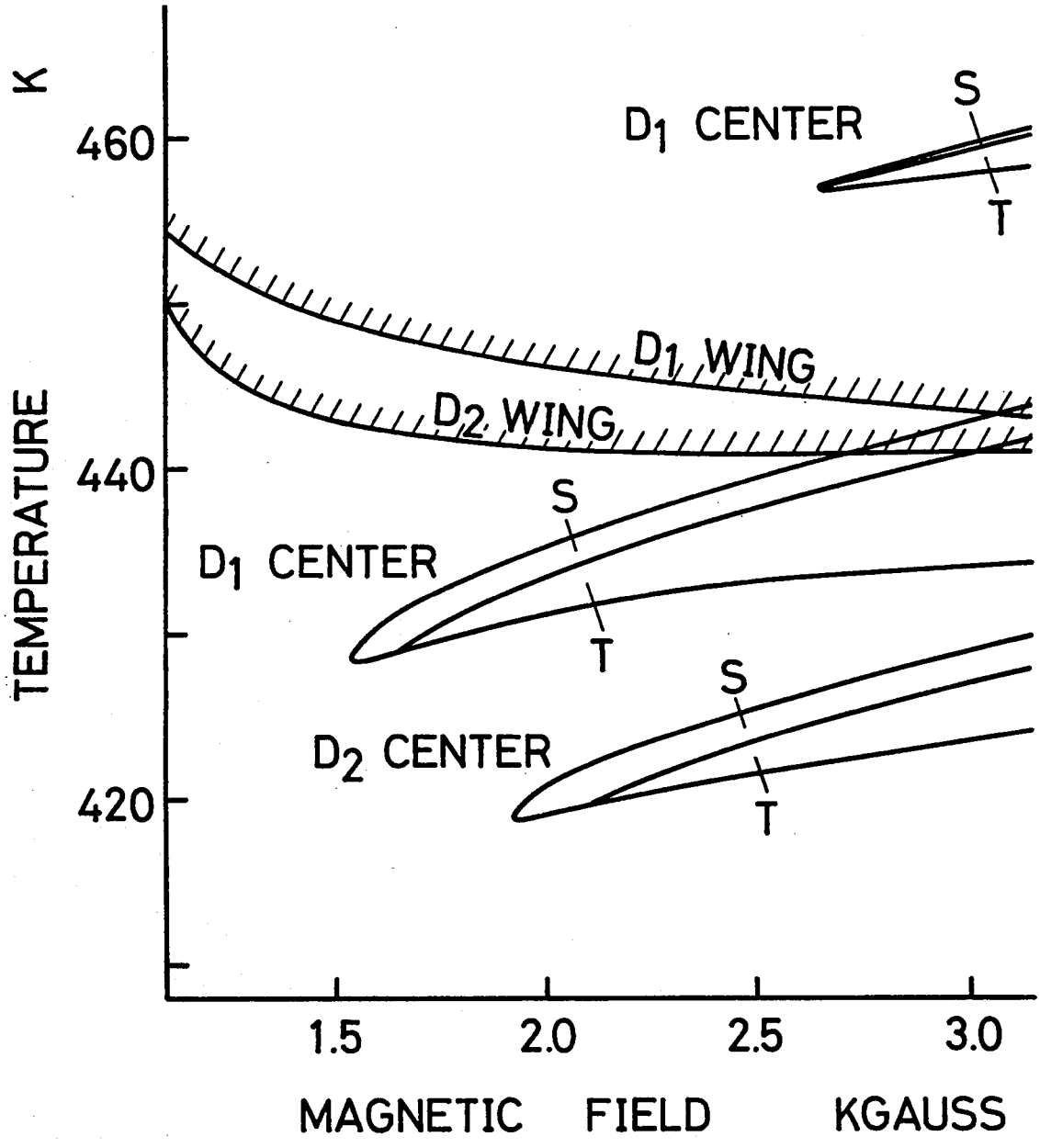


Fig. 3.7 Theoretical values of the temperature T and the magnetic field strength H for transmission larger than 0.9. S and T represent the regions where the single-mode and two-mode oscillations are expected to take place, respectively.

has single peak and two peaks, respectively. In Fig. 3.7, the regions where the single-mode and two-mode oscillation may take place are denoted by S and T, respectively. As seen in Fig. 3.7, oscillations may take place in the center regions of the $D_1$ line and $D_2$ line at temperatures below 440 K, but they do not occur simultaneously at the same value of the magnetic field strength for a given temperature. At temperatures above 440 K, oscillations may take place on the wings. The oscillation in the center region of the $D_1$ line at temperatures about 460 K comes from increasing the transmission due to the rotation angle of $3\pi/2$ instead of $\pi/2$.

## 3.3 Experimental Setup

The experimental setup is schematically shown in Fig. 3.8. The Faraday filter is inserted into the dye laser cavity with three mirrors,[106] where the Rhodamine 6G in the form of a jet stream[12),107),108)] is pumped by an argon laser of 2 W in total power. The Brewster angle window at the left side of the cell is oriented so that its principal axis agrees with that of the dye jet stream, i.e., with the polarization direction of the argon laser beam.

The Faraday filter consists of a sodium cell, polarizing elements, and a magnetic coil. We used a heat-pipe oven[109)~111)] shown in Fig. 3.9 as a sodium cell. The stainless-steel tube which is corrosion resistant to sodium has an inner diameter of 15 mm, a

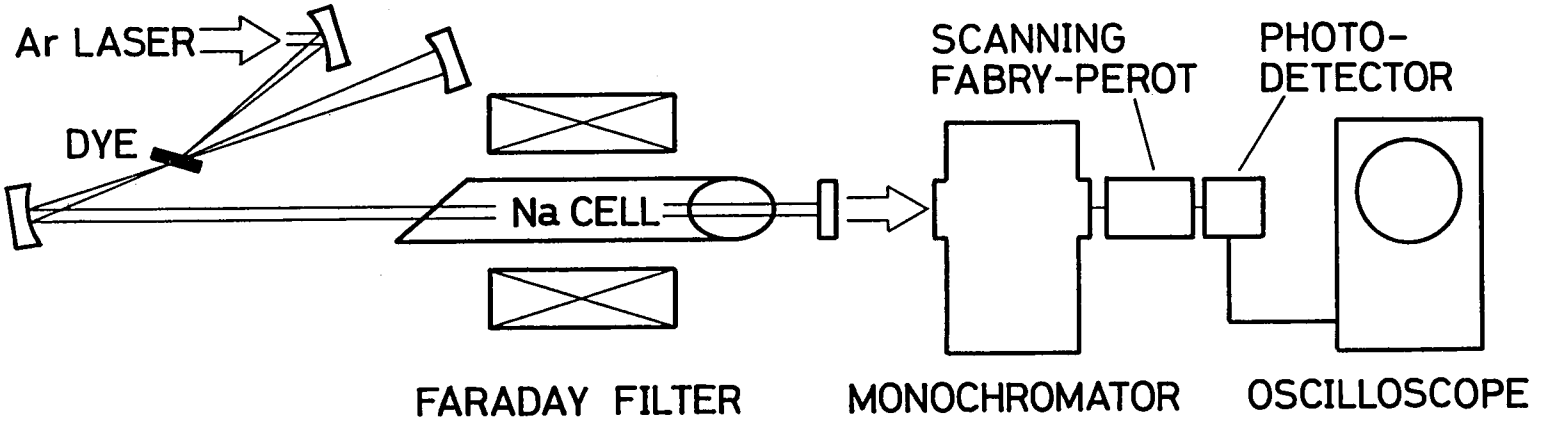


Fig. 3.8 Schematic diagram of the experimental setup.

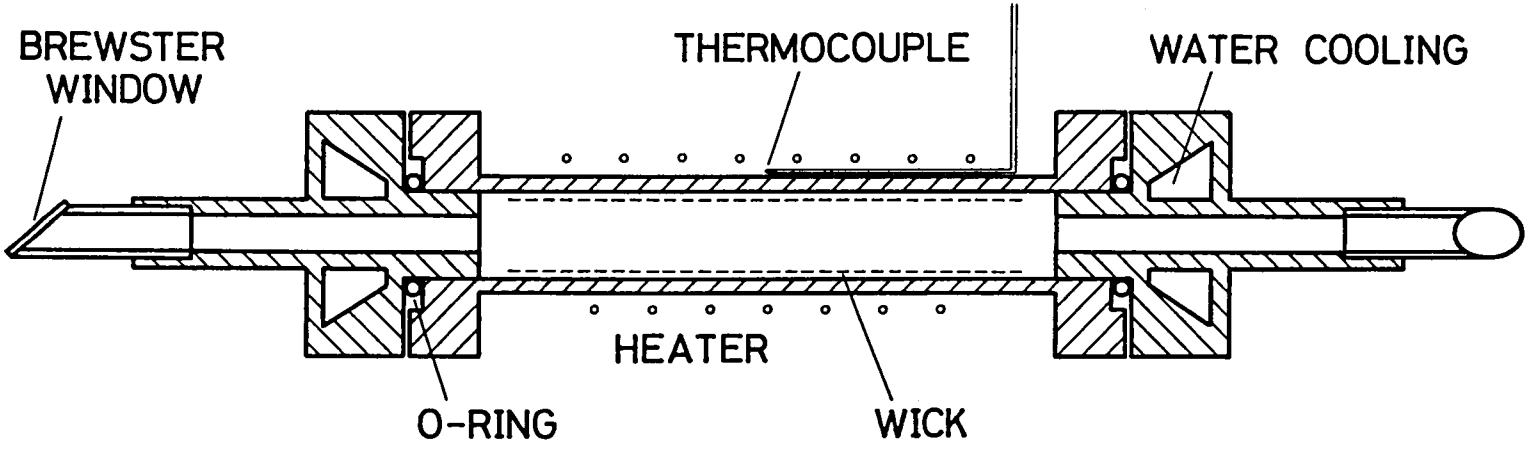


Fig. 3.9 Schematic arrangement of the heat-pipe oven.

length of 10 cm and a wall thickness of 2.5 mm. The inner wall of the tube is covered by two layers of 100-mesh #304 stainless steel as a wick. Heater coil is wrapped bipolarly around the tube with asbestos insulation. Both ends are closed by demountable units which holds brewstar-angle windows. The units are cooled by the water. The pipe is, first of all, filled with an inert gas at a suitable pressure. Heating up the central portion of the tube, a pit of sodium set on the wick melts down. The stainless-steel wick is saturated with a wetting liquid sodium. During operation the liquid evaporates at central portion due to the heat source. Since the both ends are cooled, the vapor is driven down the tube and condenses again there. The condensate is then returned by the capillary forces through the wick to the central portion. The heat-pipe oven has following properties; 1) the heat-pipe oven generates homogeneous vapors of well-defined temperature, pressure, and optical path length; 2) the vapor is confined by inert gas boundaries which prevent the sodium vapor from contacting the windows and spoiling them.

In order to load the sodium to the heat-pipe, a piece of sodium kept in the oil was taken out and washed with cyclohexane dehydrated by calcium to remove the oil, then six faces were cut away. The size of the sodium piece was about $5 \times 5 \times 20$ mm$^3$. It was then loaded to the heat-pipe cleaned by aceton. The heat pipe was evacuated and filled with helium. Complete removing of the oil from sodium surface and speedy treatment to avoid the

chemical reaction between sodium and water included in air were important points to get good heat-pipe oven. Before operation, melting of sodium was achieved by rapid heating by a gas burner, since the slow heating by the heater wrapped around the tube cannot break the layer of impurities on the sodium surface and melt down the sodium and wet the wick. After this, the buffer gas which might contain some impurities was pumped out and clean buffer gas was filled again. The pressure of helium gas was 10 torr. The oven temperature was monitored by a chromel-almel thermocouple inserted between the stainless pipe and the asbestos, and controlled automatically.

The Brewster-angle windows play roles of the polarizers. It has been pointed out in 2.5 that the Faraday filter with Brewster-angle windows has higher frequency-selectivity than that with perfect polarizers such as glan prisms.

The magnetic coil was designed to get uniform magnetic field along the optical-path up to 3 kG. It had an inner diameter of 55 mm, an outer diameter of 193 mm, a length of 216 mm and consisted of 3126 turns of 2 mm formal coated alminium wire. The solenoid was indirectly cooled by the water through the insulation oil.

The end mirror and the collimating mirror had 5-cm radius of curvature, and the output mirror with the reflectivity of 96 percent was flat. The total cavity length was 1 m, which resulted in the separation of longitudinal modes of 150 MHz.

The broadening of the sodium D lines by the collisions with

helium atoms is considered to be about 100 MHz.[112)]

The laser output was analyzed by a grating monochromator and a scanning Fabry-Perot interferometer. The focal length of the grating monochromator was 25 cm and grating constant was 1200/mm. The free spectral range and the finesse of the Fabry-Perot interferometer were 8 GHz and 200, respectively. The scanning was done with the frequency of about 50 Hz and over four free spectral range by applying the sawtooth voltage with a peak value of 150 V.

## 3.4 Experimental Results and Discussions

Using the setup described in 3.3, we made the experiments in order to determine whether or not the oscillations at the center of the D lines were possible just as predicted by the theory, and to determine experimentally the conditions for oscillations in the center regions and on the wings of the D lines. The parameters varied in the experiments were the magnetic field strength H and the temperature T of the heat-pipe oven, which could be varied from 0 to 3 kG and from the room temperature to 550 K, respectively The temperature was measured at the outside of the heat-pipe oven, so that the temperature determining the saturated vapor pressure was considered to be several tens of degrees lower than the measured one.

We have swept the magnetic field strength H, while increasing the temperature T of the heat-pipe oven as a parameter. At

about T=480 K we could get the oscillation at the $D_2$ line. Fig. 3.10(b) shows the oscillation modes observed with a scanning Fabry-Perot interferometer at T=482 K for various values of H. As seen in Fig. 3.10(b), the single-mode oscillation took place at H=2.36 kG. Upon increasing H, the mode split into two modes and the separation of the split modes increased while their intensity decreased. At about T=490 K, we could get the oscillations at the $D_1$ line, whose spectrum changed in the same manner as in the above case of the $D_2$ line (See Fig. 3.10(a)). The simultaneous oscillations at the $D_1$ and $D_2$ lines could not be observed at these temperatures.

At temperatures higher than 500 and 505 K, we could get the oscillations at the $D_2$ and $D_1$ lines, respectively. These oscillations, which were always on two longitudinal modes, took place simultaneously for higher temperatures. The intensity of these oscillations increased with the increase of H, while the two modes at both of the $D_1$ and $D_2$ lines shifted a relatively large amount toward opposite directions (See Fig. 3.11). It must be noted that even when the two modes seem to overlap each other in Fig. 3.11, the mode separation generally has the ambiguity of integral multiple of the free spectral range of the scanning Fabry-Perot interferometer, 8 GHz in the present case.

In order to know whether these oscillations took place in the center region or on the wings of the resonance line, we calculated the transmission $\tau$ of the Faraday filter in the center regions and on the wings of the $D_1$ and $D_2$ lines as functions of the

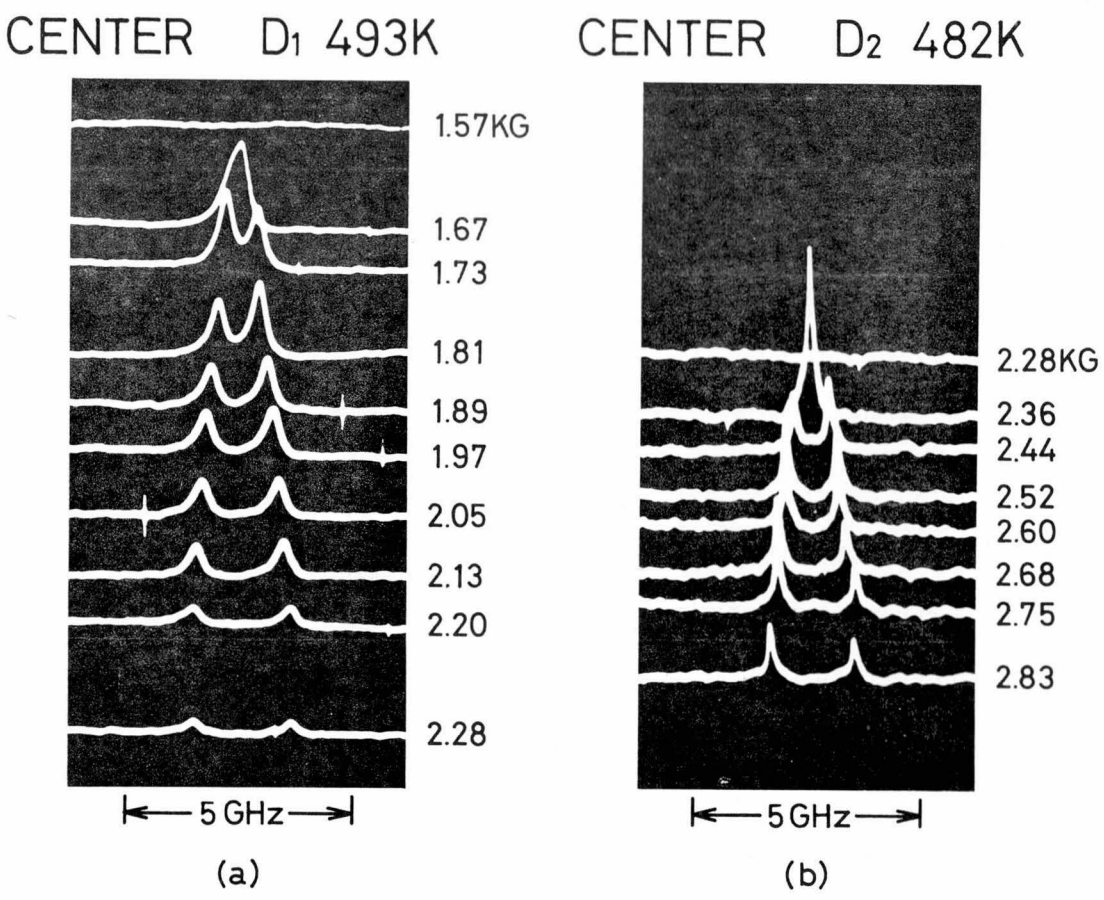


Fig. 3.10 Output spectra of the CW dye laser in the center regions of the $D_1$ and $D_2$ lines, as displayed by a scanning Fabry-Perot interferometer.

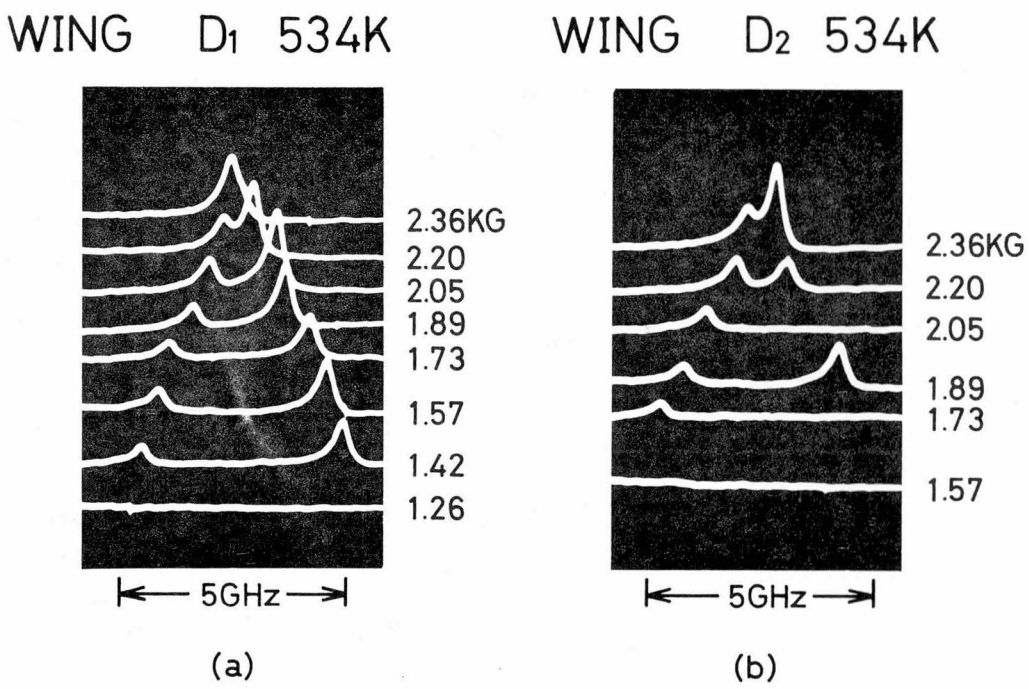


Fig. 3.11 Output spectra of the CW dye laser on the wings of the $D_1$ and $D_2$ lines, as displayed by a scanning Fabry-Perot interferometer.

magnetic field strength H for particular temperatures. As seen in Fig. 3.12, the transmission curve has single peak just at the center of the resonance lines at weak magnetic field strength and the peak value increases with the increase of H. When H is further increased, the peak splits into two peaks and the frequency separation between them increases, while the peak values decrease. On the other hand, as seen in Fig. 3.13, the transmission curve has two peaks on the wings of the lines, and the frequency separation between these two peaks and their intensity increase as the magnetic field is increased. Therefore, we can ascertain that the oscillations observed at low temperatures (shown in Fig. 3.10) take place in the center regions of the $D_1$ and $D_2$ lines. The oscillations at higher temperatures (shown in Fig. 3.11) must take place on the wings of the lines, and at the magnetic field strength where two modes seem to cross in Fig. 3.11, the mode separation should be 24 GHz. Furthermore, when we applied the laser output at low temperatures to a sodium cell outside of the cavity, we could observe the resonance fluorescence, while we could not observe it in the case of higher temperatures. This experimental result supports the above discussion.

It should be noted that the oscillation conditions for the cell temperature and the magnetic field strength, which we could obtain in this way, agreed well with theoretical one shown in Fig. 3.7, except for the fact that the temperature measured is 55-60 K higher than the calculated value. This descrepancy is caused by the error in temperature measurement as mentioned above.

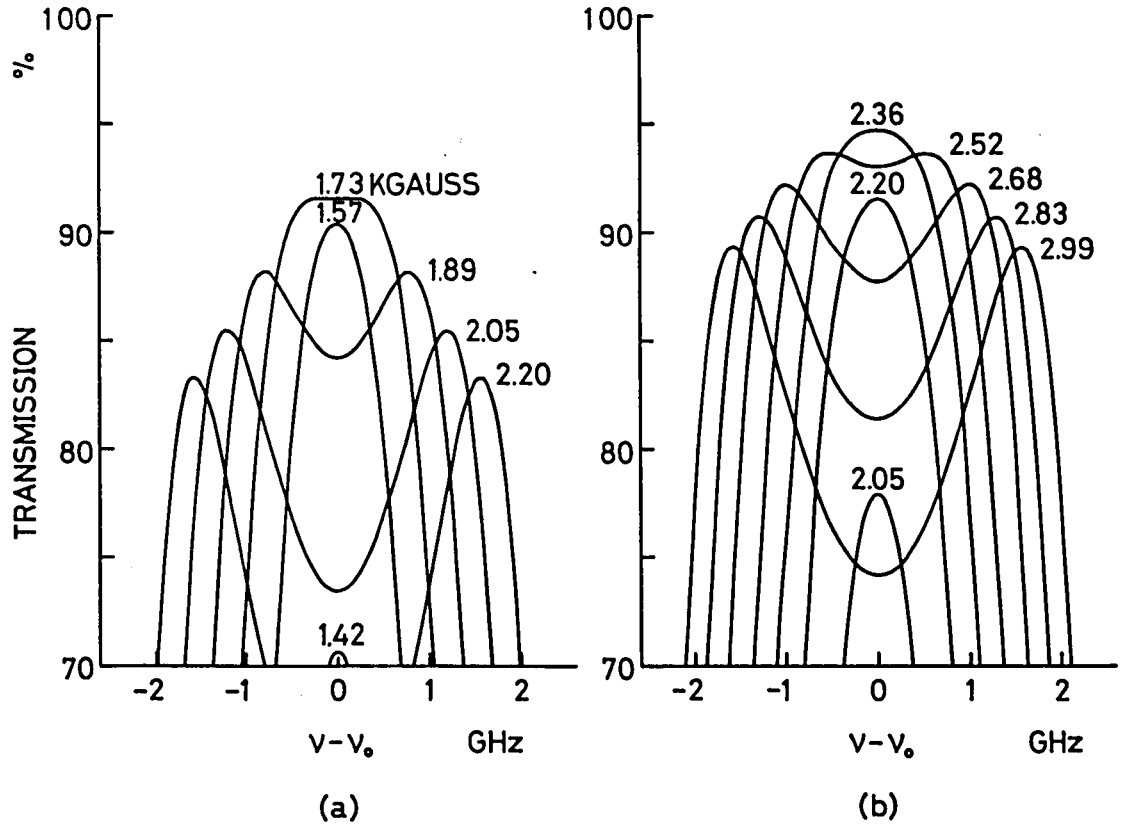


Fig. 3.12 Calculated transmissions of the Faraday filter in the center regions of the D lines, where (a) is the case of the $D_1$ line for the temperature T=430 K, and (b) is the case of the $D_2$ line for the temperature T=423 K.

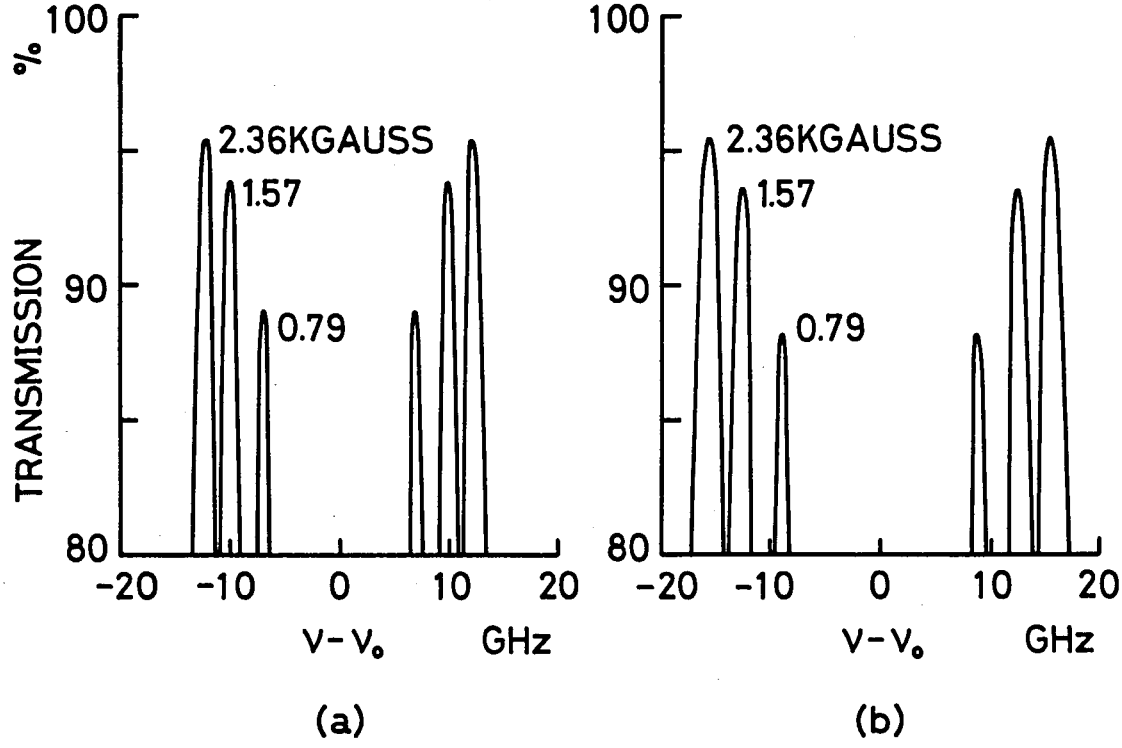


Fig. 3.13 Calculated transmissions of the Faraday filter on the wings of the D lines, where (a) is the case of the $D_1$ line for the temperature T=470 K, and (b) is the case of the $D_2$ line for the temperature T=470 K.

Next, we will consider the magnetic field dependence of the frequency of the laser output. The frequency shifts $\Delta\nu$ measured from the center of the resonance line, namely one half of the frequency separations of two modes, are shown in Fig. 3.14 and Fig. 3.15 for the oscillations on the center regions and on the wings, respectively. As seen in Fig. 3.14, in the center regions, the experimental results (circles) show the magnetic field dependence to be smaller than calculated ones (dashed lines). We consider that this discrepancy comes from the spatial hole-burning effect in the active medium of dye.[113)~115)] When the two-mode oscillation takes place at the frequencies of $\nu_1$ and $\nu_2$, the gain of the dye is spatially hole-burned at intervals of $c/2\nu_1$ and $c/2\nu_2$. Consider the case that the length of the dye is much shorter than the value of $c/(\nu_1 - \nu_2)$. Since $\nu_1 - \nu_2$ was up to about 2 GHz and the width of the jet stream of the dye was about 0.3 mm, this codition was sufficiently filled in our case. The intensity in the dye may be written as

$$I = I_0 \left\{\cos^2 kx + \cos^2(kx + \varphi)\right\} \tag{3.17}$$

$$k = \frac{2\pi}{\lambda} , \tag{3.18}$$

where $I_0$ is the intensity of each of the two modes, $\lambda$ is the laser wave length, $x$ is the length from the end mirror and $\varphi$ is the phase difference between two modes in the dye. If we assume the phase difference is $\pi/2$, the intensity becomes

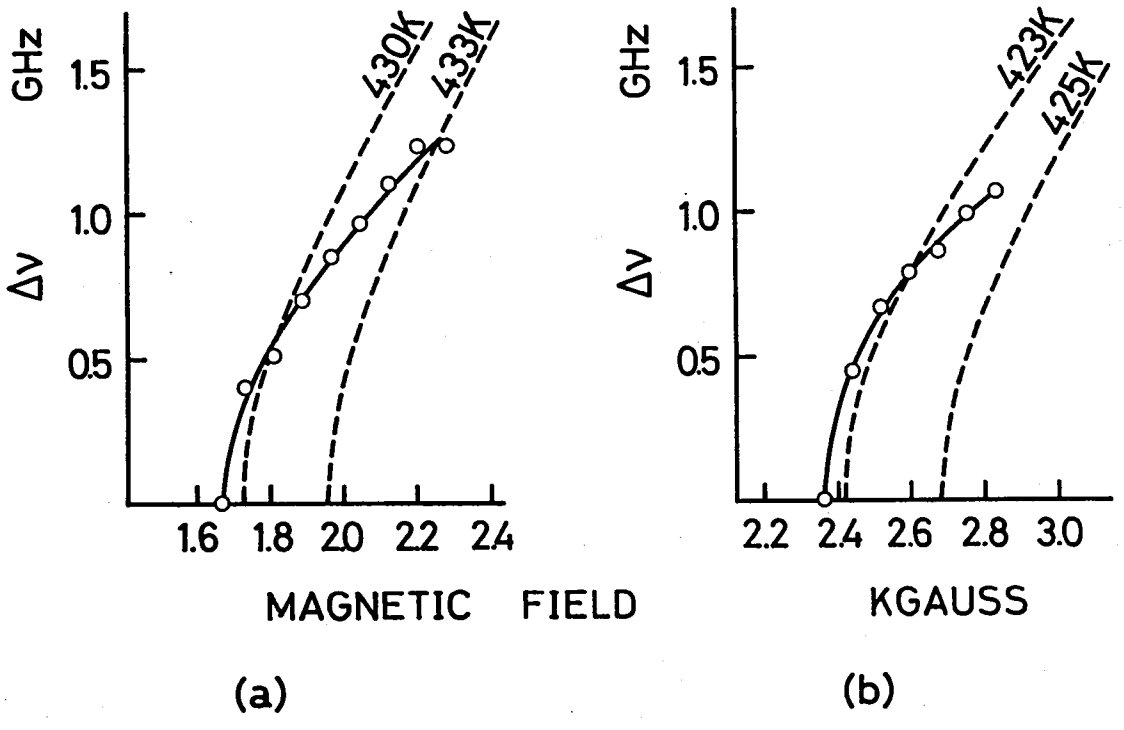


Fig. 3.14 Frequency shifts in the center regions of the D lines due to the change in the magnetic field strength H. The experimental data are represented by open circles: (a) is the case of the $D_1$ line for the temperature T=493 K, and (b) is the case of the $D_2$ line for the temperature T=482 K. The dashed and solid lines represent the theoretical shifts calculated with (3.16) and (3.26), respectively.

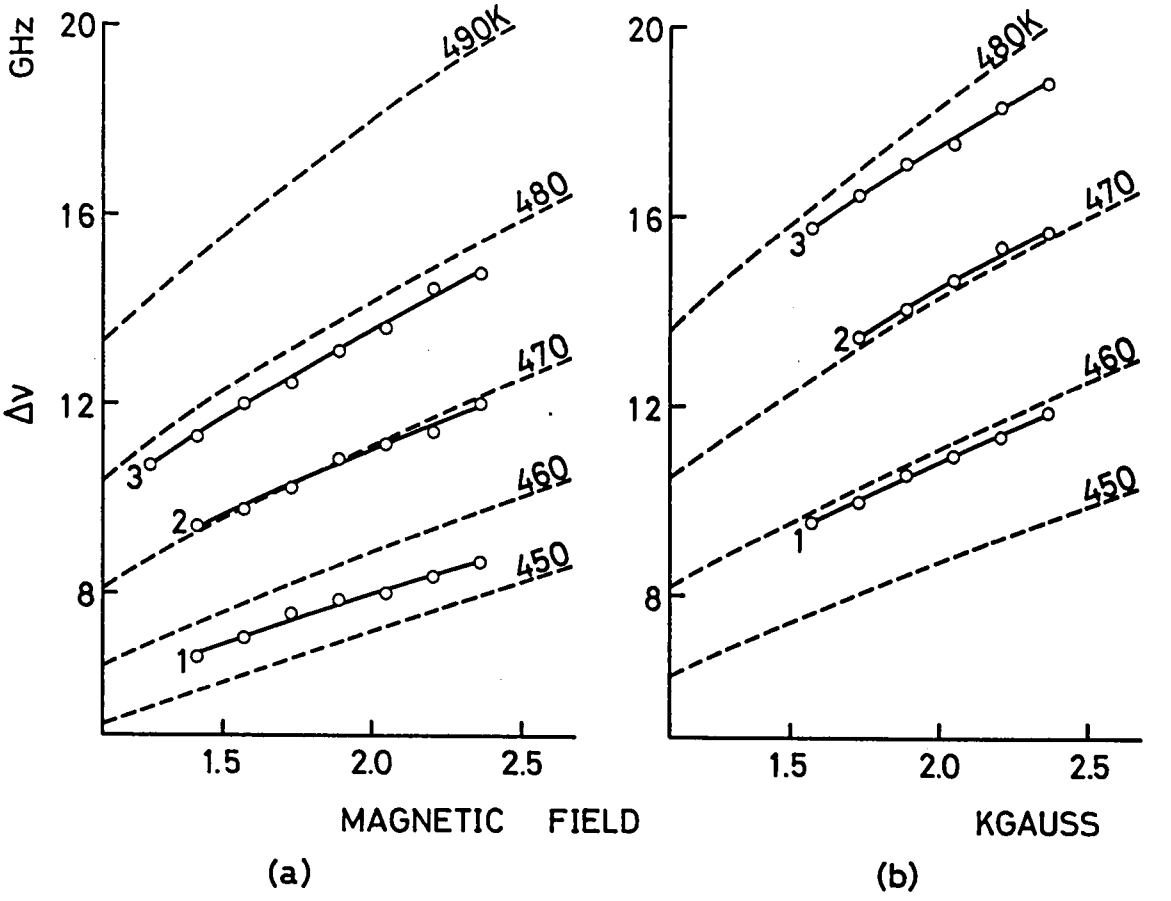


Fig. 3.15 Frequency shifts of the wings of the D lines due to the change in the magnetic field strength H. The experimental data are represented by open circles: (a) is the case of the $D_1$ line for the temperature 1:T=516 K, 2:T=534 K, 3:T=544 K, and (b) is the case of the $D_2$ line for the temperature 1:T=521 K, 2:534 K, 3:T=544 K. The dashed lines represent the theoretical shifts calculated with (3.16).

$$I = I_0 \left\{ \cos^2 kx + \cos^2 (kx + \frac{\pi}{2}) \right\} = I_0 \ . \qquad (3.19)$$

The intensity becomes the constant which is independent of the position $x$ and two oscillation modes use the active medium very efficiently. If the phase difference is not $\pi/2$, the intensity becomes the function of the position $x$, and the efficiency decreases. In other words, the holes burned in the gain curve by two-mode oscillation overlap each other when the phase difference differs from $\pi/2$. Therefore, the oscillations compete with each other when the phase difference of them in the dye is even integral of $\pi/2$, and they do not compete when it is odd integral of $\pi/2$. When the position of the dye from the end mirror is denoted by $\ell_{dm}$, the phase difference of two modes is given by

$$\varphi = 2\pi \left\{ \frac{\ell_{dm}}{c/\nu_1} - \frac{\ell_{dm}}{c/\nu_2} \right\} = \frac{2\pi \ell_{dm}}{c} (\nu_1 - \nu_2) \ , \qquad (3.20)$$

so that mode-competition occurs when $\nu_1 - \nu_2$ is even integral of $c/4\ell_{dm}$ and does not occur when $\nu_1 - \nu_2$ is odd integral of $c/4\ell_{dm}$. The gain of the dye is approximately given by

$$G' = \frac{G_0}{1 + \frac{I}{2I_s}(1+\cos^2\varphi)} \ , \qquad (3.21)$$

where $I_s$ is the satulation parameter and $G_0$ is the unsaturated gain. Defining the uncompete gain as

$$G = G_{\varphi=\pi/2} = \frac{G_0}{1 + \frac{I}{2I_s}} \ , \qquad (3.22)$$

we obtain if we assume $I/I_s \ll 1$,

$$G' = G \left\{ 1 - \frac{I}{2I_s} (1 + \cos\varphi) \right\} \tag{3.23}$$

$$= G \left\{ 1 - \frac{\alpha}{2} (1 + \cos\varphi) \right\}, \tag{3.24}$$

where $\alpha$ is the excitation parameter. Since frequencies of two oscillating modes are approximately given by $\nu_1 - \nu_0 = \nu_0 - \nu_2$ in the present case, the gain for each mode may be written in the form of

$$\left[ 1 - \frac{\alpha}{2} \left\{ 1 + \cos \frac{2(\nu_{1,2} - \nu_0)}{c/4\ell_{dm}} \right\} \right] G, \tag{3.25}$$

where $\nu_0$ is the center frequency of the absorption line. Therefore, two-mode oscillation may take place at which the function

$$\left[ 1 - \frac{\alpha}{2} \left\{ 1 + \cos \frac{2(\nu_{1,2} - \nu_0)}{c/4\ell_{dm}} \right\} \right] \tau \tag{3.26}$$

becomes maximum, where $\tau$ is the transmission of the Faraday filter given by (3.16). In the present experiment, $\ell_{dm}$ is 5 cm which gives the value of $c/4\ell_{dm}$ as 1.5 GHz. Using this value, we have calculated the oscillation frequencies as functions of the magnetic field strength. The results calculated by assuming $\alpha = 0.15$ are shown as solid lines in Fig. 3.14, where we can see an excellent agreement with experimental results.

The beam waist radius $r_o$ is given by[106]

$$(\pi r_0/\lambda)^2 \approx (\delta_{max} - \delta)(\delta - \delta_{min}) \qquad (3.27)$$

with

$$\delta = d_1 - R_1 - f$$

$$\delta_{max} = f^2/(d_2 - f), \qquad \delta_{min} = f^2/(d_2 - R_2 - f), \qquad (3.28)$$

where $d_1$ ($d_2$) is the spacing between the end (output) mirror and the colimating mirror, $R_1$ ($R_2$) is the curvature radius of end (output) mirror, and f is the focal length of the colimating mirror. In our case

$$f = 2.5 \text{ cm}, \qquad d_2 = 100 \text{ cm}, \qquad R_2 = \infty \text{ cm}.$$

Then we can estimate $r_0 = 7.7 \times 10^{-4}$ cm, so that $\pi r_0^2 = 19 \times 10^{-7}$ $cm^2$. The laser power in the dye is estimated at 200 mW, since the output power is about five mW and the transmission of the output mirror is 4 percent. Therefore the power density is 10 $kW/cm^2$. When $\alpha$=0.15, the saturation parameter is about $7 \times 10^4$ $kW/cm^2$ which is reasonable value for Rhodamine 6G.[116]

On the wings, as seen in Fig. 3.15, the magnetic field dependences of $\Delta\nu$ (solid lines) agree well with the calculated results (dashed lines). The effect of the spatial hole burning cannot be seen obviously, since the scale for $\Delta\nu$ in Fig. 3.15 is five times as large as that in Fig. 3.14.

Next, we will consider the reason why the oscillations took place only on the wings of the sodium D lines in the experiment performed by Sorokin et al., who tried to lock a flashlamp-pumped pulsed dye laser to the D lines by means of a Faraday filter. In their experiment, they varied the magnetic field strength up to 1.76 kG at which oscillations at the line center may take place within the temperature region of a few degrees as shown in Fig. 3.7. We consider that this fact gave rise to their experimental difficulties to get the oscillation at the line center. On the other hand, oscillations on the wings of lines can easily obtained for the temperatures higher than 440 K in such a magnetic field.

## 3.5 Conclusions

The oscillation frequency of a CW dye laser could be locked to both of the sodium D lines by means of a Faraday filter. The single-mode oscillations at the center of the $D_1$ and $D_2$ lines took place at temperatures about 490 and 480 K, respectively. The simultaneous oscillation at the $D_1$ and $D_2$ lines could not be observed at these temperatures. The two-mode oscillations on the both wings of the $D_1$ and $D_2$ lines took place simultaneously at temperatures higher than 505 K. The experimentally obtained conditions of the relative cell temperature and the magnetic field strength for the oscillation agreed well with those expected from the theoretical calculations. It should be noted that the

experimental results have been explained by the linear theory as expected in chapter II .

Another feature of the frequency-locking by the Faraday filter is that we can get not only the oscillation just at the center of the absorption line but also two-mode oscillation with desired frequency separation in the center region. There has been no frequency selective element having such a feature except for the Faraday filter. It is worthwile to study the physics of two-mode oscillation in a laser medium[117),118)].

# CHAPTER IV

# FREQUENCY-LOCKING TO NEON ABSORPTION LINES

## 4.1 Introduction

It has been shown in the previous chapter that the single mode oscillation of a CW dye laser at the center frequency of the sodium $D_1$ and $D_2$ lines has been achieved by the Faraday filter with a sodium cell and that the experimentally obtained conditions to get the oscillations have agreed well with those expected from the theoretical calculations. This method is applicable to the frequency-locking of a CW dye laser to other atomic lines when $Nf \gtrsim 10^{11}$ $cm^{-3}$, where $N$ and $f$ are the lower level density and the oscillator strength of the absoption line, respectively.

In this chapter, we describe the experimental and theoretical results of the frequency-locking of a CW dye laser to the absoption lines of neon by the Faraday filter. It should be emphasized that the frequency-locking by the Faraday filter is not confined to the absorption lines from the ground state and is possible to the absorption lines from the excited states, which may opens a wide area of applications. Neon has many absorption lines from the 1s states to the 2p states in the visible range as shown in Fig. 4.1. The $1s_5$ and the $1s_3$ states are metastable states and the $1s_4$ and

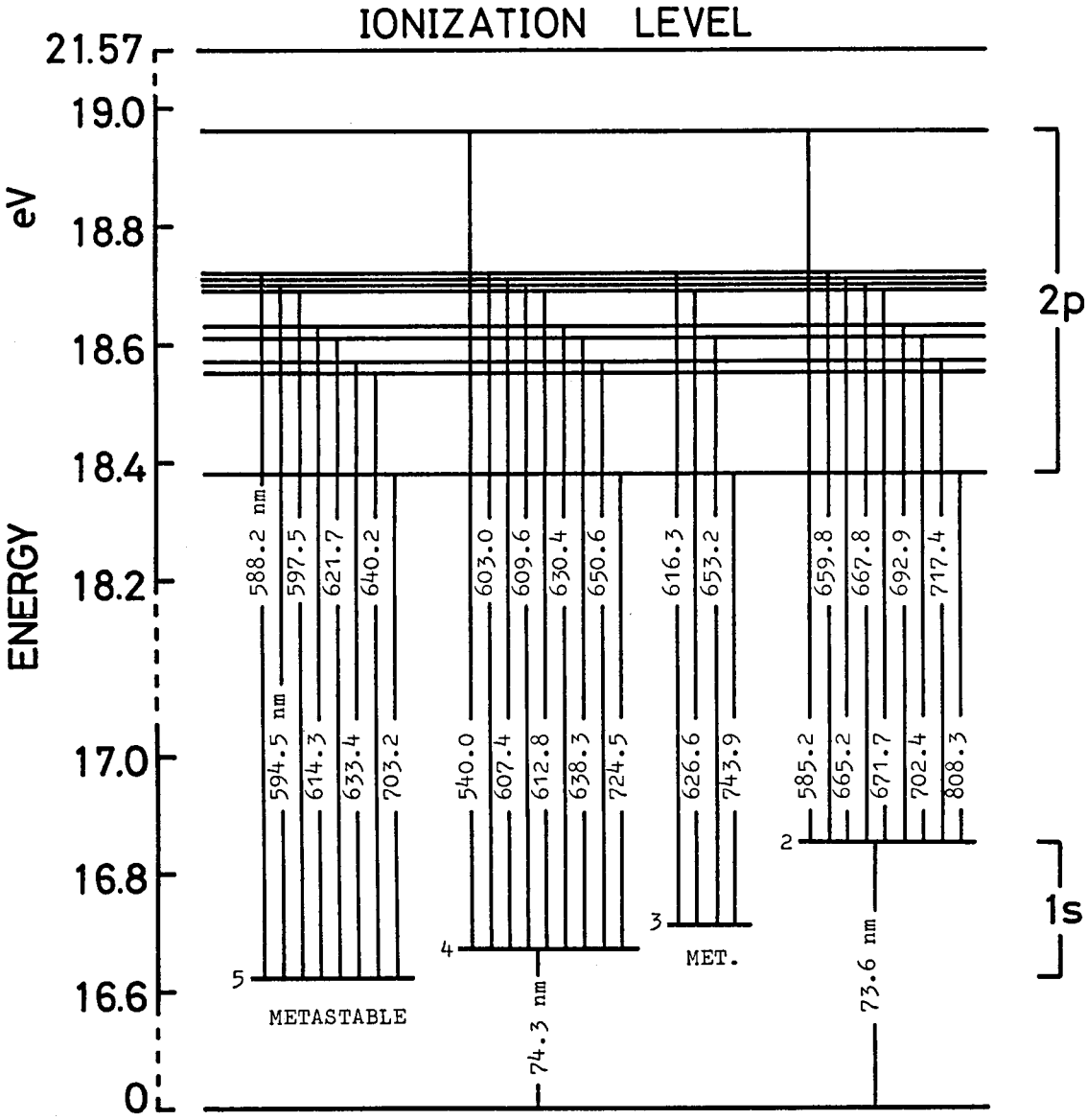


Fig. 4.1 Energy level diagram for the absorption lines from the 1s states to the 2p states of neon.[123)]

the $1s_2$ states are quasi-metastable states having long lifetimes by means of radiation trapping.[119] The total density of the 1s states can attain $10^{11} \sim 10^{12}$ $cm^{-3}$ in the positive column of a glow discharge.[120),121] Therefore there are several absorption lines to which the frequency-locking of a CW dye laser can be achieved (see Table 4.1).

Particular attention is given to the influence of isotopes on the Faraday filter. The condition for the oscillations at absorption lines and the shifts of the oscillation frequency due to the variation of the magnetic field strength are theoretically and experimentally obtained for various ratio of the mixtures of $Ne^{20}$ and $Ne^{22}$. Comparison between the experimental results and the theoretical ones is given, and a good agreement has been found. Furthermore, we have developed new technique for fine tuning of the CW dye laser in the vicinity of the absorption line by means of the isotope effect.

We have measured also the 1s densities in the positive column of the glow discharge in the presence of a magnetic field, by fitting the experimental results to the theory.

We have also found that the saturated absorption takes place at the center of several absorption lines in the Faraday filter, in addition to the optical rotation.[87]

## 4.2 Transmission of the Faraday Filter

Table 4.1 Transitions of Neon from the 1s States to the 2p States and Wavelengths Together with Parameters Assoceated with the Transitions [124),125)] The Typical Values of the 1s Densities Which Can Be Attained in the Glow Discharge and the Values of Nf Are Also Shown

| TRANSITION | λ (nm) | 2J+1 | g FACTOR | f | N ($10^{11}$cm$^{-3}$) | Nf ($10^{11}$cm$^{-3}$) | ISOTOPE SHIFT (GHz) |
|---|---|---|---|---|---|---|---|
| $1s_5$ $2p_6$ | 614.3 | 5 5 | 1.503 1.229 | 0.122 | 20 | 2.4 | 1.66 |
| $2p_4$ | 594.5 | 5 | 1.301 | 0.056 | | 1.1 | 1.72 |
| $2p_2$ | 588.2 | 3 | 1.340 | 0.040 | | 0.8 | 1.74 |
| $1s_4$ $2p_7$ | 638.3 | 3 3 | 1.464 0.669 | 0.170 | 10 | 1.7 | 1.68 |
| $2p_4$ | 609.6 | 5 | 1.301 | 0.157 | | 1.6 | 1.73 |
| $2p_3$ | 607.4 | 1 | —— | 0.114 | | 1.1 | 1.70 |
| $1s_3$ $2p_5$ | 626.7 | 1 3 | —— 0.999 | 0.394 | 5 | 2.0 | 1.65 |
| $2p_2$ | 616.4 | 3 | 1.340 | 0.273 | | 1.4 | 1.65 |

The neon Faraday filter consists of a neon discharge tube in an axial magnetic field and a polarizer positioned at each end of the discharge tube with polarization directions that form right angles to each other. When linearly polarized light passes through the discharge tube, a rotation of the polarization plane occurs, which is known as the Faraday effect. The Faraday filter has maximum transmission at the rotation angle of $\pi/2$. The transmission of the Faraday filter has large frequency-dependence in the vicinity of atomic absorption lines. The frequency giving the maximum transmission is determined by the following parameters: the population density $N$ of the 1s state of the associated absorption line, the magnetic field strength $H$, and the effective length of the discharge tube $\ell$. When the Faraday filter is inserted in the dye laser cavity, the oscillation takes place in the frequency region where the single-pass gain of the dye exceeds the cavity loss given by $1-\tau$, where $\tau$ is the transmission of the Faraday filter.

Since Rhodamine 6G is used as a dye in our experiment, we will confine ourselves to the absorption lines which are in the visible region of 570~640 nm and have the values of $Nf \gtrsim 10^{11}$ $cm^{-3}$. These absorption lines and the 1s densities which can be attained in the positive column of a glow discharge are tabulated in Table 4.1, together with the parameters for the associated transitions.

Here we will calculate the condition of $N$ and $H$ for the frequency-locking to these absorption lines. The single-pass

transmission $\tau_0$ and the rotation angle $\theta$ for linearly polarized light can be calculated in the similar way to the sodium case, and are given by eqs. (3.1)$\sim$(3.5). It should be noted that $\tau_0$ and $\theta$ are functions of the 1s density N and the magnetic field strength H.

Here, let us consider the transmission of the Faraday filter for the 614.3 nm ($1s_5$-$2p_6$) absorption line as an example. The energy level diagram in the presence of a magnetic field is shown in Fig. 4.2, together with allowed transitions and their relative spectral strength.

Since there are three stable neon isotopes, isotope shift must be taken into account to calculate the absoption and the dispersion in the vicinity of the absorption lines. Therefore, we must sum over all isotope components as well as Zeeman components performed in eqs. (3.3) and (3.4). The relative abundance of $Ne^{21}$ (0.257 percent) is small compared with those of $Ne^{20}$ (90.92 percent) and $Ne^{22}$ (8.82 percent)[122] so that $Ne^{21}$ can be neglected in the calculation. The isotope shifts between $Ne^{20}$ and $Ne^{22}$ associated with above absorption lines are shown in the last column of table 4.1.[126]

The calculated absorption coefficient k and the rotation angle $\theta$ for the 614.3 nm line are shown in Fig. 4.3(a) and (b), respectively, at the $1s_5$ density $N=1.2\times10^{12}$ $cm^{-3}$, the magnetic field strength H=2.8 kG and the effective length of the discharge tube $\ell=15$ cm. As shown in the previous chapter, the total transmission $\tau$ is given by the product of the transmission $\tau_0$ due to optical

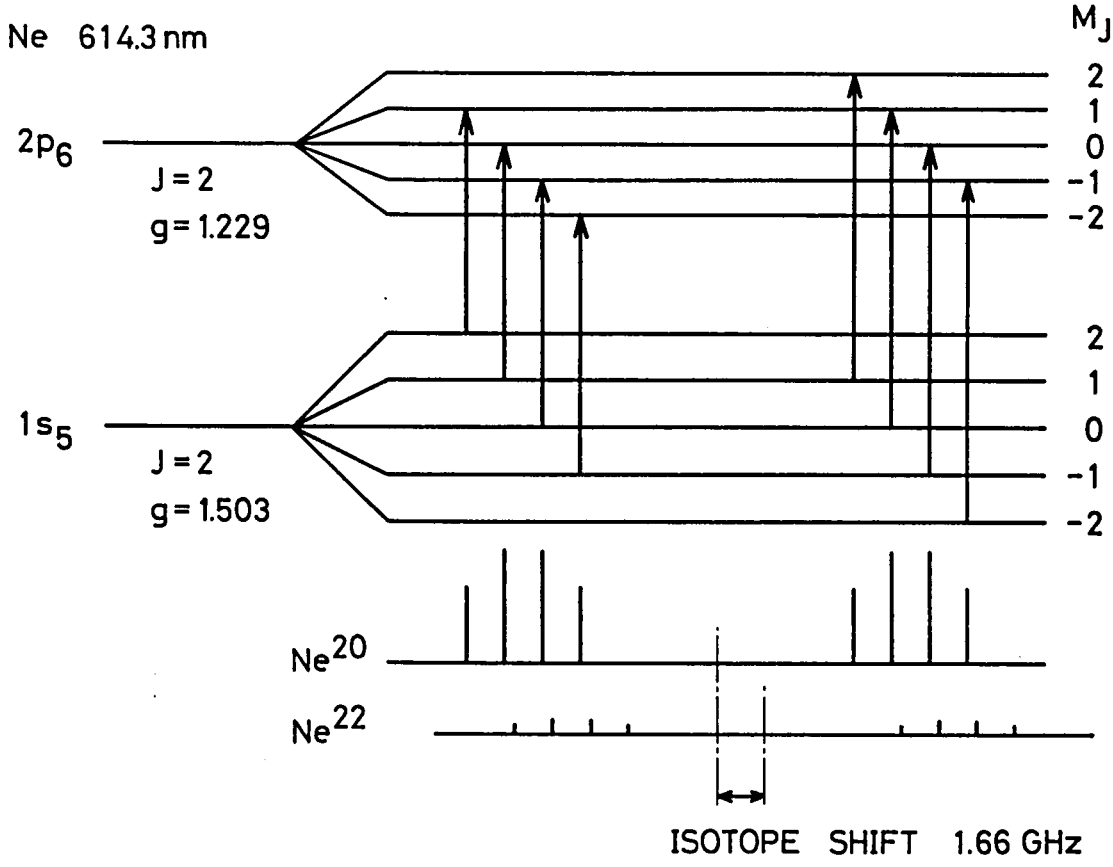


Fig. 4.2 Energy level diagram for the 614.3 nm ($1s_5$-$2p_6$) absorption line in a magnetic field and allowed $\sigma_+$ and $\sigma_-$ transition components. The corresponding spectra with their relative intensities for natural abundance neon and isotope shift are also shown in the bottom.

absorption and the transmission due to optical rotation which is given by $|b^2\cos^2\theta - \sin^2\theta|$, i.e., $\tau = \tau_0 |b^2\cos^2\theta - \sin^2\theta|$, where $b$ is the transmission of the Brewster-angle window for the electric field perpendicular to the principal axis. The values $\tau$ for the 614.3 nm line in the same case as in Fig. 4.3(a) and (b) are shown in Fig. 4.3(c). As shown in Fig. 4.3(c), the transmission curve generally has three peaks similarly to the case of the sodium D lines; one is in the center region, and the others are on the wings. It should be noted that the transmission curve is not, however, symmetric due to the presence of two isotopes $Ne^{20}$ and $Ne^{22}$.

When the Faraday filter is inserted in the dye laser cavity, the oscillation takes place in the frequency region where the single pass gain of the dye exceeds the cavity loss given by $1-\tau$, where $\tau$ is a function of the $1s_5$ density $N$ and the magnetic field strength $H$. In our experimental condition, transmission threshold is about 0.85. The conditions of the density and the mangetic field strength under which the transmission $\tau$ is larger than 0.85 have been calculated, and the results are shown in Fig. 4.4. As seen in Fig. 4.4, the oscillation on the red wing (wing on low frequency side of the absorption line) takes place at lower density and weaker magnetic field strength than those for the oscillation on the blue wing (wing on high frequency side of the absorption line).

Next, we calculate the transmission $\tau$ in the center region and on the wings of the absorption line, as functions of the magnetic

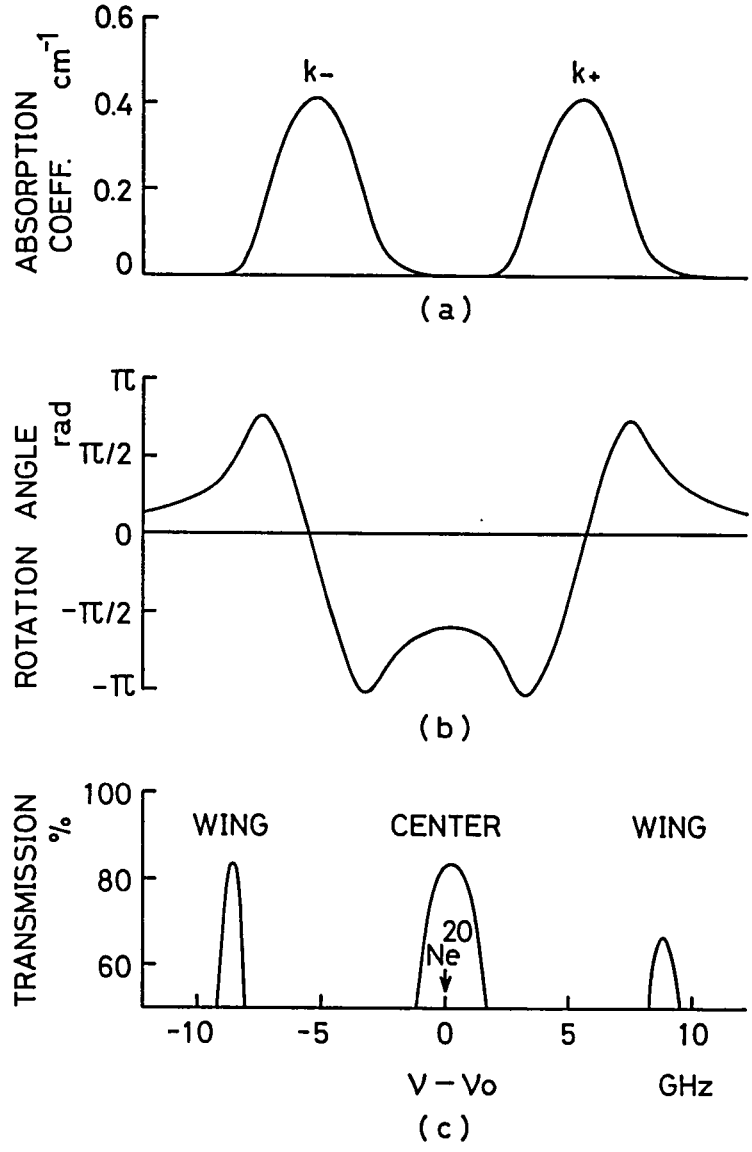


Fig. 4.3 (a) Absorption coefficients of the Faraday filter for $\sigma_+$ and $\sigma_-$ light in the case of the $1s_5$ density $N=1.2 \times 10^{12}$ $cm^{-3}$ and the magnetic field strength H=2.8 kG. (b) Single pass rotation angle for linearly polarized light.
(c) Transmission of the Faraday filter inserted into the laser cavity.

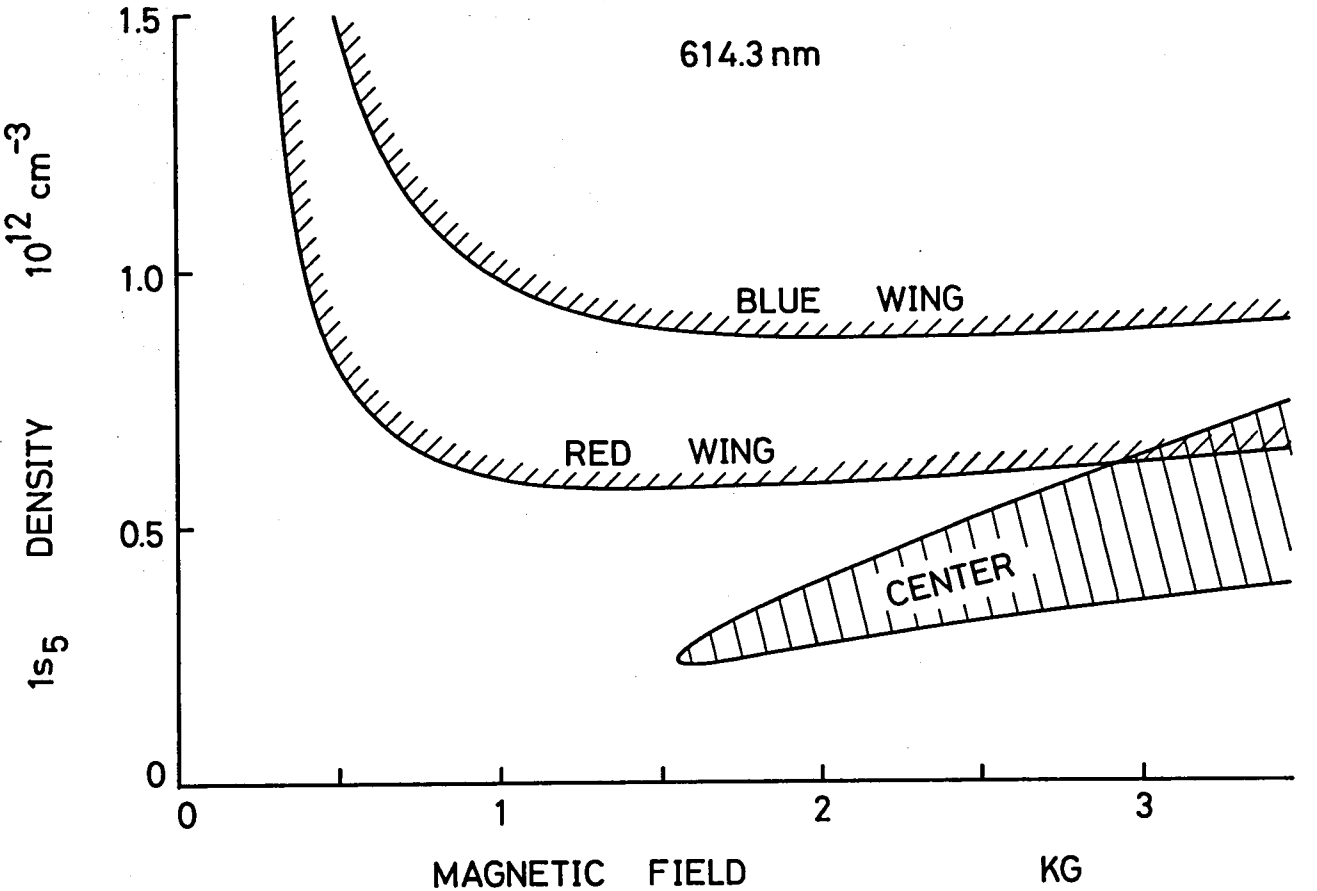


Fig. 4.4 Theoretical regions of the $1s_5$ density N and the magnetic field strength H for transmission larger than 0.85, in the case of the 614.3 nm line.

field strength H for particular $1s_5$ density. The typical results in the center region are shown in Fig. 4.5, where (a) and (b) are the cases of the Faraday filters with pure $Ne^{20}$ and natural abundance neon, respectively. As seen in Fig. 4.5(a), the transmission curve for pure $Ne^{20}$ has single peak just at the center of the $Ne^{20}$ absorption line at weak magnetic field, and the peak value increases with the increases of H. When H is further increased, the peak splits into two peaks with equal peak value and the frequency separation between them increases, while the peak values decrease. Thus, the transmission curve is symmetric in the case of a pure isotope. On the contrary, as seen in Fig. 4.5(b), the transmission curve is not symmetric in the case of natural abundance neon. There is a single peak which is shifted from the center of the $Ne^{20}$ absoption line toward the $Ne^{22}$ line center at low values of the magnetic field. The transmission at the peak increases for incrasing H, while the location of the peak shifts toward higher frequency. When H is further increased, the peak value decreases, while the peak frequency shifts toward higher frequency, and finally the second peak appears in the low frequency side as seen in Fig. 4.5(b), which is much smaller than that in the high frequency side. In this way, as H is increased up to 2.5 kG, the single peak shifts toward higher frequency without its splitting into two peaks.

Fig. 4.6(a) and (b) shows the calculated transmission of the Faraday filter on the wings of the 614.3 nm line. As seen in Fig. 4.6(a), the transmission curve for pure $Ne^{20}$ has two peaks on

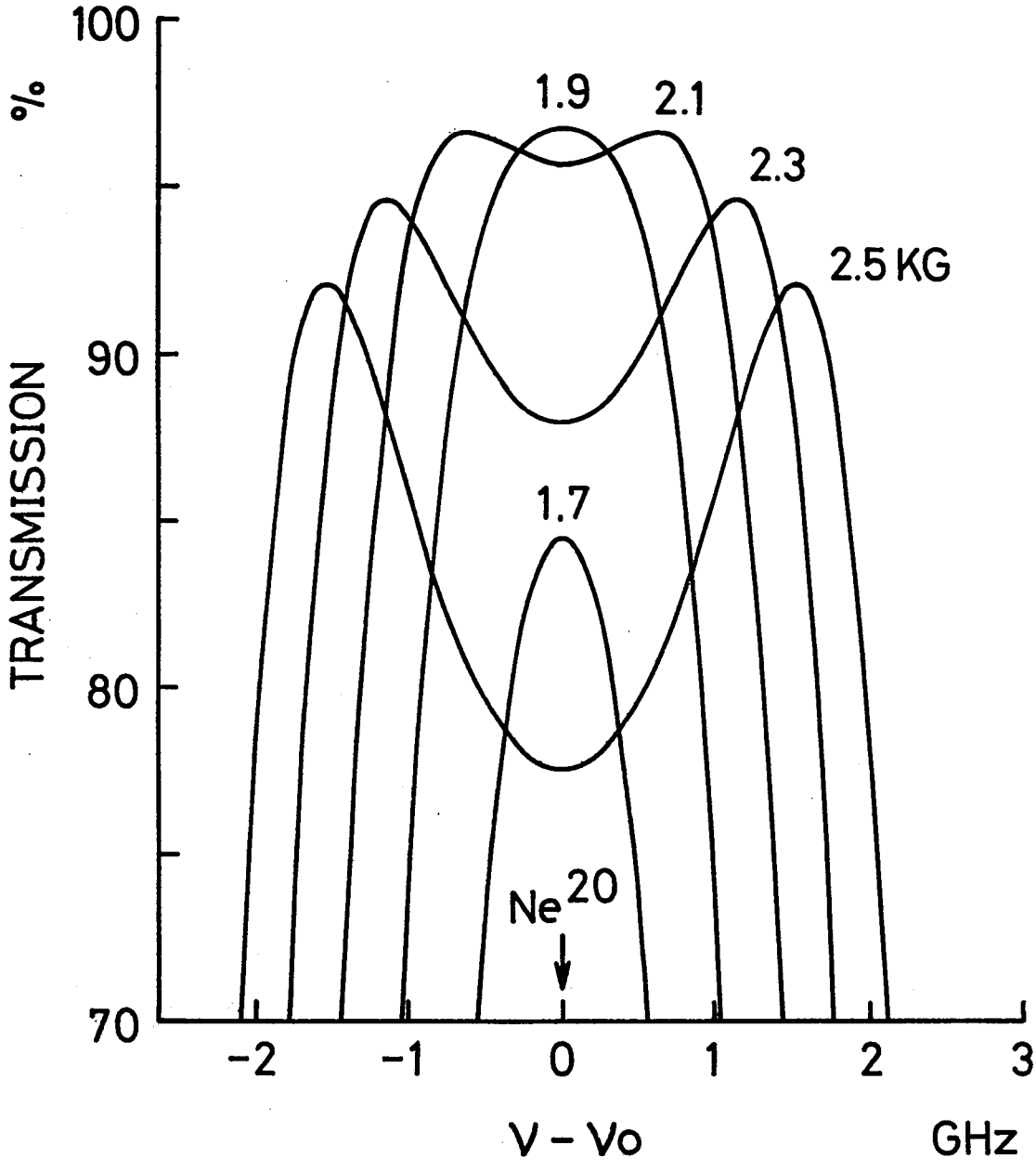


Fig. 4.5(a) Calculated transmissions of the Faraday filter in the center region of the absorption line of the 614.3 nm at the density $N=0.7\times10^{12}$ $cm^{-3}$, for the case of pure isotope $Ne^{20}$.

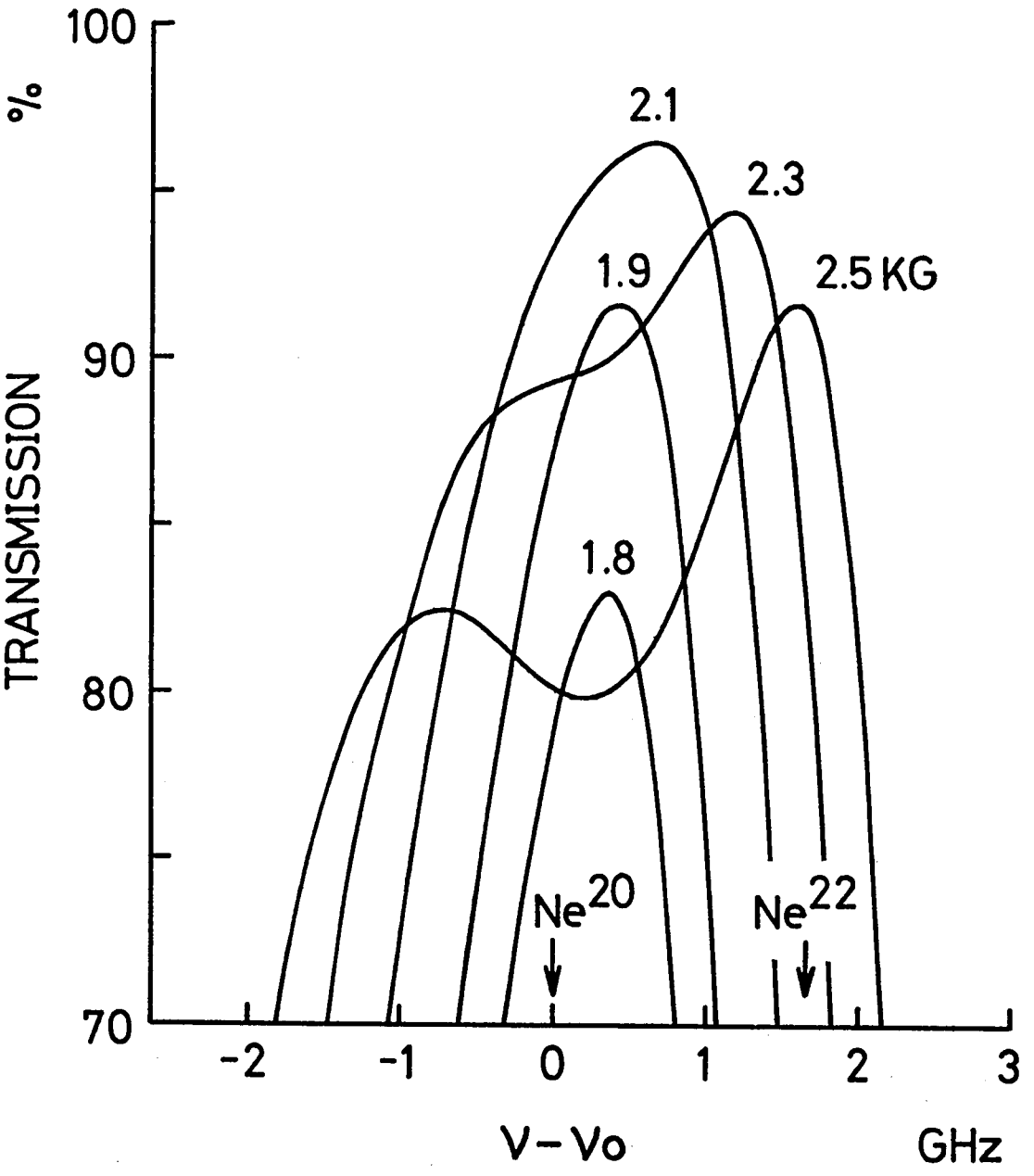


Fig. 4.5(b) Same as for Fig. 4.5(a), but for the case of natural abundance neon.

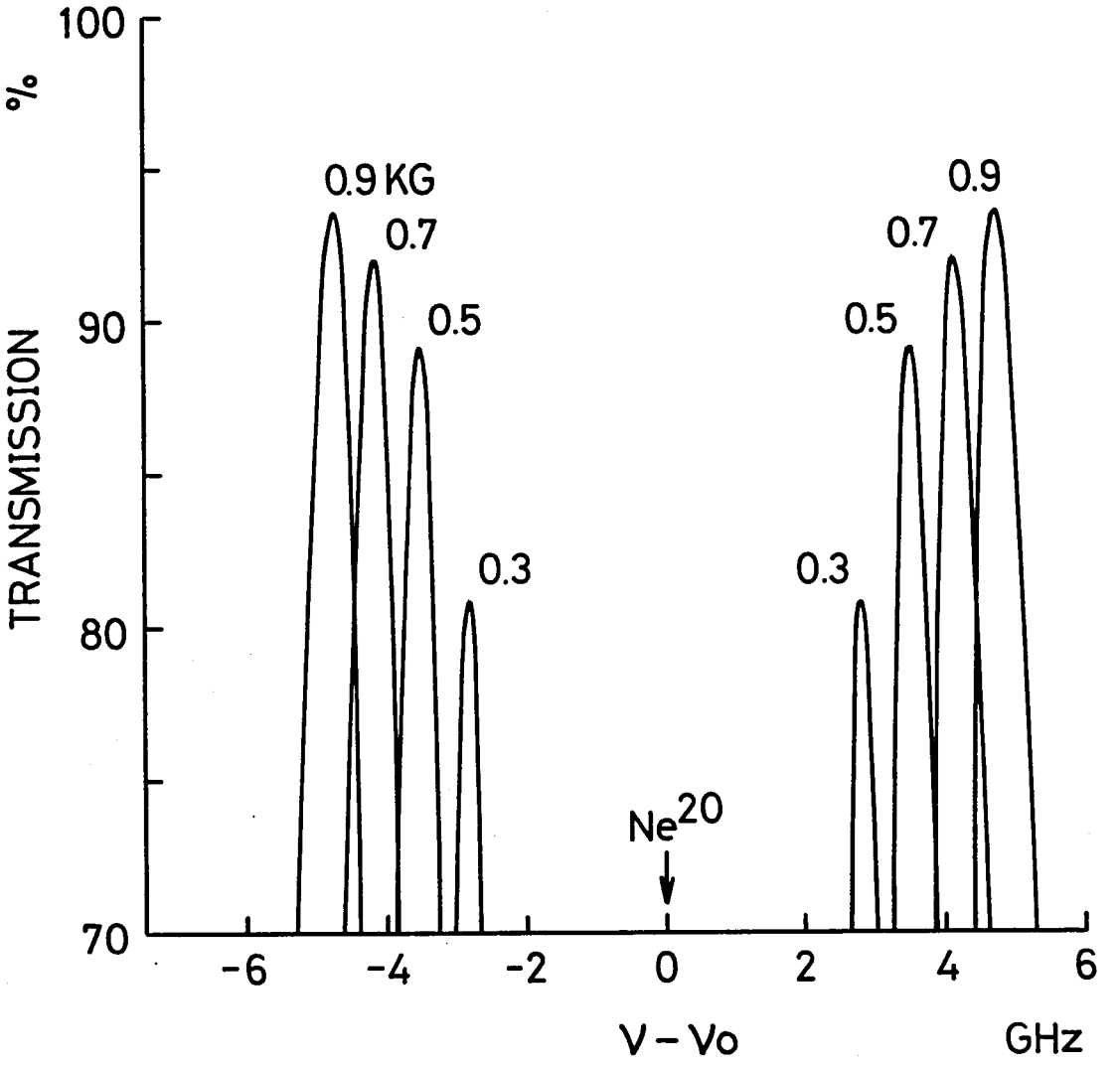


Fig. 4.6(a) Calculated transmissions of the Faraday filter on the wings of the absorption line of the 614.3 nm at the $1s_5$ density $N=2 \times 10^{12}$ $cm^{-3}$, for the case of pure isotope $Ne^{20}$.

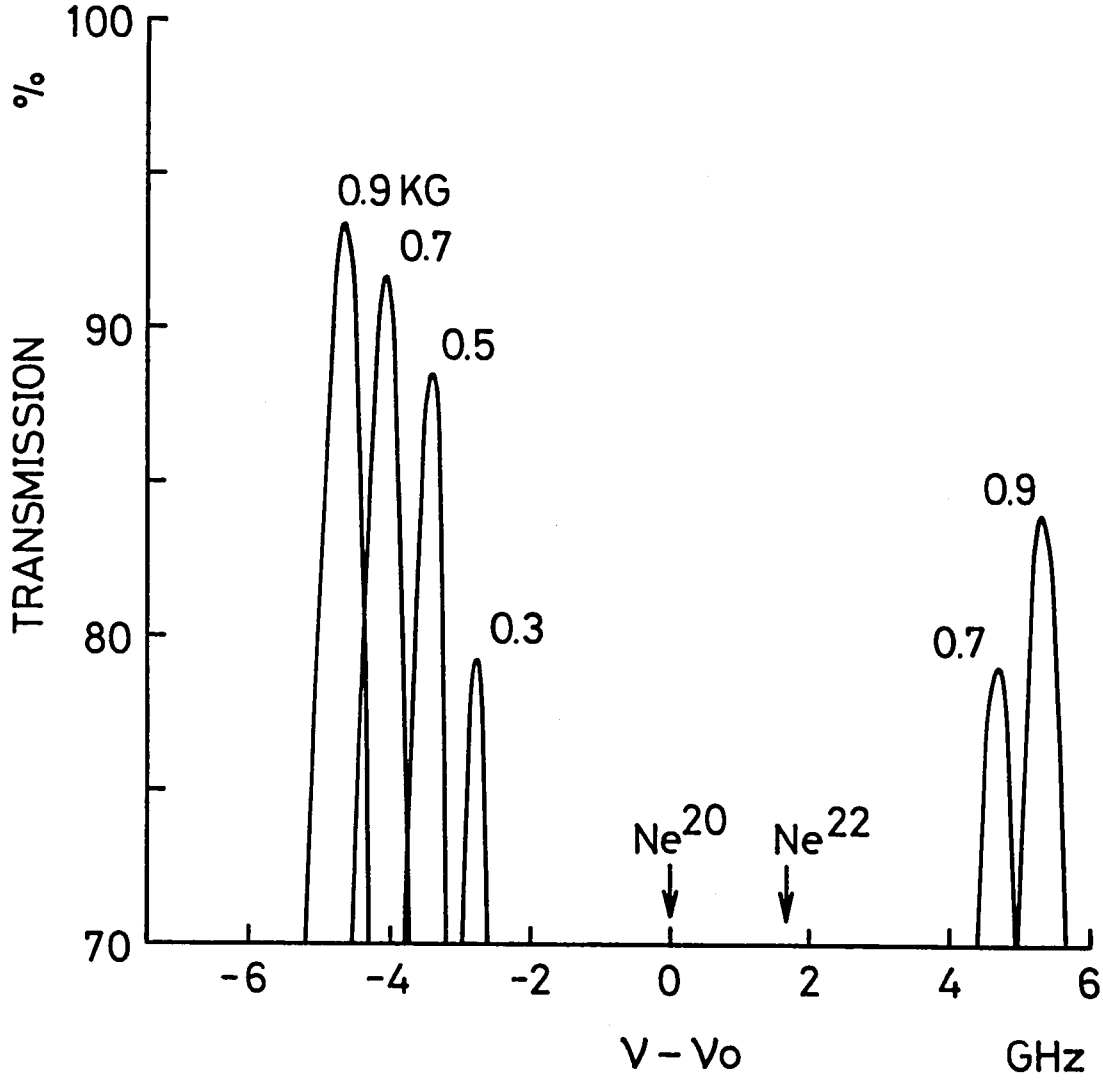


Fig. 4.6(b) Same as for Fig. 4.6(a), but for the case of natural abundance neon.

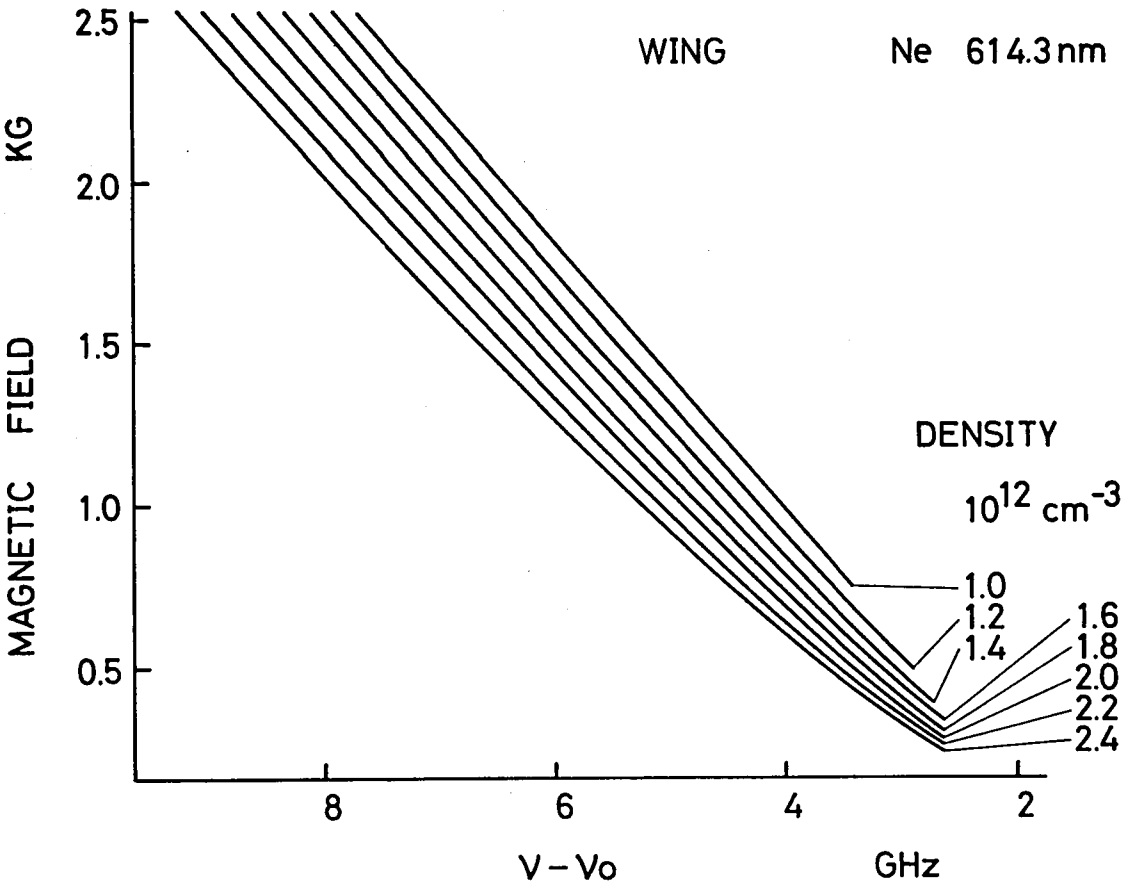


Fig. 4.7 Calculated values of the magnetic field dependence of the oscillation frequencies by the Faraday filter with natural abundance neon at the 614.3 nm line for various densities of the $1s_5$ state.

the wings of the absorption line symmetrically, and the frequency separation between two peaks and their peak values increase with the increase of the magnetic field strength H. On the contrary, as seen in Fig. 4.6(b), the transmission curve is not symmetric in the case of natural abundance neon. The peak value of the red wing exceeds that of the blue wing by a great deal. Therefore, we may obtain the single mode oscillation which shifts toward lower frequency with the increase of H. The calculated values of the magnetic field dependence of the oscillation frequencies for various densities of the $1s_5$ state are shown in Fig. 4.7.

The conditions of the 1s density and the magnetic field strength for other absorption lines, under which the transmissions of the Faraday filter are larger than 0.85, have been calculated in a similar way, and the results are shown in Fig. 4.8. In Fig. 4.8, the conditions for the center region and for the the red wing are shown for each absorption line. It becomes evident from Fig. 4.8 and f-values tabulated in Table 4.1 that oscillations at the absorption lines of neon may occur when $Nf \gtrsim 0.5 \times 10^{11}$.

## 4.3 Experimental Setup

The experimental setup is schematically shown in Fig. 4.9. The Faraday filter is inserted into the dye laser cavity with three mirrors, where the Rhodamine 6G in the form of a jet stream is pumped by an argon laser of 2 W in total power. The cavity

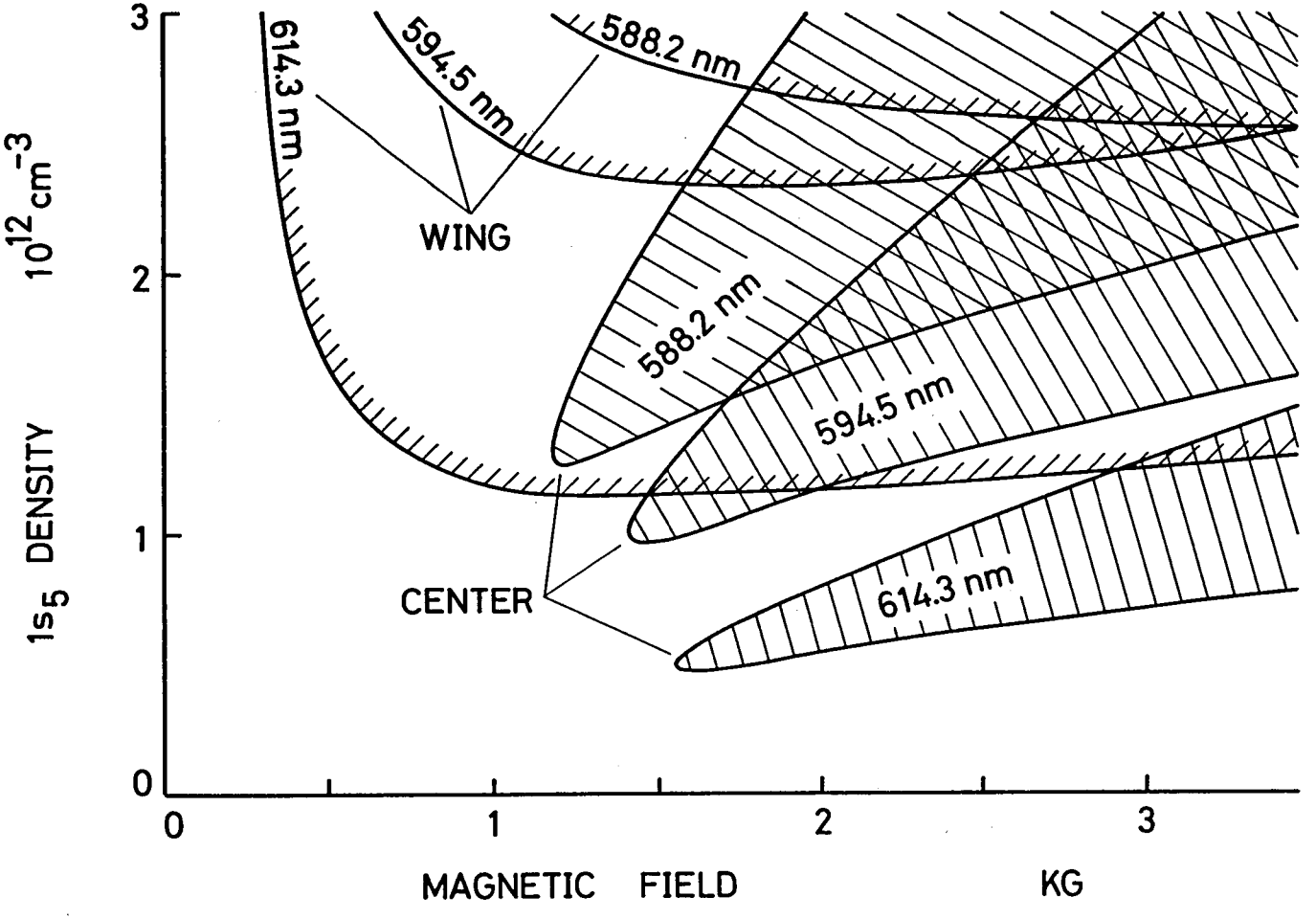


Fig. 4.8(a) Theoretical regions of the 1s density N and the magnetic field strength H for the transmission larger than 0.85, for absorption lines from the $1s_5$ state.

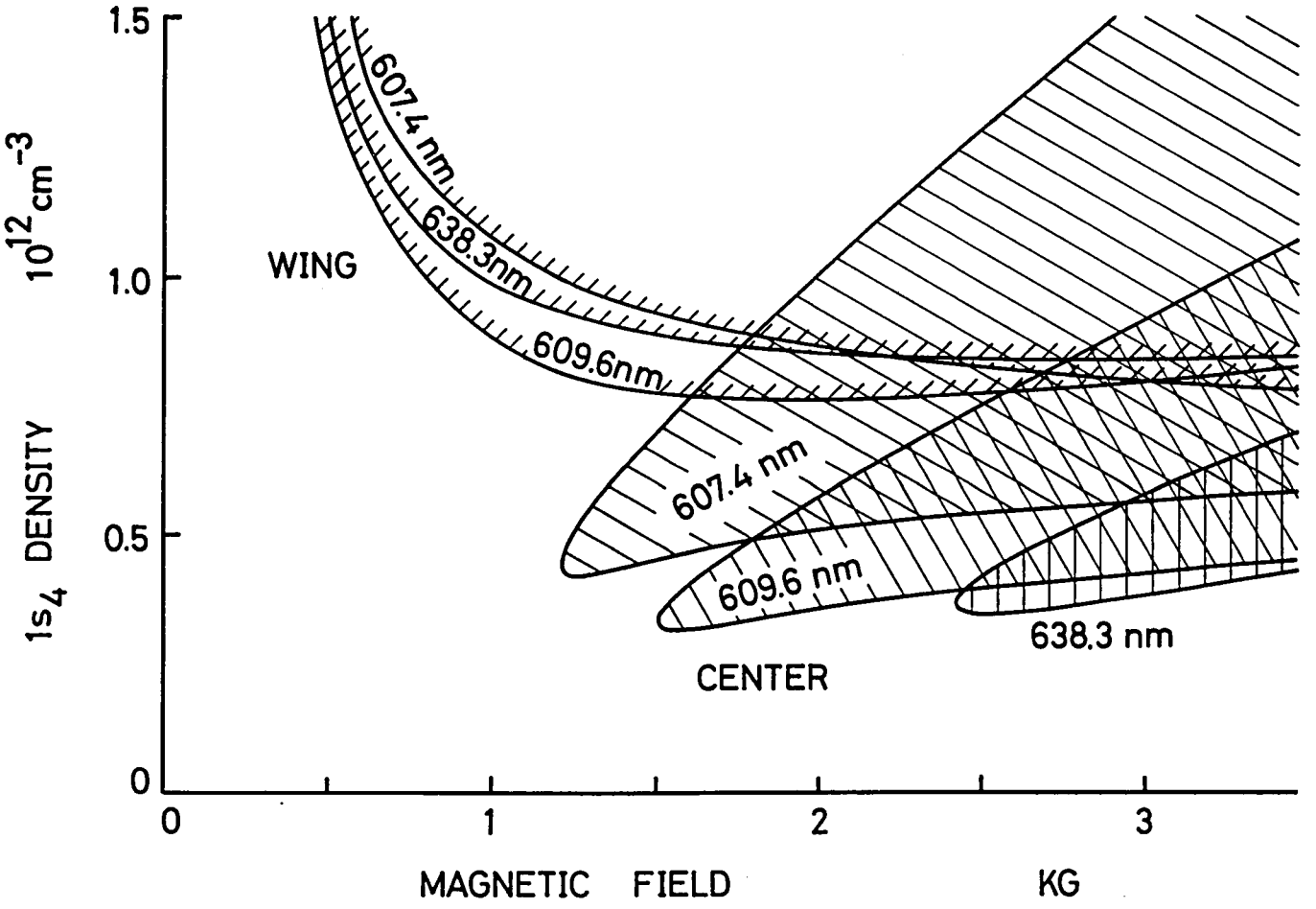


Fig. 4.8(b) Same as for Fig. 4.8(a), but for absorption lines from the $1s_4$ state.

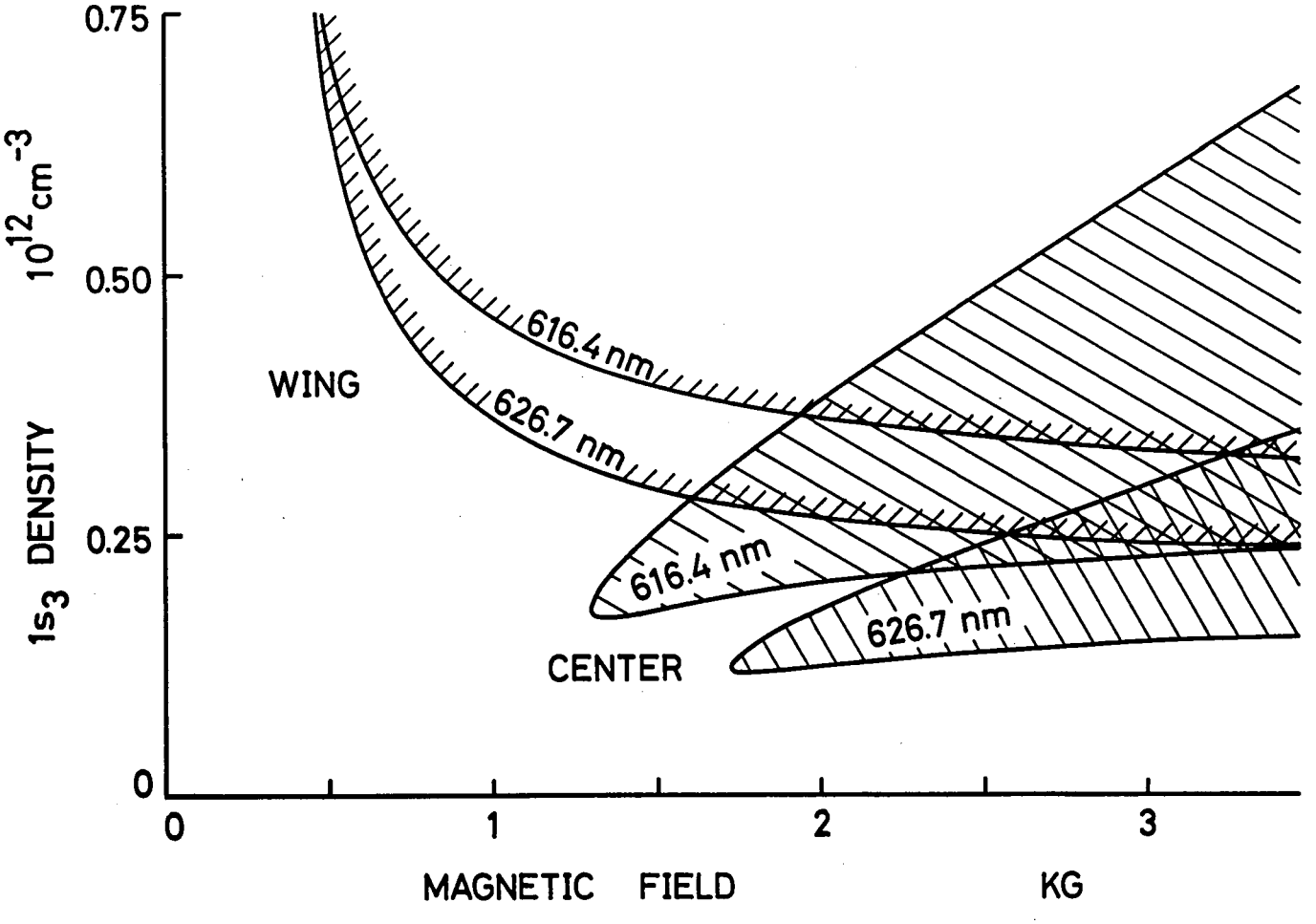


Fig. 4.8(c) Same as for Fig. 4.8(a), but for absorption lines from the $1s_3$ state.

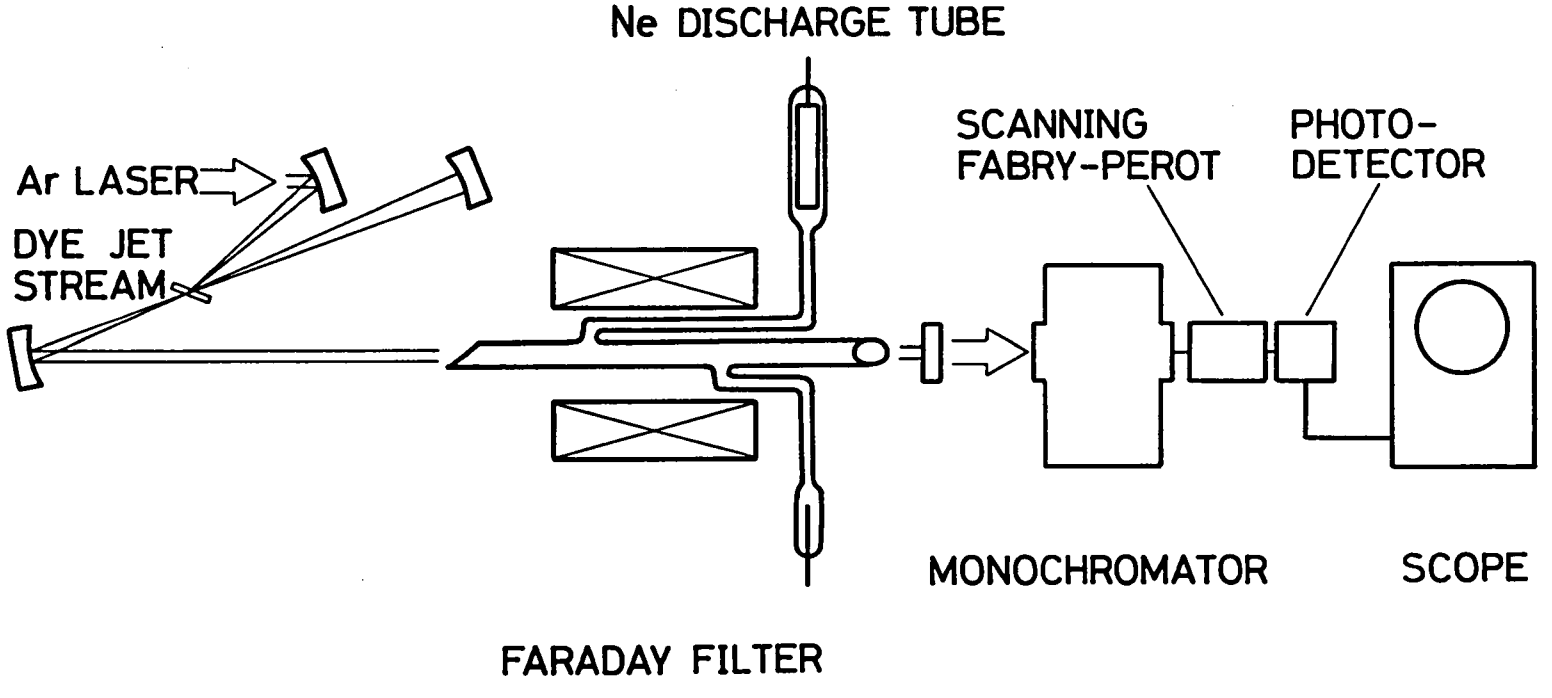


Fig. 4.9 Schematic diagram of the experimental setup.

length of the dye laser is about 1 m, which results in the mode separation of 150 MHz. The Faraday filter consists of a discharge tube and a solenoid coil. The discharge tube used has a bore of 6 mm and an effective length of 15 cm. The tube was designed so that the light propagates through the discharge in the homogeneous magnetic field to avoid the absorption of $\sigma^-$ light in the vicinity of the line center by the 1s state atoms in a weak field region of the discharge. The polarization direction of the Brewster-angle windows at both ends of the tube is a right angle to each other. The Brewster-angle window at the left side of the tube is oriented so that its polarization direction agrees with that of the dye jet stream, i.e., with the polarization direction of the argon laser beam. The neon pressure of the discharge tube is 0.5~2 torr. The dc discharge current is 10 ~ 70 mA, at which the total 1s density can attain to $10^{11} \sim 10^{12}$ $cm^{-3}$. On the other hand, the solenoid coil produces an axial magnetic field up to 2.5 kG. The laser output is analyzed by a grating monochromator and a scanning Fabry-Perot interferometer.

## 4.4 Experimental Results and Discussions

Using the setup described in section 4.3, we made experiments to determine whether or not the oscillations at neon absorption lines were possible just as predicted by the theory, and to determine experimentally the conditions for oscillations. We

swept the magnetic field, while increasing the neon pressure of the discharge tube as a parameter. The discharge current was kept constant to 40 mA. As the result, when natural abundance neon was used, the oscillations took place at six absorption lines: 614.3 nm ($1s_5$-$2p_6$), 594.5 nm ($1s_5$-$2p_4$), 588.2 nm ($1s_5$-$2p_2$), 609.6 nm ($1s_4$-$2p_4$), 607.4 nm ($1s_4$-$2p_3$), and 616.4 nm ($1s_3$-$2p_2$). It should be noted that these oscillations were in a single longitudinal mode. For oscillations locked at each absorption line, we measured the regions of the magnetic field strength for oscillation and the directions of the oscillation frequency shifts with the increase of H, and the results are shown in Fig. 4.10. In Fig. 4.10, + and - represent the directions of the shifts of the oscillation frequencies; + toward higher frequency and - toward lower frequency as the magnetic field strength H is increased.

In order to know whether the oscillation occured in the center region or on the wing of the absorption line, we applied the dye laser output beam to the other neon discharge tube in the absence of a magnetic field and observed the resonance fluorescence. As the result, in the case of Fig. 4.10(a), the resonance fluorescence was not observed for the oscillation at the 614.3 nm line in low magnetic field region, which means that the oscillation occured on the wing of the absorption line. On the other hand, since the resonance fluorescence was observed for the other oscillations, we found that the oscillations occured in the center regions of the absorption lines. In a similar way, in the case of Fig. 4.10(b), we found that the oscillations at the 614.3 nm

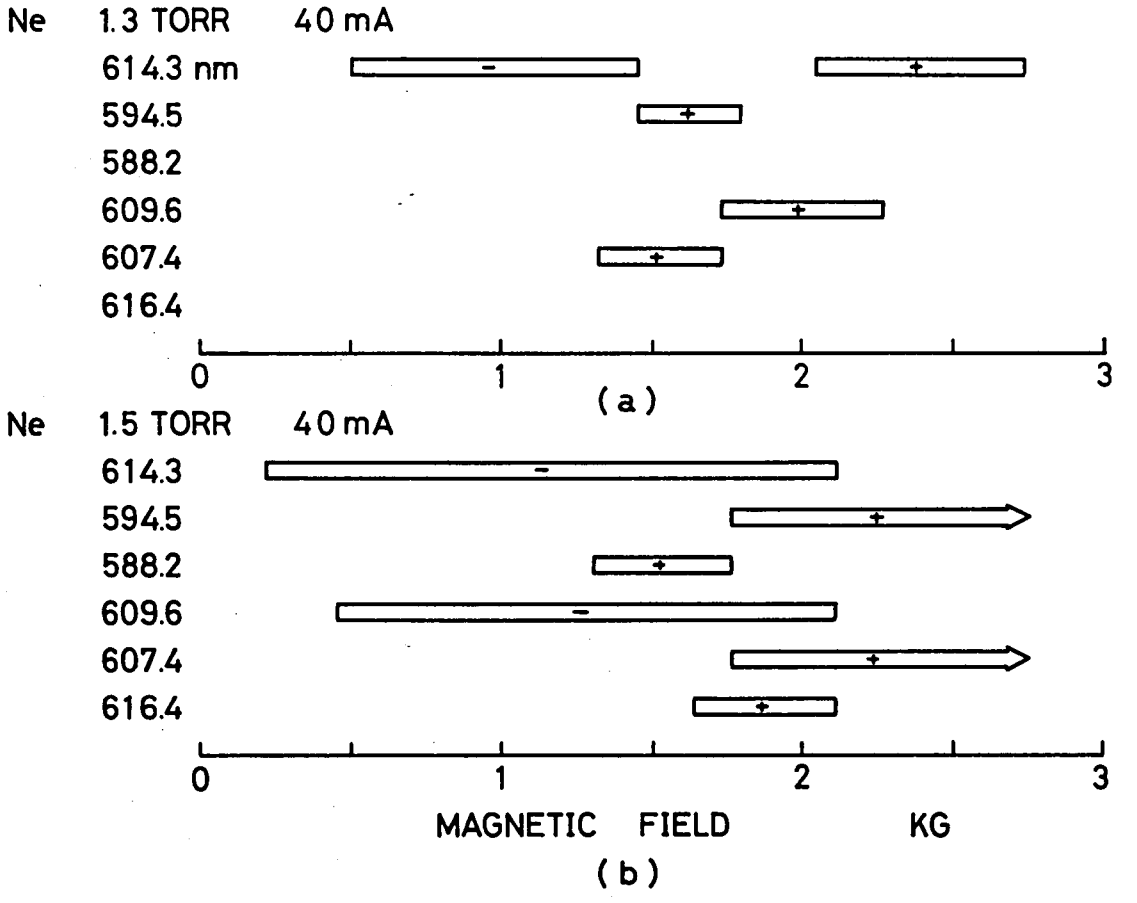


Fig. 4.10 Experimentally obtained magnetic field regions for oscillations at various absorption lines. The signs indicated show the directions of the shifts of the oscillation frequencies when the magnetic field H is increased: + toward higher frequency and - toward lower frequency. (a) Case of the neon pressure of 1.3 torr. (b) Case of the neon pressure of 1.5 torr.

and the 609.6 nm lines occured on the wings and the others in the center regions of absorption lines. From these experimental results, it is evident that the oscillation frequency shifts toward higher frequency in the center region and shifts toward lower frequency on the wing with the increase of H just as predicted by the theory. Output spectra of the dye laser on the wing of the 614.3 nm line at several magnetic fields are shown in Fig. 4.11 as an example.

Next, we will consider the magnetic field region in which oscillation takes place. It should be noted that the 1s density in the discharge tube depends significantly on the magnetic field. There have been several investigations on the measurements of the densities of the metastable states and quasi-metastable states in the positive column in the absence of a magnetic field.[120),121)] However, very little has been known about the influence of the magnetic field on the densities of these states. Consequently it must be interesting to estimate the 1s states density as function of H by comparing the experimentally obtained magnetic field regions with the calculated ones.

Here, let us consider the $1s_5$ density as an example. The $1s_5$ densities as functions of the magnetic field strength can be obtained by projecting the upper and lower limits of the experimentally obtained magnetic field regions (Fig. 4.10) to the boundary of the oscillation regions obtained theoretically, and the results are shown in Fig. 4.12, where open and filled circles are for the neon pressures of 1.3 torr and 1.5 torr, respectively.

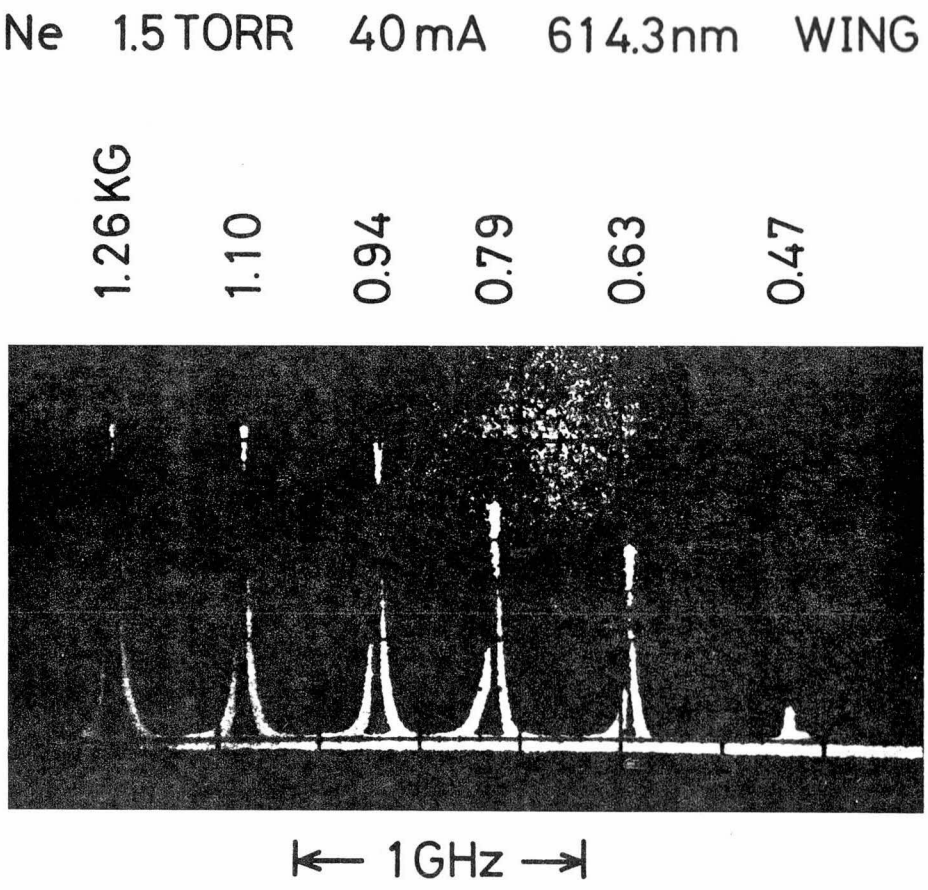


Fig. 4.11 Output spectra of the CW dye laser on the wing of the 614.3 nm line, as displayed by a scanning Fabry-Perot interferometer.

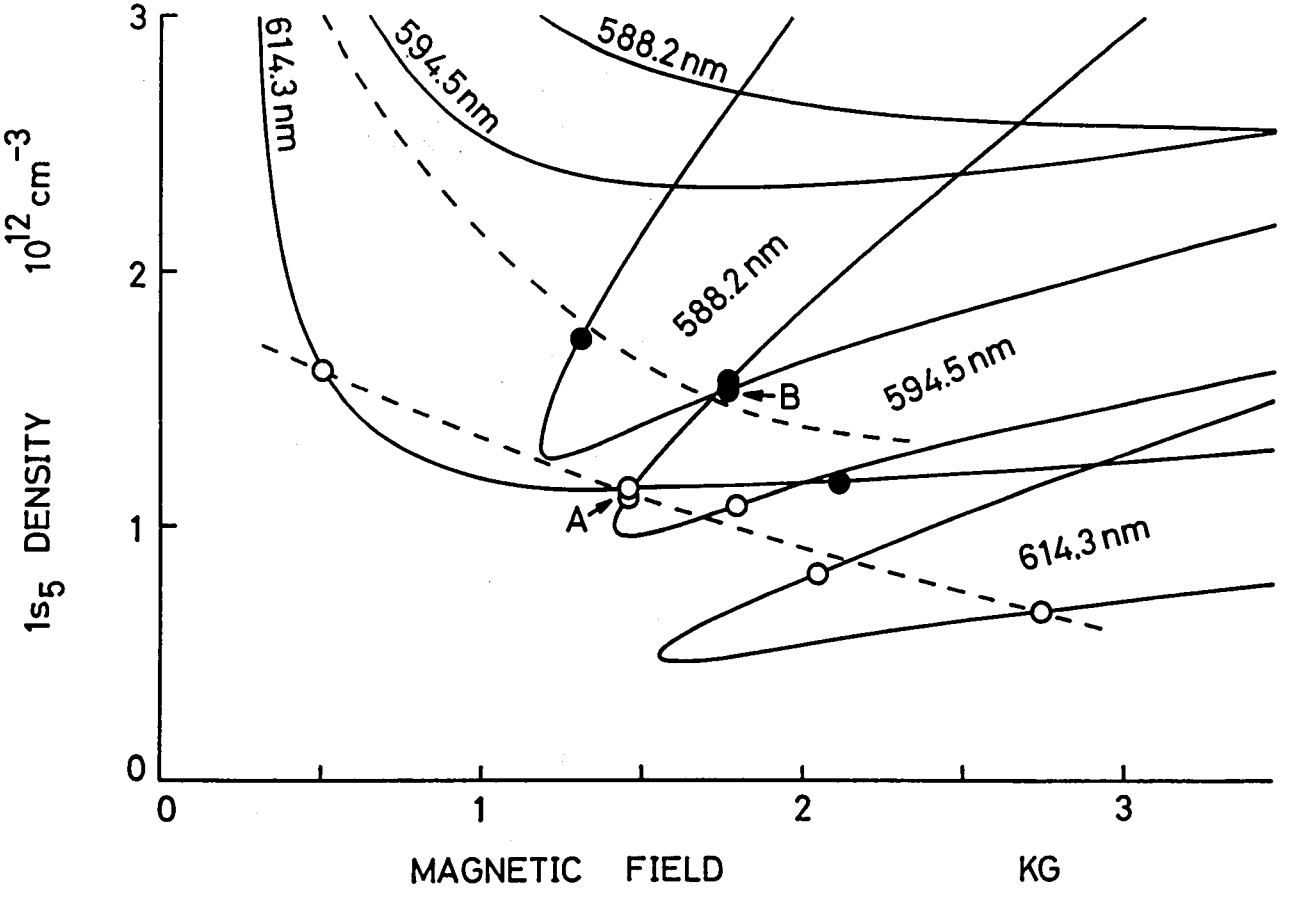


Fig. 4.12 Experimentally obtained magnetic field dependences of the $1s_5$ density. Open and filled circles show the cases of the neon pressure of 1.3 and 1.5 torr, respectively.

Supposing that transmission for the oscillation is 0.85, the experimentally obtained points at which oscillation frequencies change agree well with the crossing points of two boundaries of the theoretically obtained oscillation regions (A and B in Fig. 4.12). It is clear from Fig. 4.12 that the $1s_5$ density decreases with the increase of the magnetic field. There are two opposing effects in the glow discharge in the presence of a magnetic field; the increased concentration of electrons on the axis of a discharge tube, and the decrease in their energy.[127] The fall in the $1s_5$ density indicates a decrease in number of fast electrons, whose energies are sufficiant to excite neon atoms from the ground state to $1s_5$ state, energy separation being 16.6 eV. The densities of other state as functions of the magnetic field strength can be obtained in the same way.

## 4.5 Isotope Effect

Next, we will discuss the influence of the isotope on the transmission of the Faraday filter. The transmissions of the Faraday filter with the mixture of $Ne^{20}$ and $Ne^{22}$ are shown in Fig. 4.13, where the $1s_5$ density and the magnetic field strength are kept $7 \times 10^{11}$ $cm^{-3}$ and 2.5 kG respectively to compare the peak value of the second peak with that of the first peak (See Fig. 4.5(b) ). Parameter is the concentration of $Ne^{22}$. As seen in Fig. 4.13, when the concentration of $Ne^{22}$ is 9 percent

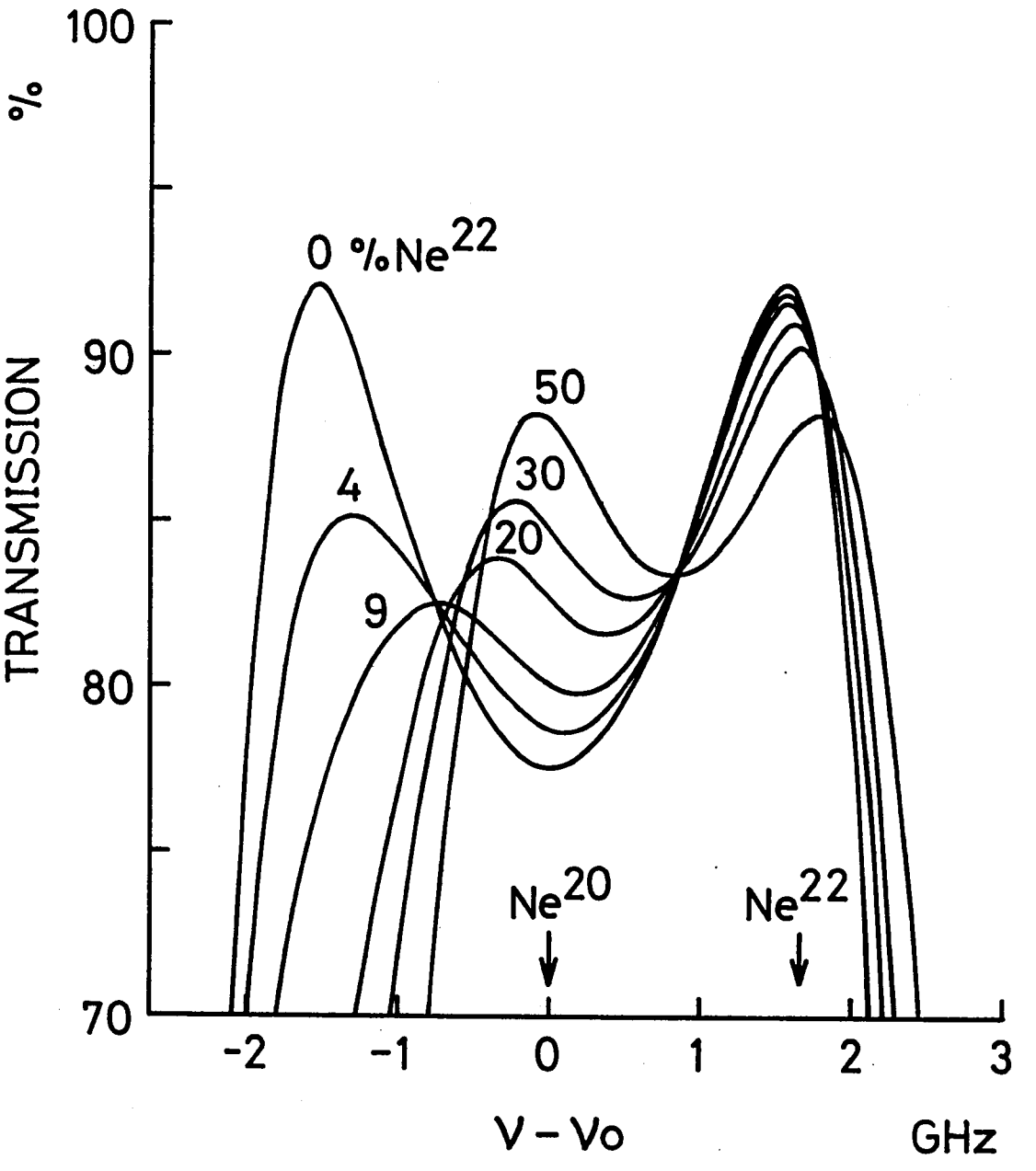


Fig. 4.13 Calculated transmissions of the Faraday filter with the mixtures of $Ne^{20}$ and $Ne^{22}$ at 614.3 nm in the case that the $1s_5$ density is $0.7 \times 10^{12}$ $cm^{-3}$ and the magnetic field strength is 2.5 kG.

($Ne^{20}$:$Ne^{22}$= 10:1) the peak value of the second (left) peak is reduced to minimum. This concentration coincides accidentally with the natural isotope abundance, so that we can use natural abundance neon ($Ne^{20}$:$Ne^{22}$= 10:1) to get the oscillation at peak in the high frequency side of the center regions. Similarly a mixture of inverse ratio ($Ne^{20}$:$Ne^{22}$= 1:10) can be used to get the oscillation at peak in the low frequency side. The same holds good for other lines.

The calculated values of the magnetic field dependence of the oscillation frequencies are shown in Fig. 4.14 in the cases of mixtures of $Ne^{20}$ and $Ne^{22}$, and pure isotopes. As seen in Fig. 4.14, the curves are symmetric in the case of pure isotopes ( A , E ) and a 1 : 1 mixture of $Ne^{20}$ and $Ne^{22}$ ( C ). When a 10 : 1 mixture ( B ) and a 1 : 10 mixture ( D ) are used, only higher frequency and lower frequency modes oscillate, respectively, as mentioned above. We can use A0-A1 and E0-E1 for the purpose of the frequency-locking to the center of the absorption lines for a long time because the oscillation frequency does not detune from the center of the absorption lines by the fluctuation of a magnetic field. We can use B0-B1 and D0-D1 for scanning of the oscillation frequencies in the vicinity of the absorption lines. Although the scanning of the oscillation frequency can be also achieved by a Faraday filter with a pure isotope, another undesired mode exists.

The single-mode oscillation just at the center was obtained with $Ne^{20}$ enriched neon (99.95 percent $Ne^{20}$) at the pressure of

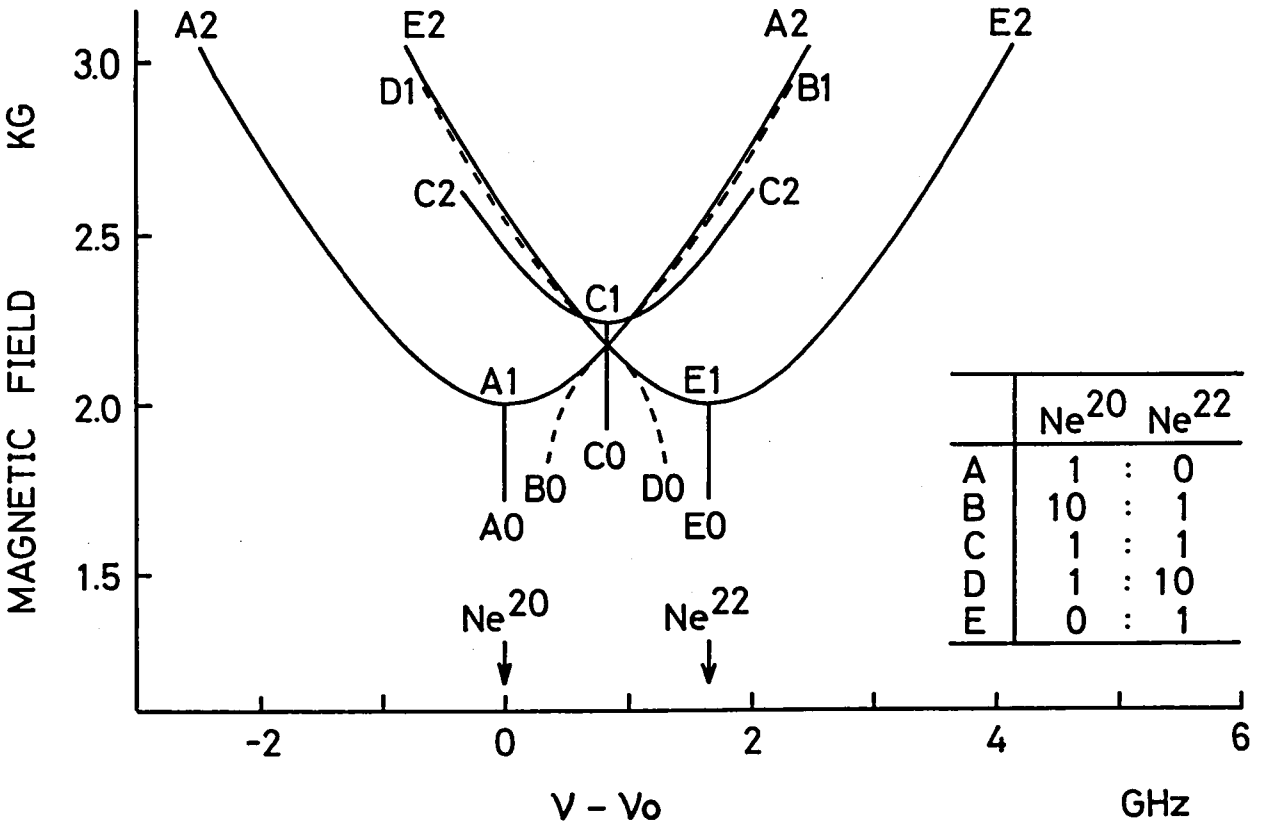


Fig. 4.14 Calculated values of the magnetic field dependence of the oscillation frequencies by the Faraday filter at 614.3 nm with pure isotopes $Ne^{20}$ (A) and $Ne^{22}$ (E), and their mixtures (B),(C) and (D) in the case of the $1s_5$ density $N=0.7 \times 10^{12}$ $cm^{-3}$.

1.3 torr and at the discharge current of 40 mA. In this case the single-mode oscillation split into two modes symmetric with respect to the line center when the magnetic field was increased. Since the cavity length was not adjusted so that the longitudinal cavity mode agreed with the line center, the oscillation took place on the nearest longitudinal cavity mode. Therefore, the precision and the stability of the frequency-locking were $\pm$75 MHz without cavity mode control.

In Fig. 4.14, we have shown the magnetic field dependence of the oscillation frequency at a certain constant $1s_5$ density. Next, we will consider the dependence on the $1s_5$ density. The calculated magnetic field dependence of the oscillation frequency for the case of natural abundance neon is shown in Fig. 4.15, where the parameter is the $1s_5$ density. At low $1s_5$ densities, the oscillation frequency shifts proportionally to the magnetic field and the tuning range is narrow. As increasing of the density, the tuning range is widened and we can sweep the oscillation frequency across the center of the absorption line of $Ne^{22}$. As seen in Fig. 4.15, by the further increasing of the density, the curve has a corner and the curve can be separated into two regions where the oscillation frequency is independent of the magnetic field and where it is dependent. At the same time, by increasing the density, the red side peak of the transmission curve appears, but it is not shown in Fig. 4.15 to simplify the figure. That is, the shape of the magnetic field dependence of the oscillation frequency varies from the type ( B ) to the type ( A ) shown in

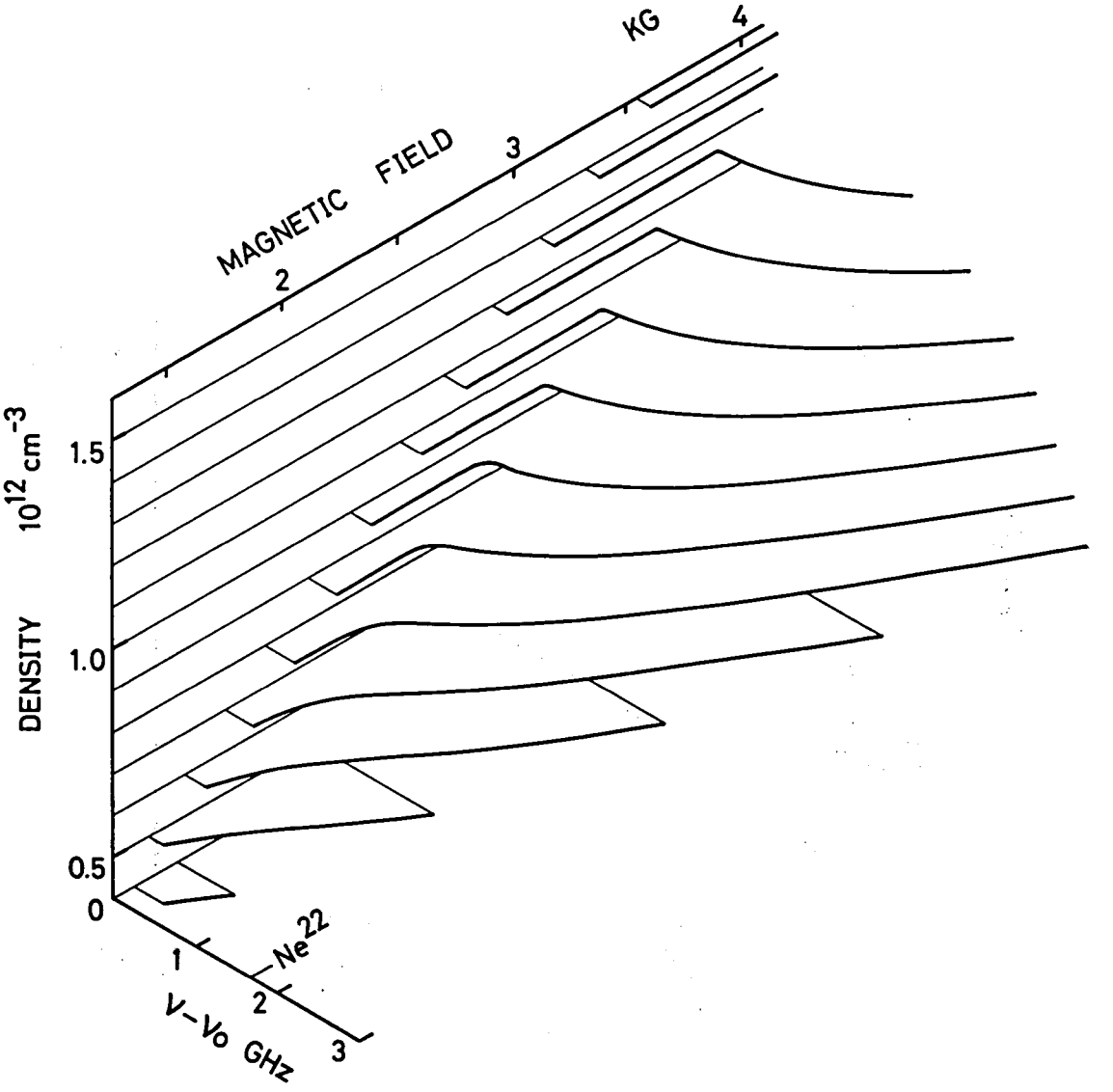


Fig. 4.15 Calculated values of the magnetic field dependence of the oscillation frequencies by the Faraday filter at 614.3 nm with natural abundance neon at various $1s_5$ densities.

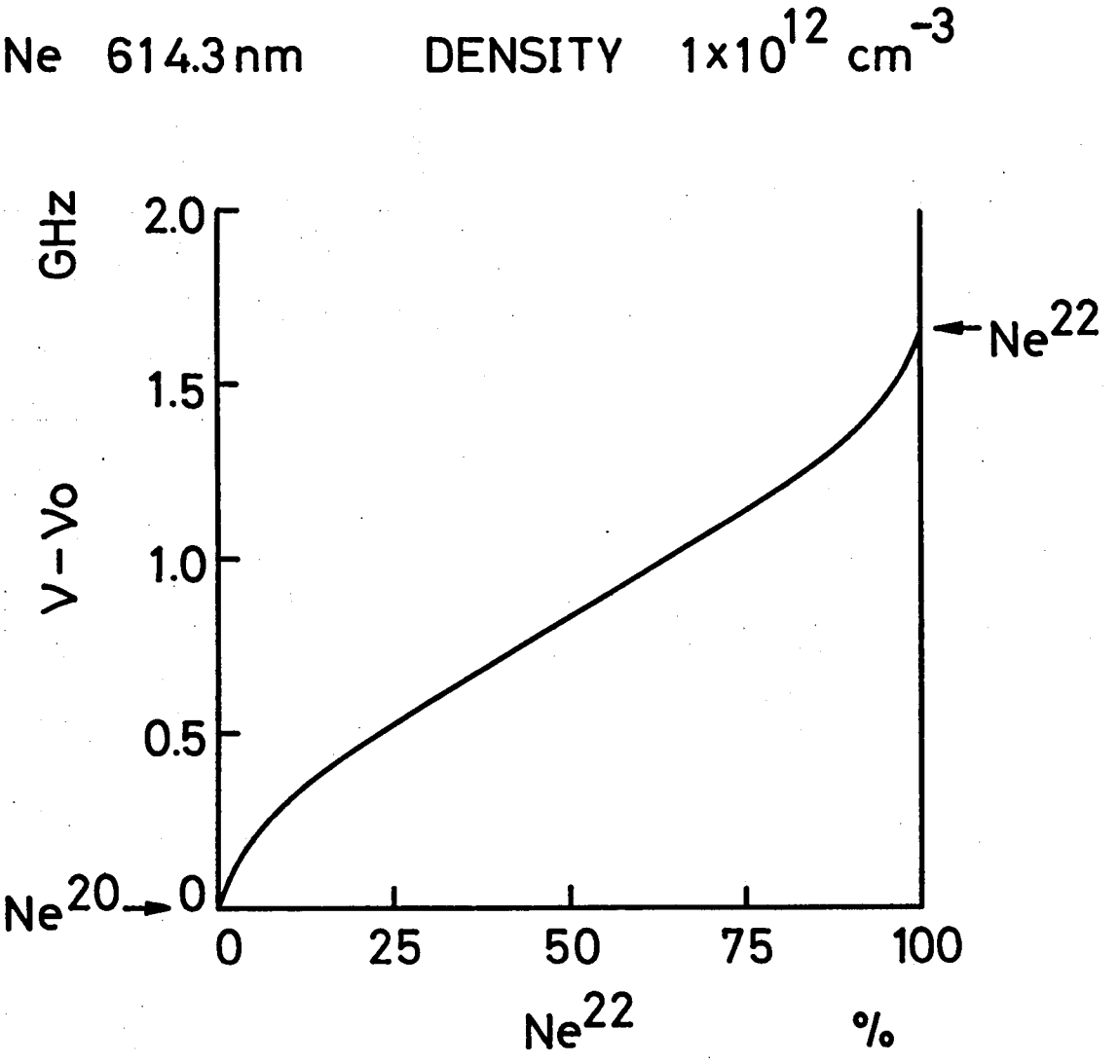


Fig. 4.16 Calculated values of the oscillation frequencies by the Faraday filter at 614.3 nm as a function of the concentration of $Ne^{22}$ in the case of the $1s_5$ density $N=1 \times 10^{12}$ $cm^{-3}$.

Fig. 4.14. It should be noted that the oscillation frequency in the region where it is independent of the magnetic field is shifted from the center of the $Ne^{20}$ absorption line toward the $Ne^{22}$ line center. This region is usefull for the case of the frequency-locking with a certain detuning from the line center for a long time, since the oscillation frequency is not changed by the fluctuation of the magnetic field and its dependence on the density is small. The detuning frequency is a function of the ratio of the mixture of $Ne^{20}$ and $Ne^{22}$ as shown in Fig. 4.16.

As a result of above discussion, it becomes evident that we can obtain the Faraday filter suitable for the desired purpose by the isotope effect.

## 4.6 Saturation Effect at Line Center

The single-mode oscillations at the absorption lines from the $1s_4$ state, such as the line at 607.4 nm ($1s_4$-$2p_3$) took place only when the longitudinal mode of cavity passed just through the center of the line. This phenomenon can be explained as an optical saturation by two $\sigma^-$ polarized monochromatic waves propagating to opposite directions, which is analogous to the ordinary saturated absorption if we do not take account of the polarization of light. Consequently, it must be convenient to discuss this in terms of the hole burning.[128] Consider an atomic system with optically coupled two levels, both of which

have the total angular momentum J=1. As shown in Fig. 4.17(a), the $\sigma^-$ polarized monochromatic waves induce four transitions in the ensemble of atoms having various velocities. When the g-factor of upper and lower states are different, these four transitions have different frequencies, so that each transition may occur in a group of atoms having a particular velocity along the direction of the light propagation. These four transitions can be devided into two groups, one having a common sublevel in the upper level, and another having it in the lower level, so that these groups can be considered separately, if the coupling between these group by the processes of spontaneous emission and relaxation by atomic collisions is weak. As shown in Fig. 4.17(b), the two light waves in $\sigma^-$ modes may burn four holes in the velocity distribution of atoms in the substate $m_L=0$ of the lower state at the velocities

$$v_z = ( \pm\Omega_U \pm \Delta\omega )/k \ , \qquad (4.1)$$

where $\Omega_U$ is the Larmor frequency in the upper state, $\Delta\omega$ is the detuning of the light frequency from the transition frequency between the substate $m_L=0$ and $m_U=0$, and k is the wave number. Therefore, if the detuning $\Delta\omega$ is zero, two holes in the positive or negative region of $v_z$ overlap to each other at $v_z=\Omega_U/k$ or $-\Omega_U/k$, which may result in the increase of the saturation at the line center. Similarly, the velocity distribution of atoms in the substate $m_U=0$ in the upper state

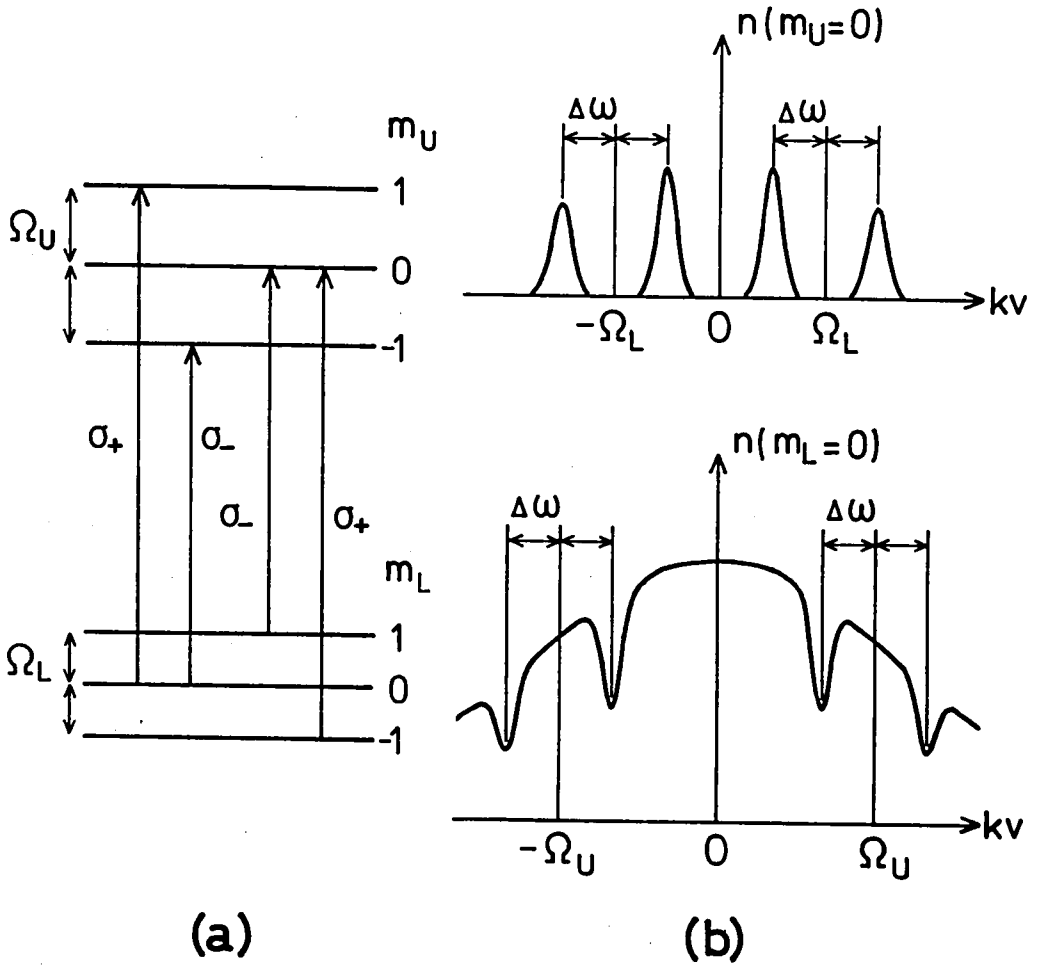


Fig. 4.17 (a) Allowed transitions between the states with J=1 by the $\sigma^-$ polarized light. (b) The positions of holes and peaks in the velocity distribution of atoms in the states with $m_L=0$ and $m_U=0$.

has four peaks and each peak overlaps to the other when $\Delta\omega=0$, which may cause also the increase of the saturation at the line center. This saturation phenomenon in a magnetic field has been studied theoretically in the case of a gas laser amplifier,[129),130)] and actually observed by Gorlicki and Dumont in the saturated absorption of neon which is placed outside of a He-Ne laser operating at 632.8 nm ($3s_2$-$2p_4$).[131)]

We could not observe above phenomenon in the oscillations at the lines originating from the $1s_5$ state. The reason might be partially due to the fact that the $1s_5$ state and the 2p states associated with these oscillations have total angular momenta larger than 2, so that the number of Zeeman components which do not contribute to the increase of saturation at $\Delta\omega=0$ is larger than that of the line from the $1s_4$ state.

Here we would like to show that the optical saturation for the absorption line from a long-life state such as the 1s states of neon takes place generally in a weak laser field, because of the fact the upper state has stronger branches for spontaneous emission. Consider here a nondegenerate two-level atom with the upper state $|a\rangle$ and the lower state $|b\rangle$, which are connected to each other by a monochromatic field with the frequency $\omega$. If the decay rates of the states $|a\rangle$ and $|b\rangle$ are denoted by $\gamma_a$ and $\gamma_b$ and the decay rate of coherence between these states by $\gamma_{ab}$, the saturation parameter[132)] can easily be calculated with a semiclassical density

formalism as

$$I_s = \frac{1}{2}(p\,E)^2 \frac{1}{\gamma_{ab}} \left(\frac{1}{\gamma_a} + \frac{\eta}{\gamma_b}\right), \qquad (4.2)$$

where $p$ is the electric dipole moment, $E$ the electric field, and $\eta$ the fraction of the decay rate from the state $|a\rangle$ to the states other than $|b\rangle$ in the total decay rate $\gamma_a$. In both cases that the state $|b\rangle$ is the ground state to which $I_s$ is given by setting $\eta=0$ in eq. (4.2) and that it is the short-life excited state, the decay rate $\gamma_a$ of the upper state plays an important role to determine the value of $I_s$. On the other hand, when $|b\rangle$ is the long-life state and $\eta$ is not zero, $I_s$ becomes independent of $\gamma_a$ and it is mainly determined by the quantity $\eta/\gamma_b$. As the result, we have generally a large saturation parameter for the absorption lines originating from the 1s states of neon. Despite this large saturation in the light absorption, the optical rotation is not significantly affected by a strong laser field, because the non-resonant atoms Doppler shifted away from the resonance contribute primarily to the dispersion.
It should be noted that $\gamma_b$ in eq. (4.2) is mainly determined by the transit-time of atoms across the laser beam for the $1s_5$ state, since it is of the order of $10^{-6}$ sec while the lifetime of this state is of the order of $10^{-4}$ sec[123),133)].

## 4.7 Faraday Filter with a He-Ne Discharge

The frequency-locking to the 638.3 nm ($1s_4$-$2p_7$) and the 626.7 nm ($1s_3$-$2p_5$) lines were not achieved by the neon Faraday filter. As seen in Fig. 4.8(b) and (c), the lowest magnetic field strength for the frequency-locking to these lines is higher than that for the other lines, so that the 1s densities in such a strong magnetic field must have been not enough to achieve the frequency-locking. We used an He-Ne discharge in order to increase the 1s densities. The frequency-locking to these two lines was achieved by a 4 : 1 mixture of He and Ne at a total pressure of 1.3 torr and a discharge current of 40 mA.

## 4.8 Conclusions

The oscillation frequency of a CW dye laser was locked to eight neon absorption lines from the 1s states to the 2p states by a Faraday filter. The oscillation took place in a single longitudinal cavity mode.

It should be noted that the frequency-locking was achieved for the absorption lines from metastable and quasi-metastable states. This gives a wide area of application to the Faraday filter.

When natural abundance neon was used, the oscillation freauency in the center region of the absoption lines shifted toward higher frequency and that on the red wing shifted toward

lower frequency with an increase in magnetic field. When $Ne^{20}$ was used, the oscillation took place just at the center of the $Ne^{20}$ absorption line, and it split into two modes symmetric with respect to the line center when the magnetic field was increased. This is just as predicted by the theory. From these experimental results and theoretical calculations, we developed a technique for fine tuning of the CW dye laser in the vicinity of the absorption line by means of isotope effect.

We measured also the 1s densities in the positive column of the glow discharge in the presence of a magnetic field by fitting the experimental results to the theory.

We observed a saturation phenomenon in the single-mode oscillation at a line center caused by two $\sigma^-$ polarized monochromatic waves propagating to opposite directions.

# CHAPTER V

# FREQUENCY-LOCKING TO A HELIUM ABSORPTION LINE

## 5.1 Introduction

In this chapter, we describe the frequency-locking of a CW dye laser to the 587.6 nm absorption line ($2^3P$-$3^3D$) of helium in a gas discharge by a Faraday filter. The $2^3P$ state is not metastable nor quasi-metastable state, but has the large population density of the order of $10^{12}$ $cm^{-3}$ in the positive column of a glow discharge.[134)~136)] The oscillator strength of this absorption line is 0.167[124)] so that the product of the lower level density and the oscillator strength Nf becomes larger than $10^{11}$ $cm^{-3}$, i.e., satisfies the condition for the frequency-locking by a Faraday filter.

Particular attention is given to the influence of fine structure of the upper and lower states of an absorption line on the Faraday filter. The $2^3P$ and $3^3D$ states have fine structures,[137)] and the fine structure couplings are not solved in the magnetic field region where the frequency-locking occurs.[138)~141)] Therefore the transmission of the Faraday filter has complicated magnetic field dependence. We have obtained experimentally a narrow spectrum located on blue wing of the line, which is

predicted by the theoretical calculation to be the easiest mode to get.

## 5.2 Transmission of the Faraday Filter

The energy level diagram of helium is shown in Fig. 5.1. We will calculate the transmission of the Faraday filter at the 587.6 nm absorption line. The triplet fine structures of the $2^3P$ and $3^3D$ states are shown in Fig. 5.2, where the corresponding spectra and their relative intensities are also shown. The fine structure couplings are partially solved in the magnetic field region where we have interest for the Faraday filter. The energy levels do not linearly depend on the magnetic field strength and the transition strengths for $\sigma$ lights are functions of the magnetic field strength. That is, $\beta_j$ and $g$ in eqs. (3.3),(3.4) and (3.5) become functions of the magnetic field.

The Zeeman Hamiltonian for the $2^3P$ and $3^3D$ states can be written as[138]

$$\mathcal{H} = \mathcal{H}_{fs} + g_S \mu_0 \vec{S} \vec{H} + g_L \mu_0 \vec{L} \vec{H} , \qquad (5.1)$$

where $\mathcal{H}_{fs}$ contains the spin-orbit and spin-spin operators which lead to the fine structure. $\vec{L}$ and $\vec{S}$ are the total orbital and spin angular momentum operators, respectively. $g_S$ and $g_L$ are the usual electronic spin and orbital g-factors, respectively,

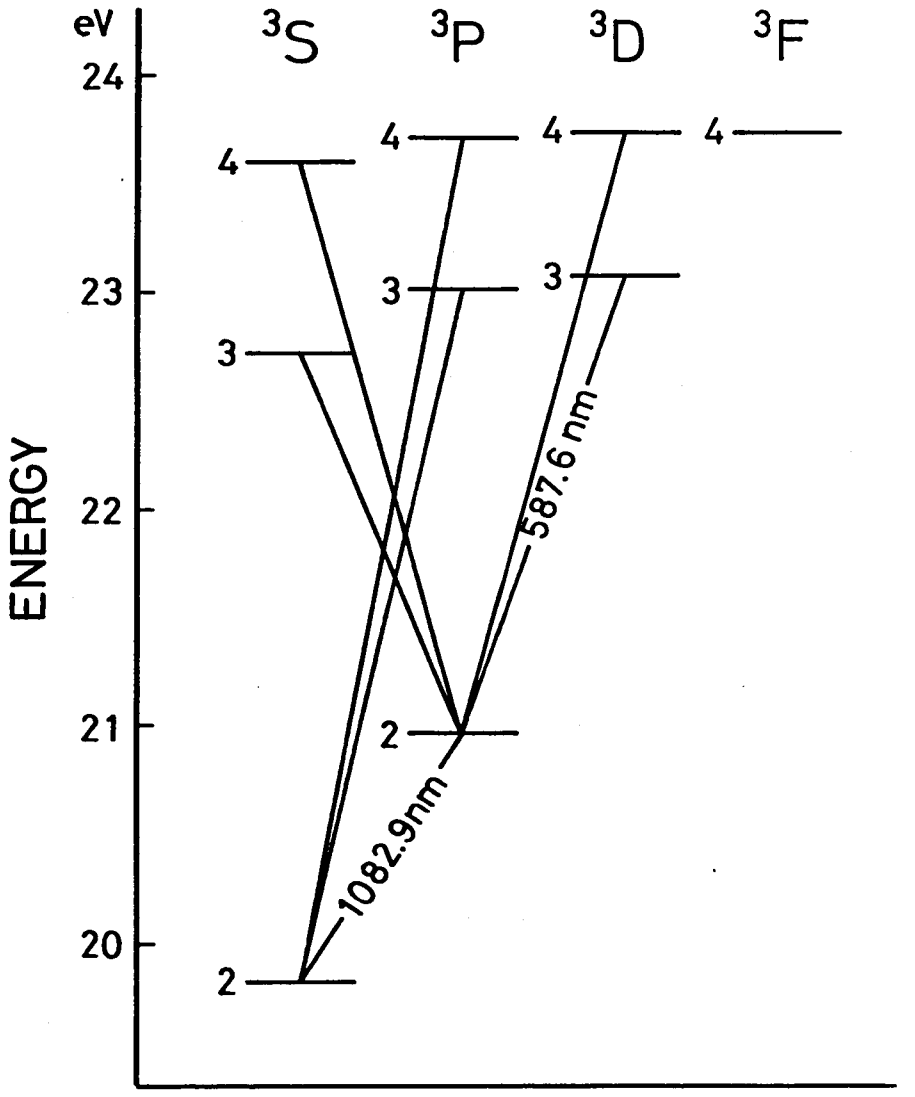


Fig. 5.1 Energy level diagram of orthohelium. The ground state and the ionization limit which lie 19.82 eV below the metastable $2^3S$ state and at 24.59 eV are omitted.

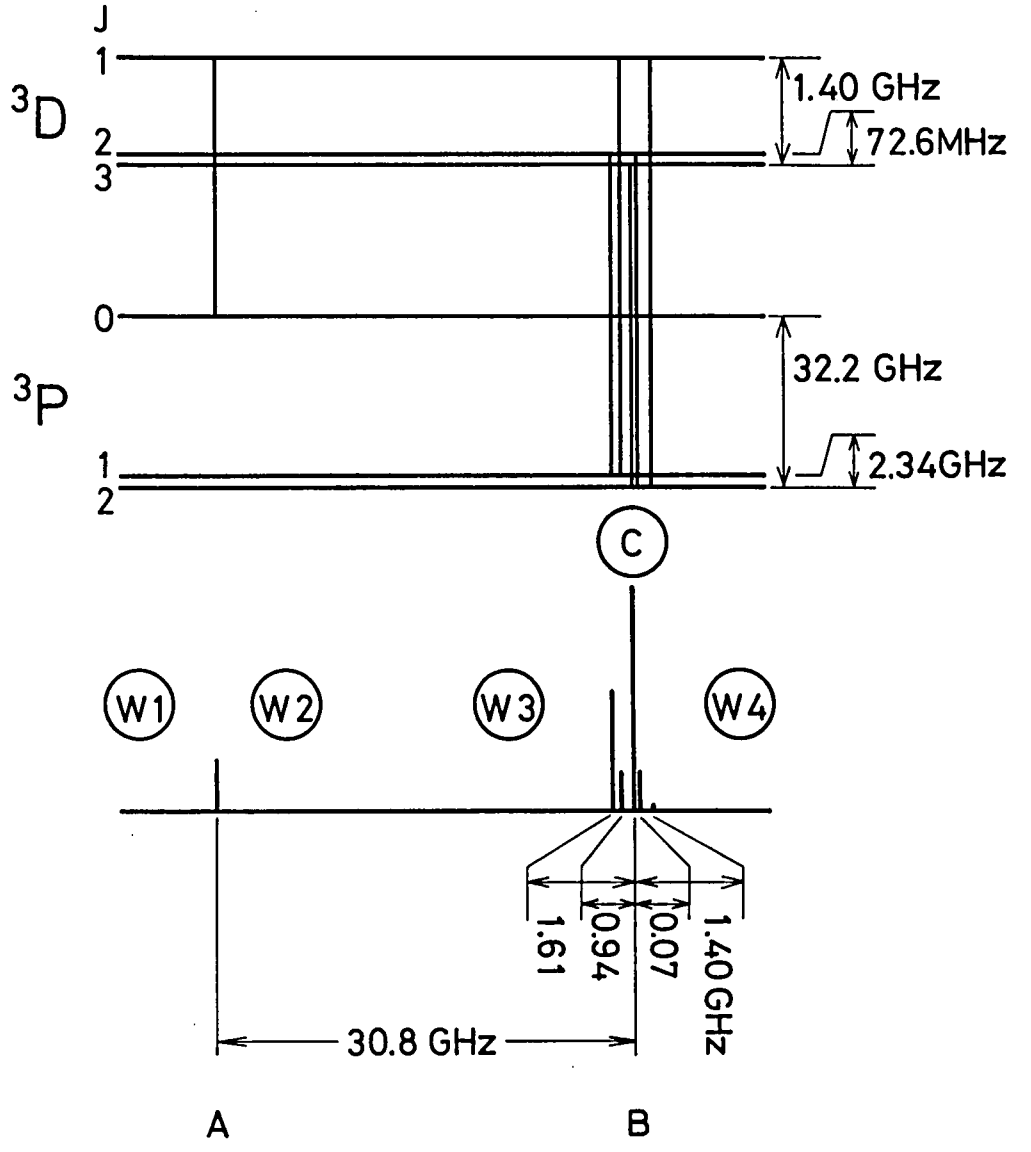


Fig. 5.2 Fine structures of the $^3P$ and $^3D$ states and allowed transition components. The corresponding spectra with their relative intensities are also shown in the bottom. W1, W2, W3, W4 and C denote the frequency regions where the frequency-locking occurs under the condition shown in Fig. 5.6.

and which are given as $g_L=1$, $g_S=2.00232$, and $\mu_0$ is the Bohr magneton. If we assume that $\vec{H}$ is the uniform magnetic field in the z direction

$$\mathcal{H} = \mathcal{H}_{fs} + g_S \mu_0 S_z H + g_L \mu_0 L_z H, \tag{5.2}$$

where H is the amplitude of the magnetic field.

Since $\mathcal{H}_{fs}$ is diagonal in J, we will be concerned only with its eigen-values $E_J$ in a representation wherein J is itself diagonal. The Zeeman Hamiltonian $\mathcal{H}$ is not diagonal in J, owing to the presence of the field-dependent terms. These terms couple states which have the same $m_J$. It is convenient to set up the Hamiltonian in a representation in which the angular-momentum eigenfunctions $|J\ m_J\rangle$ are the bases. The energy levels are obtained by solving the secular equations. The eigenfunctions $|J\ m_J\rangle$ are linear combinations of products of eigenfunction of $L_z$ and $S_z$ separately,

$$|J,m_J\rangle = \sum_{m_L} \sum_{m_S} \langle m_L\ m_S | J\ m_J\rangle\ |m_L\ m_S\rangle \tag{5.3}$$

$$m_J = m_L + m_S\ , \tag{5.4}$$

where $\langle m_L\ m_S \mid J\ m_J\rangle$ are Clebsch-Gordan coefficients.[142] These coefficients are tabulated in Tables 5.1 and 5.2 for the $2^3P$ state and the $3^3D$ state, respectively.

In magnetic field H the angular momenta $\vec{L}$ and $\vec{S}$ are somewhat uncoupled, so that J loses its significance as a good

Table 5.1 Clebsch-Gordan Coefficients $\langle m_L\ m_S \mid J\ m_J \rangle$ for the State $2^3P$

| | | $m_L$ / $m_S$ | | | | | | | | |
|---|---|---|---|---|---|---|---|---|---|---|
| | | 1 / 1 | 1 / 0 | 0 / 1 | 1 / -1 | 0 / 0 | -1 / 1 | 0 / -1 | -1 / 0 | -1 / -1 |
| $J, m_J$ | 2, 2 | 1 | | | | | | | | |
| | 2, 1 | | $\frac{1}{\sqrt{2}}$ | $\frac{1}{\sqrt{2}}$ | | | | | | |
| | 1, 1 | | $\frac{1}{\sqrt{2}}$ | $-\frac{1}{\sqrt{2}}$ | | | | | | |
| | 2, 0 | | | | $\frac{1}{\sqrt{6}}$ | $\frac{2}{\sqrt{3}}$ | $\frac{1}{\sqrt{6}}$ | | | |
| | 1, 0 | | | | $\frac{1}{\sqrt{2}}$ | 0 | $-\frac{1}{\sqrt{2}}$ | | | |
| | 0, 0 | | | | $\frac{1}{\sqrt{3}}$ | $-\frac{1}{\sqrt{3}}$ | $\frac{1}{\sqrt{3}}$ | | | |
| | 2,-1 | | | | | | | $\frac{1}{\sqrt{2}}$ | $\frac{1}{\sqrt{2}}$ | |
| | 1,-1 | | | | | | | $\frac{1}{\sqrt{2}}$ | $-\frac{1}{\sqrt{2}}$ | |
| | 2,-2 | | | | | | | | | 1 |

Table 5.2 Clebsch-Gordan Coefficients $\langle m_L\ m_S \mid J\ m_J \rangle$ for the State $3^3D$

| | | $m_L$ / $m_S$ | | | | | | | | | | | | | |
|---|---|---|---|---|---|---|---|---|---|---|---|---|---|---|---|
| | | 2 / 1 | 2 / 0 | 1 / 1 | 2 / -1 | 1 / 0 | 0 / 1 | 1 / -1 | 0 / 0 | -1 / 1 | 0 / -1 | -1 / 0 | -2 / 1 | -1 / -1 | -2 / 0 | -2 / -1 |
| $J, m_J$ | 3, 3 | 1 | | | | | | | | | | | | | | |
| | 3, 2 | | $\frac{1}{\sqrt{3}}$ | $\frac{2}{\sqrt{3}}$ | | | | | | | | | | | | |
| | 2, 2 | | $\frac{2}{\sqrt{3}}$ | $-\frac{1}{\sqrt{3}}$ | | | | | | | | | | | | |
| | 3, 1 | | | | $\frac{1}{\sqrt{15}}$ | $\frac{6}{\sqrt{15}}$ | $\frac{2}{\sqrt{5}}$ | | | | | | | | | |
| | 2, 1 | | | | $\frac{1}{\sqrt{3}}$ | $\frac{1}{\sqrt{6}}$ | $-\frac{1}{\sqrt{2}}$ | | | | | | | | | |
| | 1, 1 | | | | $\frac{2}{\sqrt{5}}$ | $\frac{3}{\sqrt{10}}$ | $\frac{1}{\sqrt{10}}$ | | | | | | | | | |
| | 3, 0 | | | | | | | $\frac{1}{\sqrt{5}}$ | $\frac{3}{\sqrt{5}}$ | $\frac{1}{\sqrt{5}}$ | | | | | | |
| | 2, 0 | | | | | | | $\frac{1}{\sqrt{2}}$ | 0 | $-\frac{1}{\sqrt{2}}$ | | | | | | |
| | 1, 0 | | | | | | | $\frac{3}{\sqrt{10}}$ | $-\frac{2}{\sqrt{5}}$ | $\frac{3}{\sqrt{10}}$ | | | | | | |
| | 3,-1 | | | | | | | | | | $\frac{2}{\sqrt{5}}$ | $\frac{8}{\sqrt{15}}$ | $\frac{1}{\sqrt{15}}$ | | | |
| | 2,-1 | | | | | | | | | | $\frac{1}{\sqrt{2}}$ | $\frac{1}{\sqrt{6}}$ | $\frac{1}{\sqrt{3}}$ | | | |
| | 1,-1 | | | | | | | | | | $\frac{1}{\sqrt{10}}$ | $\frac{3}{\sqrt{10}}$ | $\frac{2}{\sqrt{5}}$ | | | |
| | 3,-2 | | | | | | | | | | | | | $\frac{2}{\sqrt{3}}$ | $\frac{1}{\sqrt{3}}$ | |
| | 2,-2 | | | | | | | | | | | | | $\frac{1}{\sqrt{3}}$ | $-\frac{2}{\sqrt{3}}$ | |
| | 3,-3 | | | | | | | | | | | | | | | 1 |

quantum number. We will nevertheless label states by a symbol $\mathcal{J}$ which denotes the J-value from which the state derives in zero field.

The matrix $\langle J' m_J' | \mathcal{H} | J\ m_J \rangle$ can be obtained by using Tables 5.1 and 5.2. The results are tabulated in Tables 5.3 and 5.4. The energy levels are obtained by diagonalizing these matrices. The calculated energy levels as functions of the magnetic field are shown in Fig. 5.3 and Fig. 5.4 for the $2^3P$ and the $3^3D$ states, respectively.

The wave function for state $|\mathcal{J}\ m_J\rangle$ is written as

$$|\mathcal{J}\ m_J\rangle = \sum_J \langle J\ m_J | \mathcal{J}\ m_J\rangle\ |J\ m_J\rangle \ , \qquad (5.5)$$

where the coefficients $\langle J\ m_J | \mathcal{J}\ m_J\rangle$ can be calculated from the eigenvalues of the matrix $\langle J' m_J' | \mathcal{H} | J\ m_J\rangle$, so that $\sum_J |\langle J\ m_J | \mathcal{J}\ m_J\rangle|^2 = 1$.

The electric dipole matrix elements are diagonal in $S_z$, and it will be convenient to expand $|\mathcal{J}\ m_J\rangle$ as linear combination of the products $|m_L\rangle$ and $|m_S\rangle$. Then we obtain

$$\begin{aligned} |\mathcal{J}\ m_J\rangle &= \sum_J \langle J\ m_J | \mathcal{J}\ m_J\rangle\ |J\ m_J\rangle \\ &= \sum_J \langle J\ m_J | \mathcal{J}\ m_J\rangle \left\{ \sum_{m_S} \langle m_L\ m_S | J\ m_J\rangle\ |m_L\ m_S\rangle \right\} \\ &= \sum_{m_S} \left\{ \sum_J \langle J\ m_J | \mathcal{J}\ m_J\rangle \langle m_L\ m_S | J\ m_J\rangle\ |m_L\ m_S\rangle \right\} \end{aligned}$$

Table 5.3 Secular Matrix $\langle J' m_J' | \mathcal{H} | J\ m_J \rangle$ for the State $2^3P$

| | | $J$ $m_J$ | | | | | | | | |
|---|---|---|---|---|---|---|---|---|---|---|
| | | 2 2 | 2 1 | 1 1 | 2 0 | 1 0 | 0 0 | 2 -1 | 1 -1 | 2 -2 |
| $J', m_J'$ | 2, 2 | (1) | | | | | | | | |
| | 2, 1 | | (2) | (10) | | | | | | |
| | 1, 1 | | (10) | (3) | | | | | | |
| | 2, 0 | | | | (4) | (11) | | | | |
| | 1, 0 | | | | (11) | (5) | (12) | | | |
| | 0, 0 | | | | | (12) | (6) | | | |
| | 2,-1 | | | | | | | (7) | (10) | |
| | 1,-1 | | | | | | | (10) | (8) | |
| | 2,-2 | | | | | | | | | (9) |

$$(1) = E_2 + (g_L + g_S)\mu_0 H \qquad (10) = \frac{1}{2}(g_L - g_S)\mu_0 H$$

$$(2) = E_2 + \frac{1}{2}(g_L + g_S)\mu_0 H \qquad (11) = \sqrt{\frac{1}{3}}(g_L - g_S)\mu_0 H$$

$$(3) = E_1 + \frac{1}{2}(g_L + g_S)\mu_0 H \qquad (12) = \sqrt{\frac{2}{3}}(g_L - g_S)\mu_0 H$$

$$(4) = E_2$$

$$(5) = E_1$$

$$(6) = E_0$$

$$(7) = E_2 - \frac{1}{2}(g_L + g_S)\mu_0 H$$

$$(8) = E_1 - \frac{1}{2}(g_L + g_S)\mu_0 H$$

$$(9) = E_2 - (g_L + g_S)\mu_0 H$$

Table 5.4 Secular Matrix $\langle J' m_J' | \mathcal{H} | J\ m_J \rangle$ for the State $3^3D$

| | | $J$ / $m_J$ | 3 | 3 | 2 | 3 | 2 | 1 | 3 | 2 | 1 | 3 | 2 | 1 | 3 | 2 | 3 |
|---|---|---|---|---|---|---|---|---|---|---|---|---|---|---|---|---|---|
| | | | 3 | 2 | 2 | 1 | 1 | 1 | 0 | 0 | 0 | -1 | -1 | -1 | -2 | -2 | -3 |
| | 3, 3 | | (1) | | | | | | | | | | | | | | |
| | 3, 2 | | | (2) | | (16) | | | | | | | | | | | |
| | 2, 2 | | | (16) | | (3) | | | | | | | | | | | |
| | 3, 1 | | | | | (4) | | (17) | | | | | | | | | |
| | 2, 1 | | | | | (17) | | (5) | | (18) | | | | | | | |
| | 1, 1 | | | | | | | (18) | | (6) | | | | | | | |
| | 3, 0 | | | | | | | | | (7) | | (19) | | | | | |
| $J', m_J'$ | 2, 0 | | | | | | | | | (19) | | (8) | | (20) | | | |
| | 1, 0 | | | | | | | | | | | (20) | | (9) | | | |
| | 3,-1 | | | | | | | | | | | | | (10) | | (18) | |
| | 2,-1 | | | | | | | | | | | | | (18) | | (11) | (17) |
| | 1,-1 | | | | | | | | | | | | | | | (17) | (12) |
| | 3,-2 | | | | | | | | | | | | | | | | (13) (16) |
| | 2,-2 | | | | | | | | | | | | | | | | (16) (14) |
| | 3,-3 | | | | | | | | | | | | | | | | (15) |

$(1) = E_3 + (2g_L + g_S)\mu_\cdot H$

$(2) = E_3 + \frac{2}{3}(2g_L + g_S)\mu_\cdot H$

$(3) = E_2 + \frac{1}{3}(5g_L + g_S)\mu_\cdot H$

$(4) = E_3 + \frac{1}{3}(2g_L + g_S)\mu_\cdot H$

$(5) = E_2 + \frac{1}{6}(5g_L + g_S)\mu_\cdot H$

$(6) = E_1 + \frac{1}{2}(3g_L + g_S)\mu_\cdot H$

$(7) = E_3$

$(8) = E_2$

$(9) = E_1$

$(10) = E_3 - \frac{1}{3}(2g_L + g_S)\mu_\cdot H$

$(11) = E_2 - \frac{1}{6}(5g_L + g_S)\mu_\cdot H$

$(12) = E_1 - \frac{1}{2}(3g_L - g_S)\mu_\cdot H$

$(13) = E_3 - \frac{2}{3}(2g_L + g_S)\mu_\cdot H$

$(14) = E_2 - \frac{1}{3}(5g_L + g_S)\mu_\cdot H$

$(15) = E_3 - (2g_L + g_S)\mu_\cdot H$

$(16) = \frac{\sqrt{2}}{3}(g_L - g_S)\mu_\cdot H$

$(17) = \frac{4}{3\sqrt{5}}(g_L - g_S)\mu_\cdot H$

$(18) = \frac{3}{2\sqrt{5}}(g_L - g_S)\mu_\cdot H$

$(19) = \frac{2}{\sqrt{10}}(g_L - g_S)\mu_\cdot H$

$(20) = \sqrt{\frac{3}{5}}(g_L - g_S)\mu_\cdot H$

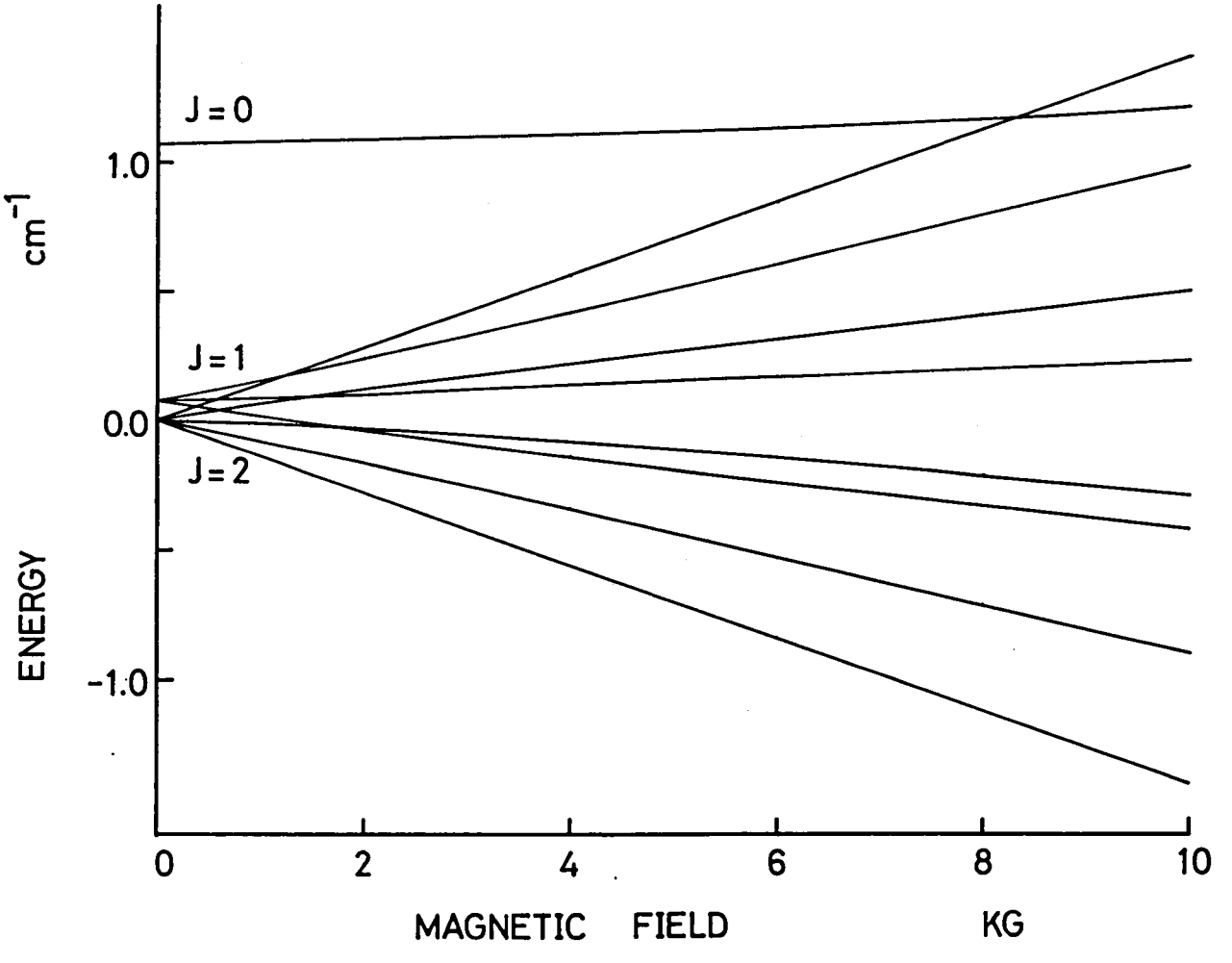


Fig. 5.3 Energy levels of $2^3P$ as a function of magnetic field.

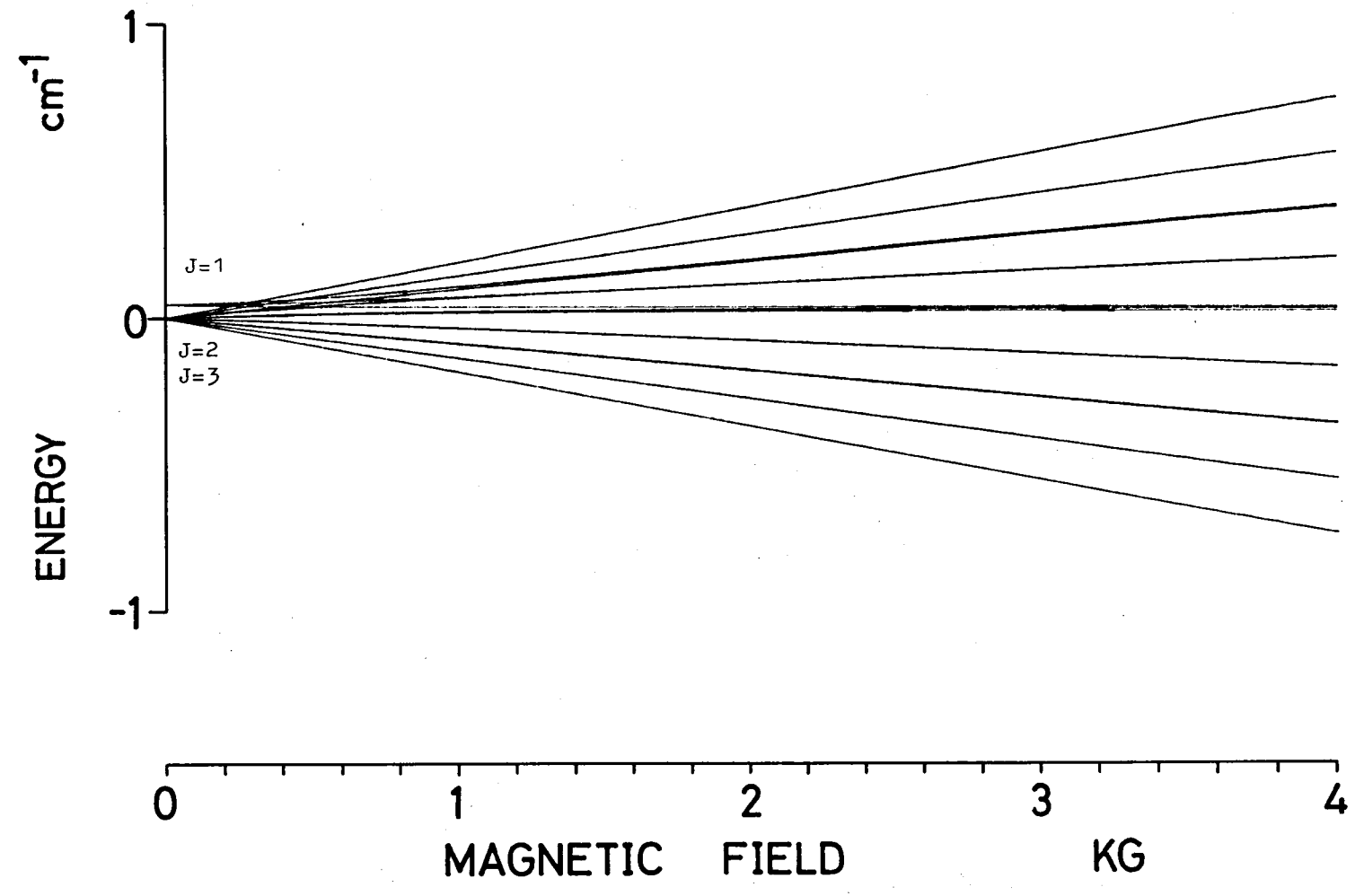


Fig. 5.4 Energy levels of $3^3D$ as a function of magnetic field.

$$= \sum_{m_S} \langle m_L\ m_S \,|\, \mathcal{J}\ m_J \rangle \,|\, m_L\ m_S \rangle \ . \qquad (5.6)$$

The electric dipole matrix elements $\langle \mathcal{J}' m_J' |\ \mathrm{d}\ | \mathcal{J}\ m_J \rangle$ can be calculated as

$$\langle \mathcal{J}' m_J' |\ \mathrm{d}\ | \mathcal{J}\ m_J \rangle$$

$$= \sum_{m_S} \sum_{m_S} \langle m_L'\ m_S' | \mathcal{J}' m_J' \rangle \langle m_L\ m_S | \mathcal{J}\ m_J \rangle \langle m_L'\ m_S' | \mathrm{d} | m_L\ m_S \rangle \ , \qquad (5.7)$$

where $\langle m_L\ m_S \,|\, \mathcal{J}\ m_J \rangle$ can be obtained from eq. (5.6)

$$\langle m_L\ m_S | \mathcal{J}\ m_J \rangle = \sum_J \langle J\ m_J | \mathcal{J}\ m_J \rangle \langle m_L\ m_S \,|\, J\ m_J \rangle \ , \qquad (5.8)$$

$\langle m_L\ m_S |\ \mathrm{d}\ | m_L\ m_S \rangle$ can be obtained by the relations similar to eqs. (2.33) and (2.34). The calculated matrix is shown in Table 5.5, where the suffices + and - indicate the $\sigma_+$ and $\sigma_-$ absorption, respectively.

We can calculate the energy levels and the transition strengths in any given field by using above equations. The absorption spectral patterns by computer calculation are shown in Fig. 5.5.

Next, we will obtain the conditions of the density N and the magnetic field H for the frequency-locking to the absorption lines. These conditions can be calculated by using eqs. (3.1), (3.2), (3.3), (3.4), and (3.16), and the spectral pattern. The calculated condition under which the transmission $\tau$ is larger than 0.85 is shown in Fig. 5.6. In Fig. 5.6, W1, W2,

Table 5.5 Electric Dipole Matrix Elements $\left|\langle m_L' \; m_S' \mid d \mid m_L \; m_S \rangle\right|^2$ between the $2^3P$ and $3^3D$ states + and - Indicate the Case of $\sigma_+$ and $\sigma_-$, Respectively

| | | $M_L$ | | | | | | | | | | | | | | |
|---|---|---|---|---|---|---|---|---|---|---|---|---|---|---|---|---|
| | | $M_S$ | | | | | | | | | | | | | | |
| | | 2 | 2 | 1 | 2 | 1 | 0 | 1 | 0 | -1 | 0 | -1 | -2 | -1 | -2 | -2 |
| | | 1 | 0 | 1 | -1 | 0 | 1 | -1 | 0 | 1 | -1 | 0 | 1 | -1 | 0 | -1 |
| | 1, 1 | $(\frac{1}{20})_+$ | | | | $(\frac{1}{120})_-$ | | | | | | | | | | |
| | 1, 0 | | $(\frac{1}{20})_+$ | | | | | $(\frac{1}{120})_-$ | | | | | | | | |
| | 0, 1 | | | $(\frac{1}{40})_+$ | | | | | $(\frac{1}{40})_-$ | | | | | | | |
| | 1,-1 | | | | $(\frac{1}{20})_+$ | | | | | $(\frac{1}{120})_-$ | | | | | | |
| $M_L', M_S'$ | 0, 0 | | | | | $(\frac{1}{40})_+$ | | | | | $(\frac{1}{40})_-$ | | | | | |
| | -1, 1 | | | | | | $(\frac{1}{120})_+$ | | | | | $(\frac{1}{20})_-$ | | | | |
| | 0,-1 | | | | | | | $(\frac{1}{40})_+$ | | | | | $(\frac{1}{40})_-$ | | | |
| | -1, 0 | | | | | | | | $(\frac{1}{120})_+$ | | | | | $(\frac{1}{20})_-$ | | |
| | -1,-1 | | | | | | | | | $(\frac{1}{120})_+$ | | | | | $(\frac{1}{20})_-$ | |

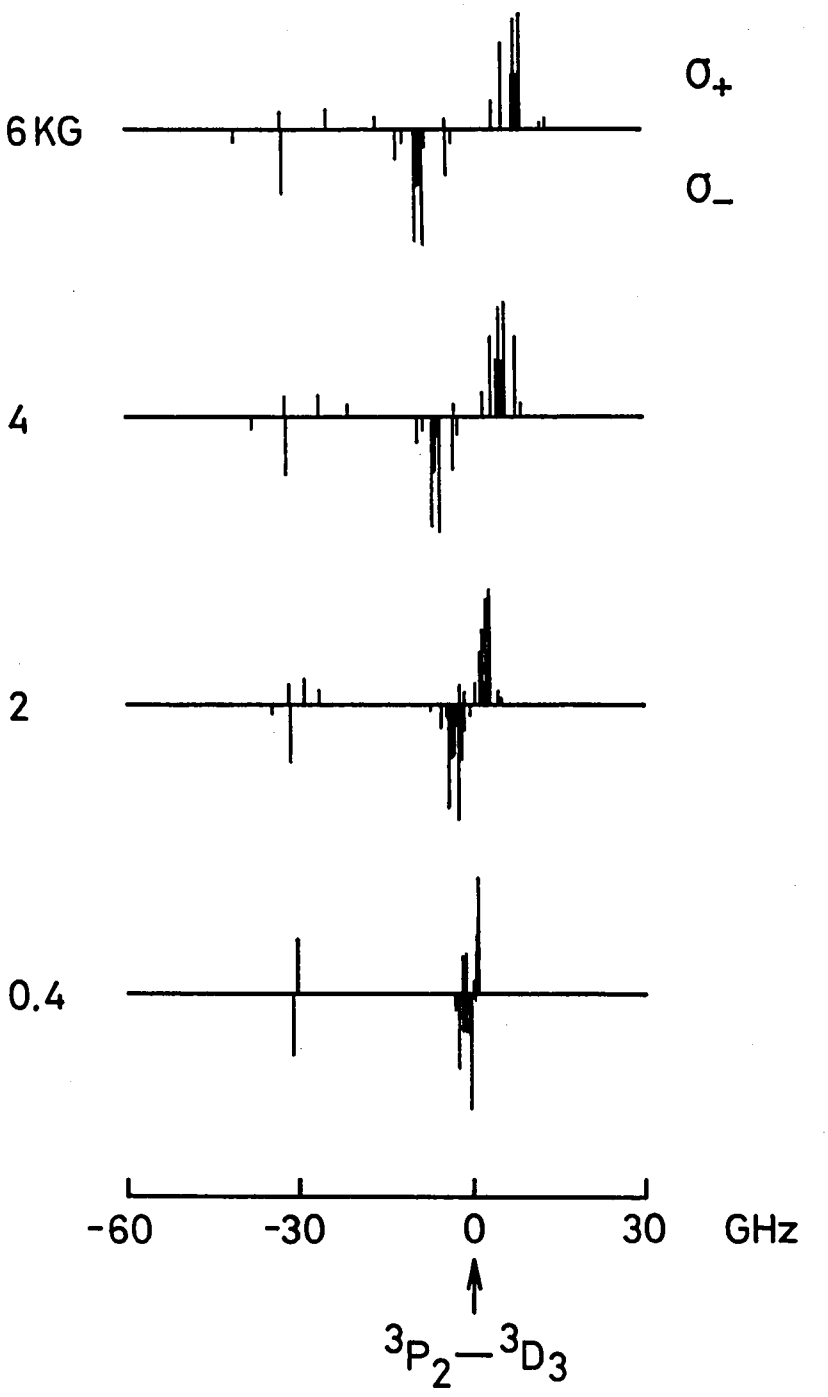


Fig. 5.5 Spectral patterns of the absorption line from $2^3P$ to $3^3D$ in various magnetic fields.

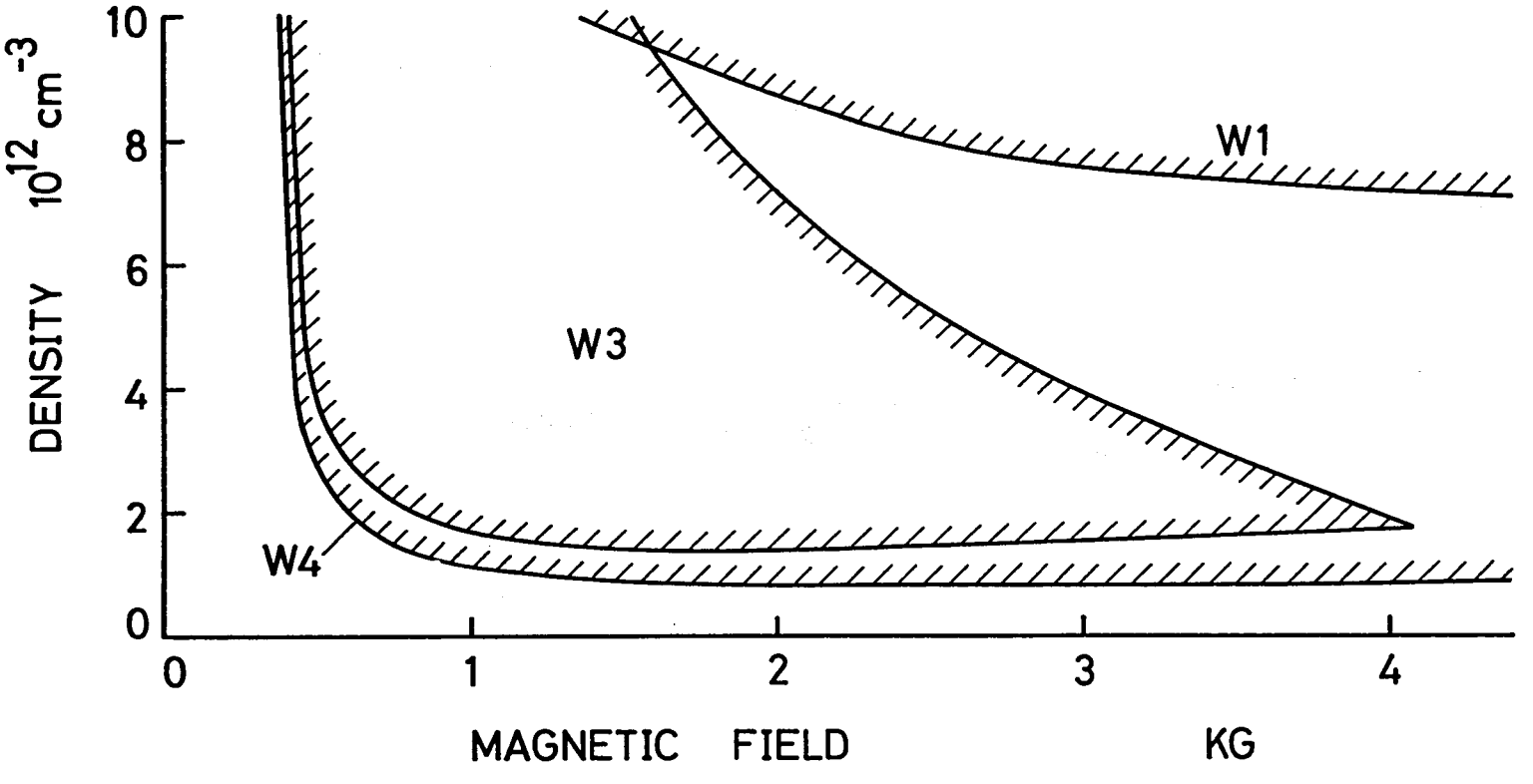


Fig. 5.6(a) Theoretical regions of the $2^3P$ density N and the magnetic field strength H for transmission larger than 0.85. W1, W2, W3, W4 and C denote the frequency region where the frequency-locking occur and which appear in Fig. 5.2.

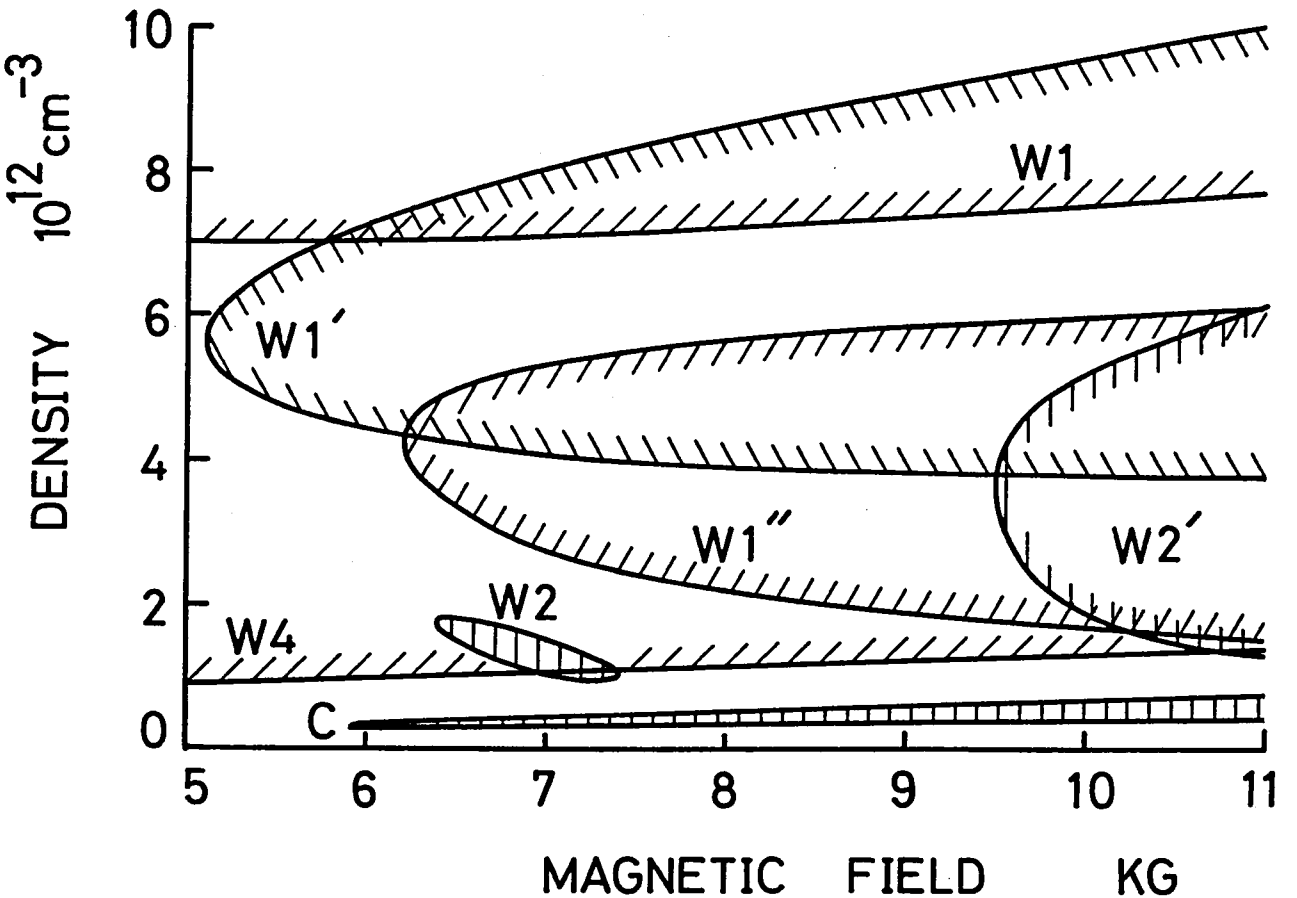


Fig. 5.6(b) Same as for Fig. 5.6(a). (strong magnetic field region)

W3, W4 and C denote the frequency region where the frequency-locking occur, and which are shown in Fig. 5.2. In these complicated spectral pattern, it may be not proper to classify the oscillations by the Faraday filter into those in the center region and those on the wing of the line. However, it is convenient to define that the oscillation is in the center region when the rotation angle $\theta < 0$ and is on the wing when $\theta > 0$ similarly to the case of normal triplet. That is, in Fig. 5.6, C and W denote the regions where the frequency-locking to the center and wing of the line occurs, respectively. As seen in Fig. 5.6, the regions W1 and W2 have some branches W1, W1′, W1″, W2 and W2′, because the spectral pattern in the magnetic field is complicated by the fine structures. The regions of the density N and the magnetic field for the frequency-locking shown in Fig. 5.6 are very complicated, however, they can be understood as the following. Since the frequency difference between the transition from $^3P_0$ to $^3D_1$ and other transitions is large compared with those between other transitions, the spectral pattern can be approximated by two absorption lines A and B located at the frequencies of the transition from $^3P_0$ to $^3D_1$ and of the center of gravity of other transitions. Since the regions W1 and W4 are located on the outside of the two lines A and B (See Fig. 5.2), influence of the line A on W4 and of the line B on W1 are small. Therefore, the regions for W1 and W4 in weak magnetic fields are similar to those of normal triplet (See Fig. 5.6(a)). As seen in Fig. 5.6(a) and (b), the minimum densities for the oscillations on the wings W1 and W4 are $7.0 \times 10^{12}$

$cm^{-3}$ and $0.8 \times 10^{12}$ $cm^{-3}$, respectively. These are in inverse proportion to the spectral strength of A and B (1 : 9). The region for W3 is similar to that for W4 in weak magnetic fields and in low densities (left and lower boundary of W3 in Fig. 5.6(a)). When we increase the density N and/or the magnetic field H, $\sigma_+$ component of the line A increases and/or approaches to the red wing of the line B (See Fig. 5.2 and Fig. 5.5), so that the transmission of the Faraday filter decreases there (right boundary of W3 in Fig. 5.6(a)).

As seen in Fig. 5.5, when H is further increases, the absorption coefficient at the center of the line B decreases, so that the frequency-locking to there becomes possible. The region for this mode is denoted by C in Fig. 5.6(b).

Furthermore, we calculate the shift of the oscillation frequency by increasing of the magnetic field. As a result, we find that the oscillation frequency shifts toward higher frequency for the cases of W2 and W4, and toward lower frequency for the cases of W1 and W3 when the magnetic field is increased.

## 5.3 Experimental Results and Discussions

The experimental setup is similar to that for the neon Faraday filter shown in Fig. 4.9. The discharge tube has a effective length of 15 cm and inner diameter of 4.5 mm.

The parameters varied in the experiments were the helium

pressure, the discharge current and the magnetic field, which could be varied from 0 to 5 torr, from 0 to 70 mA and from 0 to 2.8 kG, respectively.

We have swept the magnetic field H, while increasing the helium pressure as a parameter. The frequency-locking occured in the magnetic field region higher than 1.1 kG when the helium pressure was 3.1 torr and the discharge current was 40 mA. The laser oscillated in a few longitudinal cavity modes. The oscillation frequency shifted toward higher frequency when the magnetic field was increased.

Considering the magnetic field region for the frequency-locking in Fig. 5.6 and the direction of the shift of the oscillation frequency with an increase in magnetic field, it becomes evident that the frequency-locking occured on the wing W4 and that the density of the $^3P$ state was $1.0 \times 10^{12}$ $cm^{-3}$.

When the helium pressure was lower than 2.8 torr or higher than 3.5 torr, frequency-locking could not be achieved because of insufficiency of the density of the $^3P$ state. That is, the helium pressure of 3.1 torr was near the optimum pressure to get the maximum density for the $^3P$ state. Since the density of $1.0 \times 10^{12}$ $cm^{-3}$ in our experiment agrees with th value obtained without magnetic field by Mori et al.[134], it seems that the magnetic field dependence of the population density of the $^3P$ state is small compared with the 1s densities of neon.

## 5.4 Conclusions

The frequency-locking of a CW dye laser to the absorption line from the $^3P$ state to the $^3D$ state of helium by the Faraday filter has been studied. Particular attention has been given to the influence of the fine structures of the states on the Faraday filter. By the theoretical calculations, we have obtained the condition of the lower level density and the magnetic field for the frequency-locking. The condition is complicated by the fine structures, however, we can achieve the frequency-locking to both of the line center and wing of the absorption line. In the present experiment, since the density and the magnetic field are restricted to $1.0 \times 10^{12}$ $cm^{-3}$ and 2.8 KG, respectively, we have obtained only one oscillation mode W4. We are now planning to the frequency-locking to other mode W1, W2, W3 and C, especially to the fine structures in C by increasing of the density and the magnetic field.

# CHAPTER Ⅵ

# FARADAY FILTER WITH AN INHOMOGENEOUS MAGNETIC FIELD

## 6.1 Introduction

In our study on the frequency-locking by the Faraday filter, we have used so far an uniform magnetic field in order to achieve the Faraday rotation. We have obtained successful experimental results in the frequency-locking to some atomic absorption lines of sodium, neon and helium by such a Faraday filter.[86)~88)]

By the Faraday filter with uniform magnetic field, we can select the absorption line to which the frequency-locking occurs by choosing adequate values of the lower level density N and the magnetic field strength H. However, the frequency-locking to the wing of another line sometimes occurs at the same time when the frequency-locking to the center of desired line is achieved. Here we take an example of neon Faraday filter. As seen in Fig. 4.8(a) in chapter Ⅳ, the frequency-locking can be carried out to three absorption lines from the $1s_5$ state: 614.3 nm ($1s_5$-$2p_6$), 588.2 nm ($1s_5$-$2p_2$) and 594.5 nm ($1s_5$-$2p_4$) lines. The selection of the oscillation at the line center of these lines can be achieved by choosing adequate values of N and H. The frequency-locking to the 614.3 nm line can be achieved without

the frequency-locking to other lines. However, when the 588.2 nm line is selected, the frequency-locking to the wing of the 614.3 nm line also occurs at the same time. These two oscillations compete each other, so that the quantum efficiency for the oscillation at the desired line decreases and the fluctuation of power increases.

The Faraday filter has maximum transmission at the rotation angle $\pi/2$. The single-pass rotation angle is given by integration of rotation angle per unit length along the optical path. The rotation angle of $\pi/2$ can be also obtained by an inhomogeneous magnetic field. We can avoid the frequency locking to wings of absorption lines by using this inhomogeneous magnetic field.

## 6.2 Transmission of the Faraday Filter with an Inhomogeneous Magnetic Field

We devide the length of the magnetic field into two parts $\ell_1$ and $\ell_2$ as shown in Fig. 6.1(a), where $H_1$ and $H_2$ are the magnetic field strength in $\ell_1$ and $\ell_2$, respectively. We assume here $\ell_1 \gg \ell_2$ or $\ell_1 \approx \ell$. We use the magnetic field $H_1$ for the frequency-locking to the line center and use the magnetic field $H_2$ for suppression of the frequency-locking to the wing. As seen in Fig. 6.2, we can reduce the transmission of the Faraday filter on the wing by adjusting $H_2$ so that the peaks of the

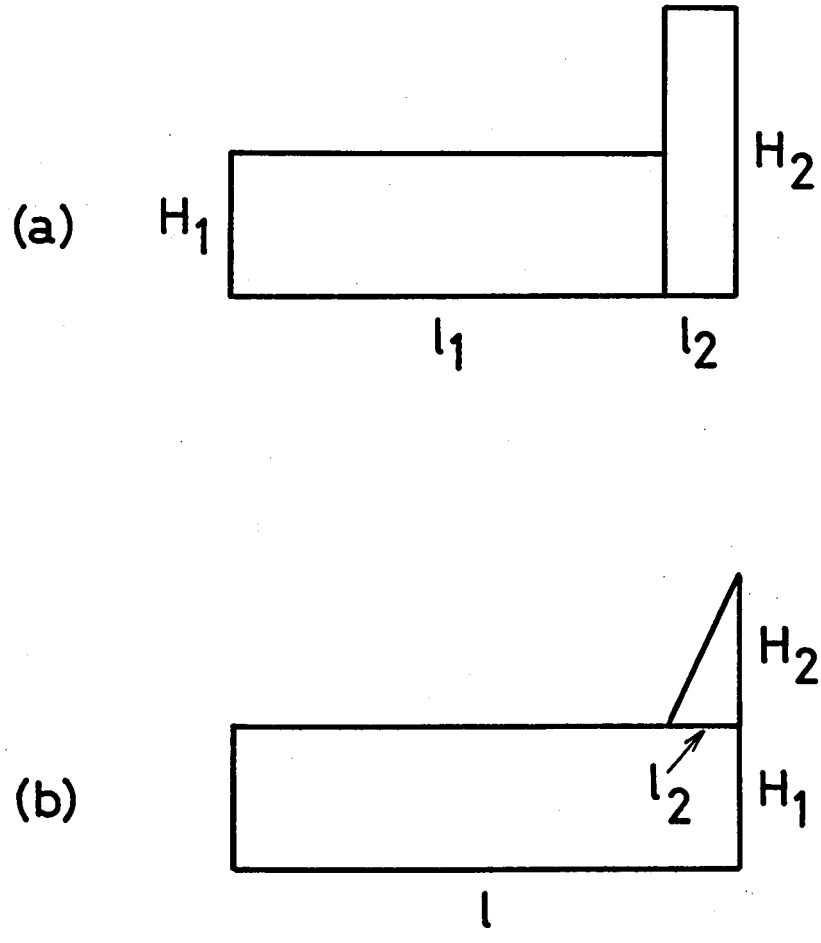


Fig. 6.1 Schematic representation of the magnetic field.
The magnetic field is divided into two parts as shown in (a) and (b).

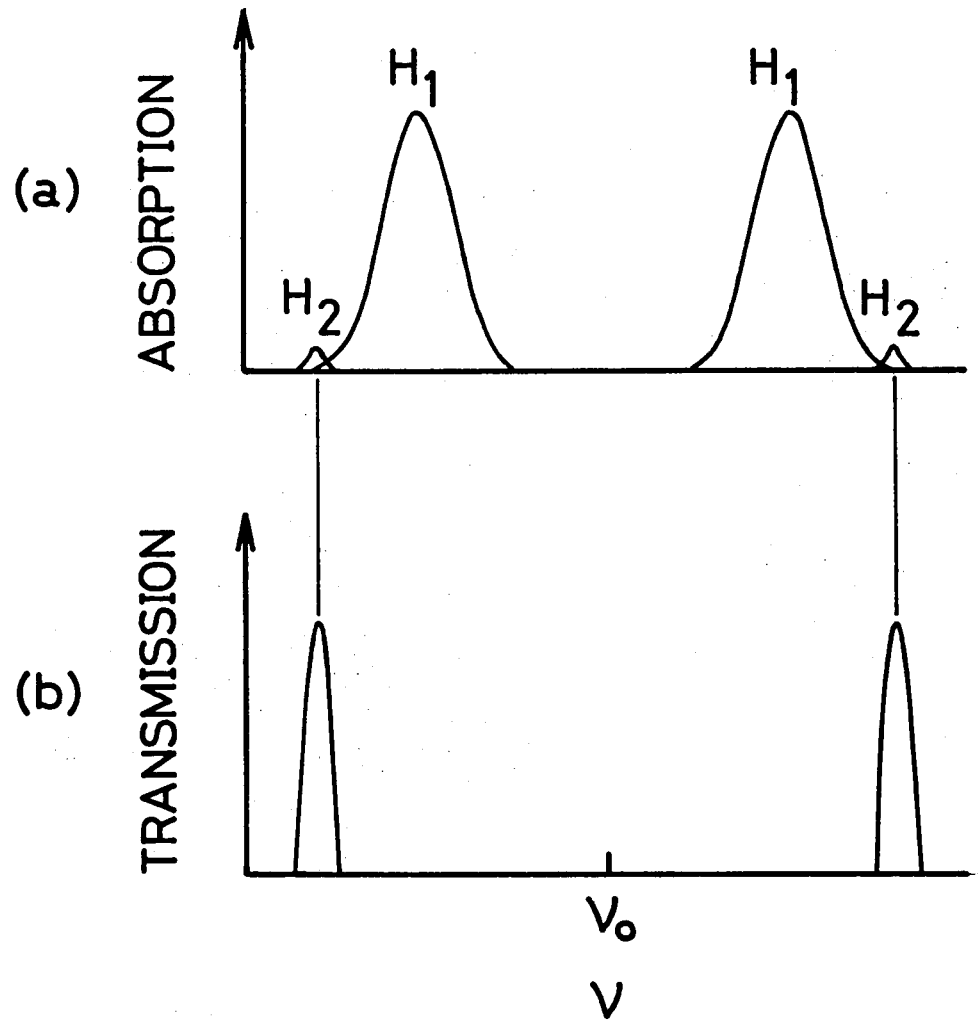


Fig. 6.2 (a) Absorption coefficients of the Faraday filter due to the magnetic field $H_1$ and $H_2$. (b) Transmission of the Faraday filter due to the magnetic field $H_1$.

absorption coefficient by $H_2$ coincide the peaks of the transmission on the wing. At this time, the change in the rotation angle at the line center due to $H_2$ is very small.

Since the peak frequency of the transmission on the wing moves with an increase in magnetic field, we must control $H_2$ for this purpose. The value of $H_2$ should be decided as the following. The frequency of the peak of the transmission on the wing does not exact linearly depend on the magnetic field $H_1$, however, it can be approximated by linear function. Therefore, we take $H_2 = \alpha H_1$, where we decide the proportional coefficient $\alpha$ so that the peaks of absorption coefficient by $H_2$ and of transmission by $H_1$ coincide at the magnetic field where the frequency-locking to the center of desired line occurs. For example, for the case of the 588.2 nm and 614.3 nm lines, we take 2.3 as $\alpha$. When $l_1$ and $l_2$ are 14 cm and 1 cm, respectively, the oscillation on the wing of the 614.3 nm line is fully suppressed as shown in Fig. 6.3. As seen in Fig. 6.3, the region for the frequency-locking at the center of the 588.2 nm line is scarcely changed. With the increase of $l_2$, the suppressing effect increases, however, the condition for the frequency-locking to the line center differs from one obtained in an uniform magnetic field.

The suppression of the frequency-locking to the wing can be also achieved by another type of magnetic field. The magnetic field is divided into two parts as shown in Fig. 6.1(b). In this case, since $H_2$ has a slope, the losses for $\sigma_{\pm}$ lights are distributed over the frequency region where the peaks of the

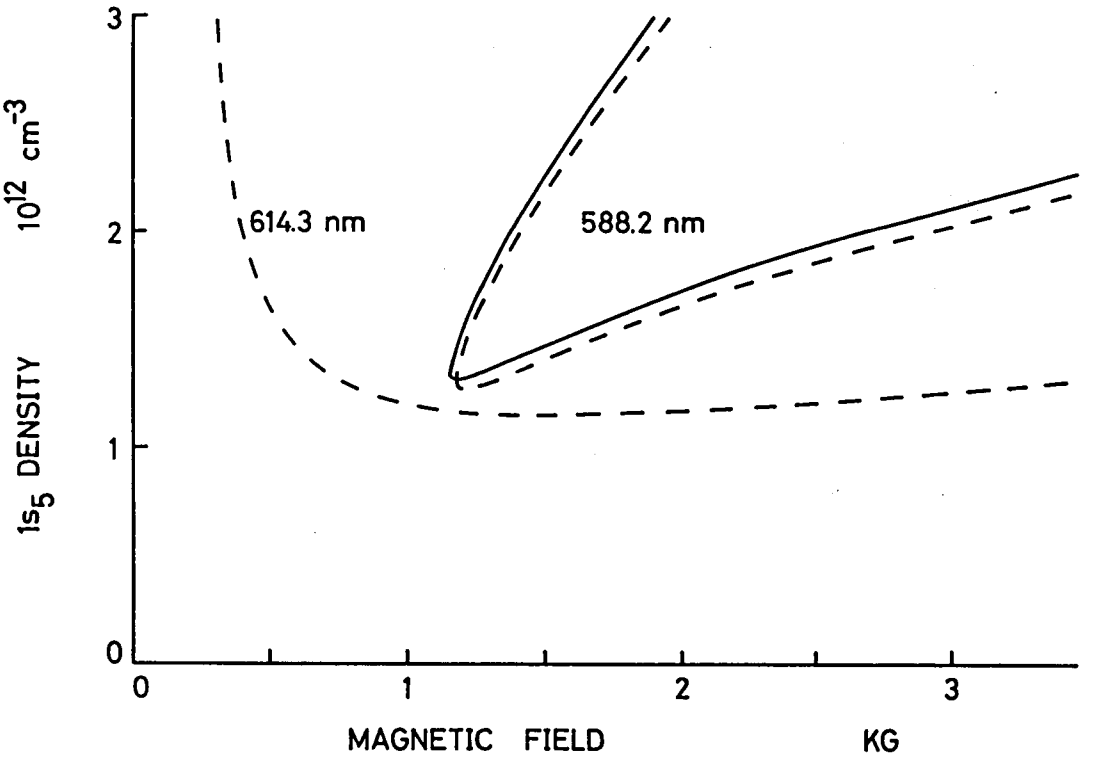


Fig. 6.3 Theoretical regions of the $1s_5$ density N and the magnetic field strength H for transmission larger than 0.85, The dashed and solid lines represent the region by the uniform and inhomogeneous magnetic field.

Table 6.1 Lower Limit of the Magnetic Field Region Where the Transmission of the Faraday Filter Is Larger than 0.75 and 0.85 on the Red and Blue Wings * Represents That the Value Is Larger than 4.1 kG

| $\ell_2$ cm | $H_2$ kG | transmission | | | |
|---|---|---|---|---|---|
| | | 0.75 | | 0.85 | |
| | | red wing | blue wing | red wing | blue wing |
| 4.5 | 0.63 | 0.35 | 0.79 | 0.63 | 1.79 |
| 4.5 | 0.94 | 0.66 | 1.16 | 1.83 | * |
| 4.5 | 1.10 | 1.04 | 1.67 | * | * |
| 4.5 | 1.26 | * | * | * | * |
| 4.5 | 1.57 | * | * | * | * |
| 4.5 | 1.89 | * | * | * | * |
| 1.5 | 1.10 | 1.23 | 1.48 | * | * |
| 1.5 | 1.26 | * | * | * | * |
| 0.5 | 1.26 | 1.13 | 1.20 | * | * |
| 0.5 | 1.42 | 1.57 | 1.64 | * | * |
| 0.5 | 1.57 | 2.11 | * | * | * |

transmission on the wings are scanned with an increase in the magnetic field. The magnetic field region for the frequency locking on the wing has been calculated for various values of $\ell_2$ and $H_2$. The calculated results are shown in Table 6.1 where the lower level density is $2.0 \times 10^{12}$ $cm^{-3}$. As seen in Table 6.1, by this method, we can suppress the oscillation on the wing of the absorption line. This method is convenient compared with one mentioned above in a practical experimental setup, because we can prepare this magnetic field by setting a piece of permanent magnet inside the ordinary uniform magnetic field.

## 6.3 Conclusions

It becomes evident by theoretical calculations that the frequency-locking only to the center of an absorption line can be achieved by using an inhomogeneous magnetic field for the Faraday filter.

Although the experiment for this theory has not been done, we are now planning the experiment.

# CHAPTER VII

## SUMMARY AND CONCLUDING REMARKS

We have made the theoretical and experimental investigations on the frequency-locking of a CW dye laser to atomic absorption lines of sodium, neon and helium.

In chapter I, we have briefly reviewed the principles of a CW dye laser operation. We have analyzed the gain and threshold of a CW dye laser. It has been shown that the oscillation frequency of a dye laser can be tuned by a dispersive element inserted in the laser cavity and that the oscillation frequency agrees the frequency with the maximum transmission of the element. We have reviewed the methods used heretofore for this purpose, and compared them with the method using the Faraday filter.

In chapter II, we have studied on the theory of the Faraday filter and calculated the transmission of the Faraday filter in the vicinity of absorption lines.

We have described absorption and anomalous dispersion of atoms in the vicinity of an absorption line and the Zeeman effect as an introduction to the resonant Faraday effect. If the resonant Faraday effect is employed, the transmission of the Faraday filter has large frequency-dependence in the vicinity

of the absorption line. The frequency with the maximum transmission is given by a density of medium, a magnetic field strength, and a length of a Faraday cell. The maximum transmission can be obtained at the center of an absorption line by choosing adequate values of these quantities.

We have also analyzed the laser cavity system with a Faraday filter, and found that the Faraday filter with partial polarizers is more suitable than that with perfect polarizers for the frequency-locking of a dye laser.

When a Faraday filter is inserted in a laser cavity, atoms in the Faraday filter are irradiated by intense laser light. We have considered the saturation effect on the Faraday filter. It has been shown that the feature of the Faraday filter does not change for the worse by the saturation effect because the absorption coefficient decreased but the refraction index is not decreased by the saturation. In other words, we can calculate the transmission of the Faraday filter and the condition for the frequency-locking by the linear theory.

In chapter III, we have studied the frequency-locking to the sodium D lines.

The single-mode oscillations at the center of the $D_1$ and $D_2$ lines took place at temperatures about 490 K and 480 K, respectively. The simultaneous oscillation at $D_1$ and $D_2$ lines could not be observed at these temperatures. The two-mode oscillations on the both wings of the $D_1$ and $D_2$ lines took place simultaneously at temperatures higher than 505 K. The experimentally obtained

conditions of the relative cell temperature and the magnetic field strength for the oscillation agreed well with those expected from theoretical calculations.

We have considered the magnetic field dependence of the frequency of the laser output. The frequency shifts from the center of the absorption line show the magnetic field dependence smaller than calculated ones. This discrepancy has been explained by the theory including the spatial hole-burning effect in the active medium of dye.

In chapter Ⅳ, we have studied the frquency-locking to the absorption lines of neon.

The oscillation frequency of a CW dye laser was locked to eight neon absorption lines from the 1s states to the 2p states by a Faraday filter. The oscillation took place in a single longitudinal mode of cavity. It should be noted that the frequency-locking was achieved for the absorption lines from metastable and quasi-metastable states. This gives wide area of application to the Faraday filter.

When natural abundance neon was used, the oscillation frequency in the center region of the absorption line shifted toward higher frequency and that on the red wing shifted toward lower frequency with the increase of the magnetic field. When $Ne^{20}$ was used, the oscillation took place just at the center of the $Ne^{20}$ absorption line, and it split into two modes symmetrically with respect to the line center when the magnetic field was increased. This is just as predicted by the theory. From these experimental

results and theoretical calculations, we have developed a technique for fine tuning of the CW dye laser in the vicinity of the absorption line by means of isotope effect.

We have measured also the 1s densities in the positive column of the glow discharge in the presence of a magnetic field, by fitting the experimental results to the theory.

We have found that the saturated absorption takes place at the center of several absorption lines in the Faraday filter, in addition to the optical rotation.

In chapter V, the frequency-locking to the absorption line from the $2^3P$ state to the $3^3D$ state in a discharge tube have been carried out.

The basic calculation method for the transmission of the helium Faraday filter is similar to the one for sodium and neon. A different point is that the $2^3P$ and the $3^3D$ states have fine structure and the angular momenta $\vec{L}$ and $\vec{S}$ are somewhat uncoupled in the magnetic field region where we have interest for the Faraday filter. By the theoretical calculation we have obtained the spectral pattern as a function of the magnetic field. We have then calculated the transmission of the Faraday filter and found that it is complicated by the fine structure.

We have experimentally obtained a narrow band oscillation on the blue wing of the line which is expected by the theoretical calculation to be easiest mode. The shift of the oscillation frequency with an increase in magnetic field has been explained by the theory.

It has been shown that the frequency-locking to the line center is possible in the magnetic fields above 6 kG by the theoretical analysis. Since in our experimental setup the upper limit of the magnetic field was 3 kG, the frequency-locking to the line center could not be done.

In chapter Ⅵ, we have proposed the Faraday filter by which the frequency-locking to the line center is possible without the oscillation on the wing of another absorption line. The theoretical calculation has shown that frequency-locking to the wing can be avoided without changing of the condition for the frequency-locking to the line center by the using of an inhomogeneous magnetic field.

In conclusion, it has been demonstrated that the Faraday filter is one of the most capable element for the frequncy-locking of a CW dye laser to atomic absorption lines. The advantages of the method using the Faraday filter are:

1) The frequency-narrowing and the frequency-locking of a dye laser are simultaneously achieved by a Faraday filter without any other wavelength selective elements.

2) The frequency-locking can be achieved at line center. Most other thechniques using atomic absorption lines lead to locking only on the wings of the line.

3) Although the frequency stability by the Faraday filter is not higher than that attained by the saturated absorption, the oscillation frequency cannot detune from the absorption line without complicated frequency control system including an

external feedback loop. This is due to the fact that the oscillation frequency is determined by characteristic atomic features. Therefore, this method is suitable for a long time operation of a dye laser at absorption lines.

In this thesis, we have dealt with the frequency-locking of a CW dye laser by a Faraday filter. It is also interesting to apply the Faraday filter to a pulsed dye laser. Because of high power and short pulse width in a pulsed dye laser, nonlinearlity and time dependence of a Faraday filter may become important. Therefore, the time evolution of spectrum[118),143)] of the dye laser system including a Faraday filter should be considered.

## REFERENCES


1) P. P. Sorokin and J. R. Lankard, IBM J. Res. Develop. 10, 162 (1966).

2) O. G. Peterson, S. A. Tuccio, and B. B. Snavely, Appl. Phys. Letters 17, 245 (1970).

3) F. P. Schäfer, Dye Lasers (Springer-Verlag, Berlin, 1973).

4) R. N. Hall, G. E. Fenner, J. D. Kingsley, T. J. Soltys, and R. O. Carlson, Phys. Rev. Letters 9, 366 (1962).

5) M. I. Nathan, G. Burns, W. P. Dumk, F. H. Dill, Jr., and G. Lasher, Appl. Phys. Letters 1, 62 (1962).

6) L. F. Mollenauer and D. H. Olson, Appl. Phys. Letters 24, 386 (1974).

7) L. F. Mollenauer and D. H. Olson, J. Appl. Phys. 46, 3109 (1975).

8) H. Walther, Laser Spectroscopy (Springer-Verlag, Berlin, 1976).

9) Model 375 Tunable Dye Laser Instruction Manual (Spectra-Physics, California).

10) J. M. Yarborough, Appl. Phys. Letters 24, 629 (1974).

11) E. P. Schäfer, W. Schmidt, and K. Marth, Appl. Phys. Letters 9, 306 (1966).

12) R. E. Grove, F. Y. Wu, L. A. Hackel, D. G. Youmans, and S. Ezekiel, Appl. Phys. Letters 23, 442 (1973).

13) E. P. Schäfer, W. Schmidt, and K. Marth, Phys. Letters 24A, 280 (1967).

14) I. P. Kaminow, H. P. Weber, and E. A. Chandross, Appl. Phys. Letters 18, 497 (1971).

15) P. W. Smith, P. F. Liao, C. V. Shank, T. K. Gustafson, C. Lin, and P. J. Maloney, Appl. Phys. Letters 25, 144 (1974).

16) O. G. Peterson, J. P. Webb, and M. C. McColgin, J. Appl. Phys. 42, 1917 (1971).

17) H. Walther, Physica Scripta. 9, 297 (1974).

18) P. P. Sorokin and J. R. Lankard, IBM J. Res. Develop. 10, 162 (1966).

19) P. P. Sorokin, J. R. Lankard, V. L. Moruzzi, and E. C. Hammond, J. Chem. Phys. 48, 4726 (1968).

20) M. E. Mack, J. Appl. Phys. 39, 2483 (1968).

21) B. B. Snavely, Proc. IEEE 57, 1374 (1969).

22) A. E. Siegman, D. W. Phillion, and D. J. Kuizenga, Appl. Phys. Letters 21, 345 (1972).

23) G. Yamaguchi, F. Endo, S. Murakawa, S. Okamura, and C. Yamanaka, Japan. J. appl. Phys. 7, 179 (1968).

24) G. Marowsky, Appl. Phys. Letters 26, 647 (1975).

25) G. Marowsky, F. K. Tittel, and F. P. Schäfer, Opt. Commun. 13, 100 (1975).

26) B. H. Soffer and B. B. McFarland, Appl. Phys. Letters 10, 266 (1967)

27) A. A. Friesem, U. Ganiel, and G. Neumann, Appl. Phys. Letters 23, 249 (1973).

28) E. E. Marinero, A. M. Angus, and M. J. Colles, Opt. Commun.

14, 266 (1975).

29) D. J. Bradley and A. J. F. Durrant, Phys. Letters 27A, 73 (1968).

30) G. M. Gale, Opt. Commun. 7, 86 (1973).

31) G. Holtom and O. Teschke, IEEE J. Quantum Electron. QE-10, 577 (1974).

32) D. Kato and T. Sato, Opt. Commun. 5, 134 (1972).

33) M. Okada, S. Shimizu, and S. Ieiri, Paper OQE-74-35, presented at a Quantum Electronics Group Meeting, Inst. Elect. Commun. Engrs. Japan (1974) (in Japanese).

34) M. Okada and S. Ieiri, Opt. Commun. 14, 4 (1975).

35) G. Marowsky, Rev. Sci. Instrum. 44, 890 (1973).

36) H. Matsuzawa, S. Suganomata, and H. Inaba, Paper OQE-77-86, presented at a Quantum Electronics Group Meeting, Inst. Elect. Commun. Engrs. Japan (1977) (in Japanese).

37) R. Wallenstein and T. W. Hänsch, Appl. Opt. 13, 1625 (1974).

38) M. D. Levenson and G. L. Eesley, IEEE J. Quantum Electron. QE-12, 259 (1976).

39) W. M. Fairbank, Jr., T. W. Hänsch, and A. L. Schawlow, J. Opt. Soc. Am. 65, 199 (1975).

40) F. Schuda, M. Hercher, and C. R. Stroud, Jr., Appl. Phys. Letters 22, 360 (1973).

41) F. Davidson, C-M, Chano, F. K. Tittel, and J. P. Hohimer, IEEE J. Quantum Electron. QE-10, 409 (1974).

42) S. Liberman and J. Pinard, Appl. Phys. Letters 24, 142 (1974).

43) U. Ganiel, A. Hardy, and D. Treves, IEEE J. Quantum Electron. QE-12, 704 (1976).

44) T. W. Hänsch, I. S. Shahin, and A. L. Schawlow, Phys. Rev. Letters 27, 707 (1971).

45) T. W. Hänsch, M. H. Nayfeh, S. A. Lee, S. M. Curry, and I. S. Shahin, Phys. Rev. Letters 32, 1336 (1974).

46) R. L. Barger, M. S. Sorem, and J. L. Hall, Appl. Phys. Letters 22, 573 (1973).

47) B. Couilland and A. Ducasse, Opt. Commun. 13, 398 (1975).

48) T. W. Hänsch, Appl. Opt. 11, 895 (1972).

49) W. Hartig and H. Walther, Appl. Phys. 1, 171 (1973).

50) A. Arnesen, A. Bengtsson, R. Hallin, S. Kandela, T. Noreland, and R. Lidholt, Phys. Letters 53A, 459 (1975).

51) H. T. Duong, S. Liberman, J. Pinard, and J.-L. Vialle, Phys. Rev. Letters 33, 339 (1974).

52) R. Schieder and H. Walther, Z. Physik. 270, 55 (1974).

53) R. L. Barger, J. B. West, and T. C. English, Appl. Phys. Letters 27, 31 (1975).

54) M. B. Klein, Opt. Commun. 5, 114 (1972).

55) M. B. Klein, C. V. Shank, and A. Dienes, Opt. Commun. 7, 178 (1973).

56) R. A. Keller, J. D. Simmons, and D. A. Jennings, J. Opt. Soc. Am. 63, 1552 (1973).

57) H. K. Holt, Phys. Rev. A 11, 625 (1975).

58) T. H. Hänsch, A. L. Schawlow, and P. E. Toschek, IEEE J. Quantum Electron. QE-8, 802 (1972).

59) K. Tohma, J. Appl. Phys. 47, 1422 (1976).

60) N. C. Peterson, M. J. Kurylo, W. Braun, A. M. Bass, and R. A. Keller, J. Opt. Soc. Am. 61, 746 (1971).

61) H. K. Holt, Phys. Rev. A 14, 1901 (1976).

62) C. V. Shank and M. B. Klein, Appl. Phys. Letters 23, 156 (1973).

63) A. L. Bloom and D. L. Hardwick, Phys. Letters 20, 373 (1966).

64) W. Strouse and I. Tobias, Appl. Phys. Letters 10, 342 (1967).

65) A. Yamagishi and H. Inaba, Opt. Commun. 16, 223 (1976).

66) A. Yamagishi and H. Inaba, Oyo Buturi 44, 764 (1975) (in Japanese).

67) J. P. Woerdman and M. F. H. Schuurmans, Opt. Commun. 14, 248 (1975).

68) J. L. Cojan, Ann. Phys. (Paris) 9, 385 (1954).

69) B. Bölger and C. H. Weysenfeld, IEEE J. Quantum Electron. QE-8, 529 (1972).

70) Y. H. Meyer, Opt. Commun. 19, 343 (1976).

71) Y. H. Meyer, C. Loth, and R. Astier, Opt. Commun. 25, 100 (1978).

72) B. M. Schmidt, J. M. Williams, and D. Williams, J. Opt. Soc. Am. 54, 454 (1964).

73) F. A. Jenkins and H. E. White, Fundamentals of Optics (McGraw-Hill, New York, 1957), p. 596.

74) L. J. Aplet and J. W. Carson, Appl. Opt. 3, 544 (1964).

75) R. L. Fork and L. C. Bradley, III, Appl. Opt. 3, 137 (1964).

76) E. B. Aleksandrov and V. N. Kulyasov, Opt. Spectrosc. 33,

577 (1972).

77) Y. A. Sharonov, Opt. Spectrosc. 25, 514 (1968).

78) P. P. Sorokin, J. R. Lankard, V. L. Moruzzi, and A. Lurio, Appl. Phys. Letters 15, 179 (1969).

79) L. E. Erickson and A. Szabo, Appl. Phys. Letters 18, 433 (1971).

80) Q. H. Vrehen and A. J. Breimer, Opt. Commun. 4, 416 (1972).

81) G. Magyar and H. Schneider-Muntau, Appl. Phys. Letters 20, 406 (1972).

82) J. J. Turner, E. I. Moses, and C. L. Tang, Appl. Phys. Letters 27, 441 (1975).

83) M. Maeda, O. Uchino, T. Okada, and Y. Miyazoe, Japan. J. appl. Phys. 14, 1975 (1975).

84) M. Maeda, T. Okada, O. Uchino, and Y. Miyazoe, Japan. J. appl. Phys. 15, 1731 (1976).

85) A. J. Gibson and L. Thomas, J. Phys. D: Appl. Phys. 11, L59 (1978).

86) T. Endo, T. Yabuzaki, M. Kitano, T. Sato, and T. Ogawa, IEEE J. Quantum Electron. QE-13, 866 (1977).

87) T. Yabuzaki, T. Endo, M. Kitano, and T. Ogawa, Opt. Commun. 22, 181 (1977).

88) T. Endo, T. Yabuzaki, M. Kitano, T. Sato, and T. Ogawa, IEEE J. Quantum Electron. QE-14 (1978) (in press).

89) J. C. Slater and N. H. Frank, Electromagnetism (McGraw-Hill, New York, 1947) p. 105.

90) H. E. White, Introduction to Atomic Spectra (McGraw-Hill,

New York, 1934).

91) T. Yabuzaki, M. Kitano, T. Endo, and T. Ogawa, Japan. J. appl. Phys. 16, 849 (1977).

92) P. K. Runge, Opt. Commun. 4, 195 (1971).

93) P. K. Runge, Opt. Commun. 5, 311 (1972).

94) D. M. Camm and F. L. Curzon, Can. J. Phys. 50, 2866 (1972).

95) H. M. Gibbs, G. G. Churchill, and G. J. Salamo, Opt. Commun. 12, 396 (1974).

96) Y. J. Yu and R. K. Osborn, Phys. Rev. A 15, 2404 (1971).

97) L. Rosenfeld, Theory of Electrons (Dover Publications, Inc., New York, 1965).

98) S. A. Korff and G. Breit, Rev. Modern Phys. 4, 471 (1932).

99) M. Sargent III, M. O. Scully, and W. E. Lamb, Jr., Laser Physics (Addison-Wesley Publishing Company, London, 1974), p. 372.

100) A. N. Sevchenko, A. A. Kovalev, V. A. Pilipovich and Yu. V. Razvin, Sov. Phys. Doklady 13, 226 (1968).

101) P. P. Sorokin, J. R. Lankard, E. C. Hammond, and V. L. Moruzi, IBM J. Res. Develop. 11, 130 (1967).

102) B. B. McFarland, Appl. Phys. Letters 10, 208 (1967).

103) M. Sargent III, M. O. Scully, and W. E. Lamb, Jr., Laser Physics (Addison-Wesley Publishing Company, London, 1974), p. 101.

104) F. C. M. Coolen, L. C. J. Baghuis, H. L. Hagedoorn, and J. A. van der Heide, J. Opt. Soc. Am. 64, 482 (1974).

105) A. L. Mashinskii, Opt. Spectrosc. 28, 1 (1970).

106) H. W. Kogelnik, E. P. Ippen, A. Dienes, and C. V. Shank, IEEE J. Quantum Electron. QE-8, 373 (1972).

107) F. Y. Wu, R. E. Grove, and S. Ezekiel, Appl. Phys. Letters 25, 73 (1974).

108) B. Wellegehausen, H. Welling, and R. Beigang, Appl. Phys. 3, 387 (1974).

109) C. R. Vidal and J. Cooper, J. Appl. Phys. 40, 3370 (1969).

110) G. M. Grorer, T. P. Cotter, and G. F. Frickson, J. Appl. Phys. 35, 1990 (1964).

111) T. Kobayashi, Oyo Buturi 44, 878 (1975) (in Japanese).

112) A. D. Wilson and Y. Shimoni, J. Phys. B: Atom. Molec. Phys. 8, 2415 (1975).

113) C. T. Pike, Opt. Commun. 10, 14 (1974).

114) I. V. Hertel and A. S. Stamatović, IEEE J. Quantum Electron. QE-11, 210 (1975).

115) G. Marowsky and K. Kaufman, IEEE J. Quantum Electron. QE-12, 207 (1976).

116) H. G. Danielmeyer, J. Appl. Phys. 42, 3125 (1971).

117) W. H. Makky and M. M. Ibrahim, IEEE J. Quantum Electron. QE-14, 325 (1978).

118) Y. H. Meyer and P. Flamant, Opt. Commun. 19, 20 (1976).

119) C. S. Willett, in Introduction to Gas Lasers (Pergamon, Oxford, 1974).

120) A. Ricard, J. Phys. (Paris), 30, 556 (1969).

121) O. P. Bochkova, L. P. Razumovskaya, and S. E. Frish, Opt. Spectrosc. 11, 376 (1961).

122) R. L. Heath, in Handbook of Chemistry and Physics (CRC Press, Ohio, 1976) p. B-245.

123) J. R. Dixon and F. A. Grant, Phys. Rev. 107, 118 (1957).

124) W. L. Wiese, M. W. Smith, and B. M. Glennon, Atomic Transition Probabilities, NSRDS-NBS4, vol. 1 (U. S. Government Printing Office, Washington, D. C., 1966).

125) C. E. Moore, Atomic Energy Levels, National Bureau of Standards Circular 467, vol. 1 (U. S. Government Printing Office, Washington, D. C., 1949).

126) V. I. Odintsov, Opt. Spectrosc. 18, 205 (1965).

127) G. Francis, in Handbuch der Physik, vol. 22 (Springer-Verlag, Berlin, 1956) p. 168.

128) W. R. Bennett, Jr., Appl. Opt., Suppl. 1, 24 (1962).

129) A. Dienes, Phys. Rev. 174, 400 (1968).

130) A. Dienes, Phys. Rev. 174, 414 (1968).

131) M. Gorlicki and M. Dumont, C. R. Acad. Sci. (Paris) B 279, 55 (1974).

132) W. E. Lamb, Jr., Phys. Rev. 134, 1429 (1964).

133) A. V. Phelps and J. P. Molnar, Phys. Rev. 89, 1202 (1953).

134) M. Mori, T. Goto, and S. Hattori, J. Phys. Soc. Japan 44, 1715 (1978).

135) T. Fujimoto, K. Miyazaki, and K. Fukuda, J. Quant. Spectrosc. Radiat. Transfer. 14, 337 (1974).

136) R. Mewe, Physica 47, 373 (1970).

137) J. Daley, M. Douglas, L. Hambro, and N. M. Kroll, Phys. Rev. Letters 29, 12 (1972).

138) W. E. Lamb, Jr., Phys. Rev. 105, 559 (1957).

139) F. M. J. Pichanick, R. D. Swift, C. E. Johnson, and V. W. Hughes, Phys. Rev. 169, 55 (1968).

140) S. A. Lewis, F. M. J. Pichanick, and V. W. Hughes, Phys. Rev. A 2, 86 (1970).

141) R. D. Kaul, J. Opt. Soc. Am. 58, 429 (1968).

142) E. U. Condon and G. H. Shortley, The Theory of Atomic Spectra (Cambridge University Press, Cambridge, 1951) p. 76.

143) P. Juramy, P. Flamant, and Y. H. Meyer, IEEE J. Quantum Electron. QE-13, 855 (1977).